NACA RM L51J04

NACA

RESEARCH MEMORANDUM

LOW-SPEED LONGITUDINAL CHARACTERISTICS OF A 45° SWEPTBACK WING OF ASPECT RATIO 8 WITH HIGH-LIFT AND STALL-CONTROL DEVICES AT REYNOLDS NUMBERS FROM 1,500,000 TO 4,800,000

By George L. Pratt and E. Rousseau Shields

Langley Aeronautical Laboratory
Langley Field, Va.

CLASSIFICATION CANCELLED

Authority J. W. Crowley Date 12-7-53

By T.C.F. Release form no. 1654

NATIONAL ADVISORY COMMITTEE FOR AERONAUTICS

WASHINGTON

February 28, 1952

NATIONAL ADVISORY COMMITTEE FOR AERONAUTICS

RESEARCH MEMORANDUM

LOW-SPEED LONGITUDINAL CHARACTERISTICS OF A 45° SWEPTBACK WING OF ASPECT RATIO 8 WITH HIGH-LIFT AND STALL-CONTROL DEVICES AT REYNOLDS NUMBERS FROM 1,500,000 TO 4,800,000

By George L. Pratt and E. Rousseau Shields

SUMMARY

The low-speed static longitudinal stability characteristics of a wing having 45° sweepback of the quarter-chord line, an aspect ratio of 8, a taper ratio of 0.45, and NACA 63_1A012 airfoil sections parallel to the air stream were investigated in the Langley 19-foot pressure tunnel at Reynolds numbers from 1.5×10^6 to 4.8×10^6. The effects of combinations of leading-edge and trailing-edge flaps, upper-surface flow-control fences, and a fuselage on the longitudinal stability characteristics were determined.

The basic wing had a maximum lift coefficient of 1.01, exhibited a large degree of instability throughout the lift range, and was unstable at maximum lift. With a combination of leading-edge and trailing-edge flaps and upper-surface fences, a maximum lift coefficient of 1.50 was obtained, the movement of the aerodynamic center was reduced to less than 6 percent of the mean aerodynamic chord throughout the lift range, and the pitching moment was stable at maximum lift.

INTRODUCTION

Previous investigations of sweptback wings (see, for example, references 1, 2, and 3) have shown that as the aspect ratio and sweepback are increased, it becomes increasingly difficult to provide longitudinal stability throughout the lift range with the various devices used to control the stalling of sweptback wings. In order to extend these investigations and to provide information in the low-speed range with which

to evaluate design configurations suitable for high-subsonic, long-range airplanes, an investigation has been conducted in the Langley 19-foot pressure tunnel to determine the low-speed longitudinal characteristics of a 45° sweptback wing of aspect ratio 8. A wing of this sweep - aspect-ratio combination is well in the longitudinally unstable region as set forth in reference 4, and on the basis of present manufacturing methods appears to be approaching a limit outside of which a wing would be structurally impractical.

The present paper contains the results of an investigation to determine the effects of leading-edge and trailing-edge flaps, upper-surface flow-control fences, and a fuselage on the longitudinal characteristics of the wing. The effects of leading-edge roughness on the basic wing and on a representative flap-deflected configuration were determined. The tests were conducted at a Reynolds number of 4.0×10^6 and a Mach number of approximately 0.19. Additional tests were made at Reynolds numbers from 1.5×10^6 to 4.8×10^6 on the basic wing, wing with fences, and on a representative flap-deflected configuration.

Results of measurements of the pressure distribution over the wing and the effect of a horizontal tail on the longitudinal stability are presented in references 5 and 6, respectively.

SYMBOLS

The data are referred to a wind axis with the origin located at the projection of the quarter-chord point of the mean aerodynamic chord on the plane of symmetry. Standard NACA symbols and coefficients are used.

C_L	lift coefficient (Lift/qS)
C_D	drag coefficient (Drag/qS)
C_m	pitching-moment coefficient (Pitching moment/qSc')
ΔC_m	increment of pitching-moment coefficient resulting from the addition of the fuselage
L/D	lift-drag ratio
α	angle of attack of wing chord plane with wind, degrees
q	free-stream dynamic pressure, pounds per square foot $\left(\frac{\rho V^2}{2}\right)$

R	Reynolds number $(\rho Vc'/\mu)$
M_o	free-stream Mach number
μ	viscosity of air, slugs per foot-second
ρ	density of air, slugs per cubic foot
V	free-stream velocity, feet per second
S	wing area, square feet
c'	mean aerodynamic chord parallel to plane of symmetry, feet $\left(\frac{2}{S}\int_0^{b/2} c^2 dy\right)$
c	local wing chord parallel to plane of symmetry, feet
b	wing span, feet
y	spanwise coordinate, feet
t_{max}	local airfoil section maximum thickness, feet
i_w	wing-fuselage incidence, angle between wing chord plane and longitudinal axis of fuselage, degrees
dC_m/dC_L	rate of change of pitching-moment coefficient with lift coefficient

MODEL

The model tested in this investigation had 45° sweepback of the quarter-chord line, an aspect ratio of 8.02, and a taper ratio of 0.45 (see table I). The wing was constructed of a steel core embedded in an alloy of bismuth and tin to the plan form indicated in figure 1 and contoured to NACA 63_1A012 airfoil sections parallel to the plane of symmetry. The wing tips were 2.5 percent of the wing span and were rounded to a parabolic curve plan form and cross section. The wing had no geometric twist or dihedral. Measurements were made of the torsional deflection due to aerodynamic loading at a Reynolds number of 4.0×10^6 (a free-stream dynamic pressure of approximately 120 pounds per square foot). The results indicated a nearly linear variation in twist with increasing angle of attack to a maximum value of approximately 0.2° washout from the root to the tip at maximum lift $(C_L = 1.0)$.

The dimensions and locations of the various high-lift and stall-control devices are shown in figure 2. The split-type trailing-edge flaps (fig. 2(a)) were constructed of sheet steel with a chord equal to 20 percent of the local wing chord in the undeflected position and were deflected 50° from the lower surface of the wing parallel to the air stream (60° measured in a plane perpendicular to the flap hinge line). Mounting brackets were constructed to simulate hinge-line locations of the trailing-edge flaps at 80 and 100 percent of the wing chord with spans of 35, 50, and 60 percent of the wing span with the inboard end of the flap located at the wing root. The inboard 10 percent of the trailing-edge flaps was removed to permit installation of the fuselage. For convenience in referring to the trailing-edge flaps, the flap pivoted about the 80-percent-chord line will be referred to as the split flap, and the flap pivoted about the trailing edge will be referred to as the extended split flap.

The principal dimensions of the round-nose extensible-type leading-edge flaps and the span and spanwise location are shown in figure 2(b). The flaps were constructed of a wooden block having a sheet steel nose rolled to approximately a 3/8-inch diameter. When resolved parallel to the plane of symmetry, the leading-edge flap dimensions presented in figure 2(b) resulted in a flap deflection of 30° with respect to the wing-chord plane and a constant chord of 2.75 inches. This chord is equal to 16 percent of the local wing chord at 0.40b/2 and 27 percent at 0.975b/2.

The upper-surface fences were constructed of 1/16-inch sheet steel. The 3 types of chordwise fences tested on the model are shown in figure 2(c). The "nose fence" extended aft 25 percent of the wing chord from the leading edge on the upper and lower wing surfaces. The "chord fence" extended along the upper surface from 0.05c to the trailing edge of the wing. The "complete fence" is a combination of the first two fences. An additional segment of chord fence extending from 0.35c to the trailing edge was tested at 0.89b/2. Unless specifically stated otherwise, the fences installed on the various configurations throughout the tests had a height (measured from the surface of the wing) equal to $0.6t_{max}$ at 0.575b/2 and 0.80b/2 and $0.7t_{max}$ at 0.89b/2. The fences will be referred to by type and spanwise location.

The fuselage was a body of revolution having a fineness ratio of 10 with the nose and afterbody shapes as indicated in table I and shown in figure 1. Provisions were made to test the wing at wing-fuselage incidences of 0° and 4°.

Leading-edge roughness was obtained by applying No. 60 carborundum granules to a thin coating of shellac on the leading 0.08 chord of the wing measured along the upper and lower surfaces. For the flap-deflected combination, the roughness extended along the wing leading edge inboard of the leading-edge flaps.

The wing mounted for testing on the two-support system of the Langley 19-foot pressure tunnel is shown in figure 3.

TESTS

The tests were conducted in the Langley 19-foot pressure tunnel with the air in the tunnel compressed to approximately 33 pounds per square inch, absolute. Lift and drag forces and pitching moments were measured through an angle-of-attack range from -3.5° to 31°, and unless stated otherwise, the tests were conducted at a Reynolds number of 4.0×10^6. Scale-effect tests were made at Reynolds numbers from 1.5×10^6 to 4.8×10^6 for the plain wing and plain wing with fences and from 1.5×10^6 to 4.0×10^6 for one wing-flap combination. The Mach numbers corresponding to the various Reynolds numbers are as follow:

R	M_o
1.5×10^6	0.07
2.2	.11
3.0	.14
4.0	.19
4.8	.25

The lift, drag, and pitching-moment data have been corrected for support tare and interference effects. As noted in reference 5, there was a spanwise variation in the tunnel air-stream angle in the region occupied by the model. Inasmuch as only total wing-force coefficients are considered in this paper, an average air-stream misalinement correction has been applied to the angle of attack and drag coefficients.

The angle of attack and drag have been corrected for jet-boundary effects and the pitching moment corrected for tunnel-induced distortion of the loading by the method of reference 7. These corrections are as follow and were all added to the data:

$$\Delta\alpha = 0.387C_L$$

$$\Delta C_D = 0.00634C_L^2$$

$$\Delta C_m = 0.0035C_L$$

The spanwise variation of the jet-boundary-induced angle was of the same magnitude and in a direction opposite to the 0.2° twist due to aerodynamic loading.

RESULTS

Presentation of Results

The longitudinal aerodynamic characteristics for the various configurations tested are presented in figures 4 to 31. Table II presents a summary of the maximum lift and pitching-moment characteristics.

Basic Wing

Plain wing.- The lift curves show a decreasing slope and the pitching-moment curves show a positive increase in dC_m/dC_L with an increase in angle of attack beginning at a low angle of attack (fig. 4). At the low Reynolds number and above a lift coefficient of 0.7, there was a rapid increase in lift-curve slope which became much less pronounced and occurred at a higher lift coefficient as the Reynolds number was increased. This increase in lift-curve slope was accompanied by a stable break in the pitching-moment curve which also became less severe at the higher Reynolds numbers. In the region near maximum lift the lift curves tended to level off, and the pitching moments were highly unstable. In general, an increase in Reynolds number in the range investigated caused the lift curve to be more nearly linear and reduced the variation of dC_m/dC_L throughout the lift range.

The pressure-distribution surveys presented in reference 5 indicate that the decreased lift-curve slope and positive increase in dC_m/dC_L with increasing angle of attack result from a loss in lift due to trailing-edge separation which began at low angles of attack over the tip sections of the wing. The increased lift and stable moment break in the region of $C_L = 0.7$ appear to result from a chordwise redistribution of loading as separation occurs over the complete chord of the tip sections.

The drag was decreased considerably through the moderate and upper lift range with an increase in Reynolds number (figs. 4 and 5). Reynolds number appeared to have little effect on the maximum value of the lift-drag ratios.

Wing with fences.- By the use of flow-control fences located at several spanwise positions on the upper surface of the wing, it was possible to reduce appreciably the variation of dC_m/dC_L with lift

coefficient (figs. 6 to 8). With fences at 0.575, 0.80, and 0.89b/2, the movement of the aerodynamic center was reduced to less than 6 percent of the mean aerodynamic chord throughout the lift range to approximately $0.95C_{L_{max}}$ as indicated by the variation of dC_m/dC_L (fig. 8). The pitching moment, however, remained unstable at maximum lift. As the spanwise locations of the fences of this investigation were chosen somewhat arbitrarily, they should not be construed as being an optimum for a wing of this plan form. It seems reasonable that a more thorough investigation would result in an improvement in fence type and a possible reduction in the number of fences required to obtain a linear variation of pitching moment with lift coefficient.

The effectiveness of individual fences and the effect of extending the fences chordwise around the wing leading edge are also indicated in figures 6 to 8. A fence located at 0.575b/2 resulted in a greater improvement in stability than a fence located at 0.80b/2 (fig. 6(b)) and probably results from the inner fence affecting the spanwise flow of air in the boundary layer over a larger portion of the wing. A complete fence at 0.65b/2, however, resulted in no change in the longitudinal stability characteristics from those obtained with a fence at 0.575b/2 (data not presented). The fences that extended around the leading edge of the wing (complete fences) were mainly effective near maximum lift where they reduced the large positive pitching moment obtained with the chord fences at an angle of attack beyond and several degrees prior to maximum lift. The nose fences when tested alone reduced appreciably the instability of the plain wing in the upper lift region but had little effect through the low and moderate lift coefficient range (fig. 8).

Figure 9 presents the results of varying the height of the complete fence at 0.575b/2 from $0.3t_{max}$ to $1.5t_{max}$. In the range investigated, an increase in the height of the fence produced only a small improvement in the longitudinal stability which resulted in a small trim shift near maximum lift.

Upper-surface fences improved the lift characteristics of the basic wing as indicated by a higher lift-curve slope in the upper lift range and a small increase in maximum lift (figs. 6 to 8). The drag characteristics of the wing with two fence configurations are compared to the plain wing in figure 10. The fences resulted in a small increase in drag in the lower lift range and a consequent reduction in the maximum lift-drag ratio. In the upper lift region, however, the fences resulted in an appreciable decrease in drag with a subsequent increase in the lift-drag ratios.

Within the Reynolds number range available for the present tests $\left(1.5 \times 10^6 \text{ to } 4.8 \times 10^6\right)$, an increase in Reynolds number improved the stability at the lower Reynolds numbers (fig. 11). The data indicate little Reynolds number effect on stability, however, at Reynolds numbers

above 3.0×10^6 and 2.2×10^6 for a single and multiple fence arrangement, respectively.

In general, the improvement in the aerodynamic characteristics of the wing in the upper lift region by the addition of upper-surface fences appears to result from the ability of the fences to delay the trailing-edge separation on the tip sections of the wing by interrupting the spanwise flow of air in the boundary layer. The pressure-distribution data of reference 5 show that the lifting ability of the tip sections was maintained to a much higher angle of attack for the wing with fences installed.

Wing with Flaps

Trailing-edge flaps.- Split-type trailing-edge flaps resulted in little improvement in the longitudinal stability characteristics of the wing (fig. 12). An increase in the span of the flaps from 0.35b/2 to 0.60b/2 improved the stability slightly through the low and moderate lift range but produced a more abrupt unstable break in the pitching-moment curve as the wing stalled. The longitudinal stability characteristics with the extended split flaps were similar to those obtained with the split flaps.

The maximum lift coefficient was increased from a value of 1.01 for the plain wing to values of 1.34 and 1.45 by the 0.60b/2 split and extended split flaps, respectively. The trailing-edge flaps produced an abrupt loss in lift after maximum lift had been attained, whereas the plain wing exhibited a leveling off of the lift curves at maximum lift. At zero angle of attack, the increments in lift coefficient due to flaps were equal to 0.51 and 0.57 for the 0.6b/2 split and extended split flaps, respectively. An attempt to calculate the increment in lift due to the flaps by the simplified method of reference 3 resulted in values considerably less than the experimental values.

Leading-edge flaps.- With the leading-edge flaps installed, the variation of dC_m/dC_L was appreciably less than for the basic wing; however, considerable undesirable changes in stability remained throughout the lift range. At maximum lift, the pitching-moment curves broke in a stable direction.

A comparison of the lift characteristics of the plain wing (fig. 4(a)) and the wing with leading-edge flaps deflected (fig. 13) shows that the leading-edge flaps resulted in a higher lift-curve slope through the moderate and upper lift coefficient range and produced an increment of maximum lift coefficient of approximately 0.2. A change in leading-edge flap span from 0.35b/2 to 0.575b/2 resulted in only small changes in maximum lift. As can be seen from the curves of figure 13, there was

an initial break in the lift curve at a lift coefficient of approximately 1.1 and a small increase in lift with further increase in angle of attack. The change in lift-curve slope at a lift coefficient of approximately 1.1 is associated with the unstable break in pitching moment obtained for the shorter spans of leading-edge flap at the same lift coefficient and results from a loss in lift over the wing inboard of the inboard end of the leading-edge flap, as indicated by wool tuft studies and pressure distribution measurements (data not published). The longer spans of flap move the initial stall inboard and reduce the loss in lift behind the center of moments, thereby reducing the instability. The effectiveness of the leading-edge flaps in providing stability appears to result from their ability to maintain lift over the outboard portion of the wing. By the selection of the proper flap span, the stalled and unstalled areas may be balanced to provide the desired stability.

Combinations of leading-edge and trailing-edge flaps.- When the leading-edge and trailing-edge flaps were tested in combination, the model exhibited varying degrees of instability which were dependent on the span of both the leading-edge and trailing-edge flaps (figs. 14 to 16). In general, the longer spans of leading-edge flaps and the shorter spans of trailing-edge flaps provided the most favorable pitching-moment characteristics near maximum lift. The chordwise location of the trailing-edge flaps had little effect on the longitudinal stability characteristics with the leading-edge flaps installed.

An examination of figures 14 to 16 indicates that, for many combinations (particularly the configurations having the longer spans of leading-edge flaps), the initial leveling off or break in the lift curve is followed by a small increase in lift at higher angles of attack. For purposes of comparison, the maximum value of lift coefficient obtained will be used in discussing the maximum lift characteristics of the wing with flaps deflected, although it is realized that this may not be a usable value of lift coefficient from the standpoint of longitudinal stability. In most cases, maximum lift occurs after the pitching-moment curves have broken in a stable or unstable direction.

The maximum values of lift coefficient obtained are presented in figure 17 for the various combinations of flaps. With the leading-edge flaps deflected, the 0.6b/2 split flap produced only an increment of maximum lift coefficient of approximately 0.10 to 0.15. Several of the shorter spans of split flap actually produced a decrease in maximum lift over that obtained with the leading-edge flaps alone. The extended split flaps improved the maximum lift characteristics appreciably, and the 0.6b/2 trailing-edge flap resulted in an increment of maximum lift coefficient of approximately 0.25 with the leading-edge flaps installed.

The drag characteristics are presented for a representative group of flap-deflected configurations in figures 18 to 20. The data indicate that the extended split flaps produced an appreciably smaller increment in drag than a corresponding span of split flaps. A change in leading-edge flap span from 0.35b/2 to 0.575b/2 produced only a small increment of drag.

An increase in Reynolds number in the range 1.5×10^6 to 4.0×10^6 reduced the variation of dC_m/dC_L and improved the lift-curve slopes throughout the upper lift range with the leading-edge and trailing-edge flaps installed (fig. 21).

Effect of fences with flaps deflected.- The data of figures 12 to 16 indicate that two upper-surface fences located at 0.575b/2 and 0.80b/2 reduced appreciably the variation of dC_m/dC_L throughout the upper lift range obtained with the leading-edge and trailing-edge flaps installed. Figure 22 indicates that the addition of a third fence at 0.89b/2 resulted in a further slight improvement in the variation of pitching-moment coefficient with lift coefficient (compare with data of figs. 13 and 14(b)). The effectiveness of the fences in improving the longitudinal stability, as in the case of the plain wing, appears to result from the interference with the spanwise flow of air in the boundary layer over the outboard rear portion of the wing.

The effectiveness of the individual fences at 0.575b/2 and 0.80b/2 is indicated in figure 23 for one flap combination. Contrary to the results obtained for the plain wing (fig. 6), with the leading-edge flaps deflected, the outboard fence (0.80b/2) produced the greatest improvement in the longitudinal stability characteristics. The data of figure 16 compared with similar flap configurations of figures 14 and 15 also indicate the increased effectiveness of the outboard fence over the inboard fence. The decreased effectiveness of the inboard fence with the flaps deflected may result from the proximity of the fence to a vortex off the inboard end of the leading-edge flap which probably interferes with the spanwise flow of air in the boundary layer.

Figures 14 to 16 show that the lift-curve slope and maximum-lift characteristics of the wing with flaps were improved slightly in the higher angle-of-attack range by the addition of the fences. As in the case of the plain wing, fences increased the drag slightly in the lower lift range but decreased the drag at higher values of lift coefficient (figs. 18 to 20).

The most satisfactory of the flap and fence configurations tested from the standpoint of longitudinal stability and maximum lift characteristics appears to be the 0.500b/2 leading-edge flap and 0.500b/2 extended split flap with the upper-surface fences located at 0.575b/2 and 0.80b/2

(fig. 15(a)). This combination had a maximum lift coefficient of 1.50, the movement of the aerodynamic center amounted to less than 6 percent of the mean aerodynamic chord as indicated by the variation of dC_m/dC_L throughout the lift range, and the pitching moment was stable at maximum lift.

Leading-Edge Roughness

The results of testing the plain wing and one flap-deflected combination (Reynolds number of 4.0×10^6) with roughness applied along the leading edge of the wing are presented in figure 24. For the flap-deflected combination, the roughness extended along the wing leading edge inboard of the leading-edge flaps.

The roughness resulted in a lower lift-curve slope and a positive increase in dC_m/dC_L for both the plain and flapped configurations through most of the lift range and, in general, produced results similar to those obtained for the smooth wings tested at lower Reynolds numbers (see figs. 4 and 21). Reference 5 presents the results of pressure-distribution measurements on the plain wing with leading-edge roughness and indicates that roughness resulted in a lower lift-curve slope, an earlier separation, and a lower maximum lift over the tip sections of the wing.

Wing-Fuselage Combination

Plain wing-fuselage combination.- The installation of a fuselage on the wing resulted in a decrease in stability throughout the lift range (figs. 25 to 27). At the lower lift coefficients, the aerodynamic center for the wing-fuselage combination for $i_w = 0^\circ$ and $i_w = 4^\circ$, respectively, was approximately 11 percent and 9 percent of the mean aerodynamic chord forward of its location for the wing alone as indicated by the curves of figure 26. As can be seen, a change of wing-fuselage incidence from 0° to 4° resulted in a movement of the aerodynamic center of approximately 2 percent of the mean aerodynamic chord which is slightly larger than the effects obtained for unswept-wing - fuselage combinations (references 8 and 9).

Figure 27 shows the increment in pitching-moment coefficient due to the fuselage (fuselage-on pitching-moment coefficient minus fuselage-off pitching-moment coefficient) plotted against angle of attack for the 2 wing fuselage incidences tested. The data indicate a negative trim change due to the fuselage at the low angles of attack and a positive increase with increasing angle of attack, which resulted in large positive pitching moments at high angles of attack. The principal effect of wing-fuselage incidence was a trim change which remained nearly constant through the angle-of-attack range.

The lift-curve slope was improved slightly in the higher lift range, and the maximum lift coefficient was increased approximately 0.05 by the addition of the fuselage at either wing-fuselage incidence. The incidence of 4° resulted in a slight decrement in lift at zero angle of attack which should be expected because of the negative attitude of the fuselage at zero wing angle of attack.

The fuselage increased the drag by a constant increment of approximately 0.008 through the lower lift range at both wing incidences (figs. 25(c) and 4(c)). The improved lift characteristics in the high lift range with the fuselage installed were accompanied by a decrease in drag coefficient at the lift coefficients above 0.90. The Reynolds number effects with the fuselage installed were similar to those obtained on the wing without fuselage (figs. 4 and 25).

Wing-fuselage combination with fences.- The upper-surface fences appeared to maintain their effectiveness by reducing the variation of dC_m/dC_L through the upper lift range with the fuselage installed on the wing (fig. 28). In the lower lift range the fences installed on the wing-fuselage combination did not produce the linear variation of pitching moment with lift coefficient as obtained by the fences on the basic wing. This is shown more clearly in figure 26 which presents the values of dC_m/dC_L through the lift range for the fence on and off configurations and shows the positive increase in the slope of the pitching-moment curve with increasing lift coefficient to be appreciably greater for the fuselage-installed configurations with fences through the lower lift range. As in the case of the plain wing, the fences on the wing-fuselage combination improved the lift characteristics slightly in the upper lift range.

Wing-fuselage combination with flaps.- The addition of a fuselage to the wing with leading- and trailing-edge flaps deflected altered the stability characteristics of the wing appreciably. The data of figures 29 to 31 show that the leading-edge flaps no longer produced a stable break in the pitching moment at high angles of attack for most flap-deflected configurations. This lack of stability with the leading-edge flaps appears to result from the large positive increments in pitching moment due to the fuselage at high angles of attack. Examination of the data of figure 27 shows that the increment in pitching-moment coefficient due to the fuselage is considerably greater for the flap-deflected condition shown than for the plain wing-fuselage combination at high angles of attack. At the lower angles of attack the variation of increment in pitching-moment coefficient with angle of attack is approximately the same for the flaps on and off configurations. The shift in the two curves (flaps on and flaps off for a given incidence) is due primarily to the split flap which extended inboard to the plane of symmetry with the fuselage off but had the inboard 10 percent removed for the fuselage-on tests to permit installation of the fuselage, which resulted in an additional trim change.

Fuselage incidence had little effect on the stability characteristics of the wing-fuselage combination with flaps deflected. The increment in pitching moment due to incidence was not affected appreciably at the lower angles of attack for the flap-deflected condition of figure 27 but was decreased slightly at the higher angles of attack.

An analysis similar to that presented in figure 27 for a configuration having an extended split flap of longer span and upper-surface fences (data of figs. 30 and 31) produced qualitatively and approximately quantitatively the same results as were obtained for the flap configuration of figure 27.

The data of figures 29 to 31 indicate that the upper-surface fences decreased the variation of dC_m/dC_L through the upper lift range for the various flap-deflected wing-fuselage combinations.

The fuselage had little effect on the lift coefficient at which the lift curves initially leveled off for the combinations having split flaps deflected but resulted in a slight increase in lift coefficient with the extended split flaps deflected at either wing-fuselage incidence (figs. 30 and 31). At higher angles of attack, the fuselage resulted in a further small increase in lift which was slightly greater at $i_w = 0^\circ$ than at $i_w = 4^\circ$. The lift-curve slope was increased slightly through the lift range for the various flap-deflected configurations by the addition of the fuselage at either incidence.

Although the fuselage of this investigation had a large detrimental effect on the longitudinal stability characteristics of the wing including the more favorable flap combinations, a subsequent investigation of the stability contribution of a horizontal tail on the wing-fuselage combination (reference 6) showed that satisfactory longitudinal stability characteristics could be obtained for the wing with flaps and fences through the lift range.

CONCLUDING REMARKS

The following remarks may be made in conclusion of an investigation of the low-speed longitudinal characteristics of a 45° sweptback wing of aspect ratio 8 with various high-lift and stall-control devices:

1. The basic wing exhibited a large degree of instability resulting from trailing-edge separation beginning at low angles of attack over the tip sections of the wing.

2. By controlling the spanwise flow of air over the tip sections of the wing through the use of upper-surface fences installed at several locations along the span, the movement of the aerodynamic center was reduced to less than 6 percent of the mean aerodynamic chord throughout the lift range to $0.95C_{L_{max}}$. The pitching moment remained unstable at maximum lift, however.

3. Leading-edge flaps resulted in stability at maximum lift and increased the maximum lift coefficient from 1.01 for the basic wing to approximately 1.22. Considerable variations in stability existed throughout the lift range, however, which were reduced markedly by upper-surface fences.

4. In combination, the longer spans of leading-edge flaps and the shorter spans of trailing-edge flaps provided the most favorable pitching-moment characteristics at maximum lift. The chordwise location of the trailing-edge flaps had little effect on the longitudinal stability characteristics, but split-type flaps located along the trailing edge of the wing produced improved maximum-lift characteristics over the flaps located along the 80-percent-chord line. Upper-surface fences improved the stability characteristics of the wing for all flap combinations investigated.

5. With a configuration having leading-edge and trailing-edge flaps each equal to 50 percent of the wing semispan and having upper-surface fences located at 57.5 and 80 percent of the wing semispan, the maximum lift was 1.50, the movement of the aerodynamic center was less than 6 percent of the mean aerodynamic chord, and the pitching moment was stable at maximum lift.

6. Installation of a fuselage on the wing resulted in a large destabilizing moment which was not eliminated by the use of leading-edge flaps and fences. A change of the incidence of the wing on the fuselage produced only a small effect on the longitudinal stability.

Langley Aeronautical Laboratory
National Advisory Committee for Aeronautics
Langley Field, Va.

REFERENCES

1. Graham, Robert R., and Conner, D. William: Investigation of High-Lift and Stall-Control Devices on an NACA 64-Series 42° Sweptback Wing with and without Fuselage. NACA RM L7G09, 1947.

2. Salmi, Reino J.: Effects of Leading-Edge Devices and Trailing-Edge Flaps on Longitudinal Characteristics of Two 47.7° Sweptback Wings of Aspect Ratio 5.1 and 6.0 at a Reynolds Number of 6.0×10^6. NACA RM L50F20, 1950.

3. Koven, William, and Graham, Robert R.: Wind-Tunnel Investigation of High-Lift and Stall-Control Devices on a 37° Sweptback Wing of Aspect Ratio 6 at High Reynolds Numbers. NACA RM L8D29, 1948.

4. Shortal, Joseph A., and Maggin, Bernard: Effect of Sweepback and Aspect Ratio on Longitudinal Stability Characteristics of Wings at Low Speeds. NACA TN 1093, 1946.

5. Graham, Robert R.: Low-Speed Characteristics of a 45° Sweptback Wing of Aspect Ratio 8 from Pressure Distributions and Force Tests at Reynolds Numbers from 1,500,000 to 4,800,000. NACA RM L51H13, 1951.

6. Salmi, Reino J., and Jacques, William A.: Effect of Vertical Location of a Horizontal Tail on the Static Longitudinal Stability Characteristics of a 45° Sweptback-Wing - Fuselage Combination of Aspect Ratio 8 at a Reynolds Number of 4.0×10^6. NACA RM L51J08, 1951.

7. Sivells, James C., and Salmi, Rachel M.: Jet-Boundary Corrections for Complete and Semispan Swept Wings in Closed Circular Wind Tunnels. NACA TN 2454, 1951.

8. Jacobs, Eastman N., and Ward, Kenneth E.: Interference of Wing and Fuselage from Tests of 209 Combinations in the NACA Variable-Density Tunnel. NACA Rep. 540, 1935.

9. Anscombe, A., and Raney, D. J.: Low-Speed Tunnel Investigation of the Effect of the Body on C_{m_o} and Aerodynamic Centre of Unswept Wing-Body Combinations. Rep. No. Aero. 2323, British R.A.E., April 1949.

TABLE I.- GEOMETRY OF MODEL

Wing:	
Area, square feet	14.02
Span, feet	10.61
Aspect ratio, b^2/S	8.02
Taper ratio, ratio of tip chord to root chord	0.45
Mean aerodynamic chord, feet	1.39
Airfoil section, parallel to plane of symmetry	NACA 63_1A012
Sweepback of quarter-chord line, degrees	45
Sweepback of leading edge, degrees	46.3
Geometric twist, degrees	0
Dihedral, degrees	0
Fuselage:	
Fineness ratio, ratio of fuselage length to max. diameter	10.0
Ratio of fuselage length to wing span	1.0
Height of wing root leading edge above center line of fuselage, fraction of maximum fuselage diameter	0.25
Incidence, i_w, angle between root chord line and center line of fuselage, degrees	0 and 4
Length of fuselage, mean aerodynamic chords	7.63
Distance of quarter-chord point of mean aerodynamic chord from nose of fuselage, $i_w = 0^o$, mean aerodynamic chords	4.20
Fuselage nose shape	$\frac{r}{r_o} = \left[1 - \left(1 - \frac{x}{l}\right)^2\right]^{1/2}$
Fuselage afterbody shape	$\frac{r}{r_o} = \left[1 - \left(1 - \frac{x}{l}\right)^2\right]^{3/4}$

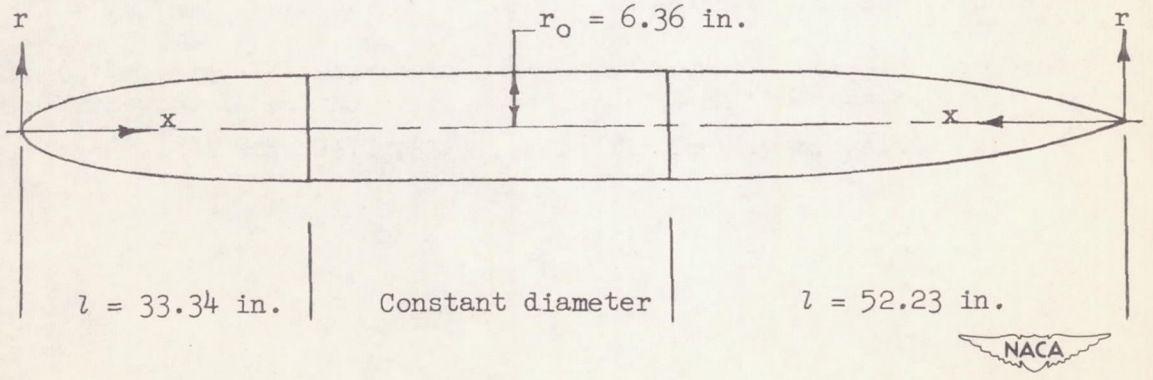
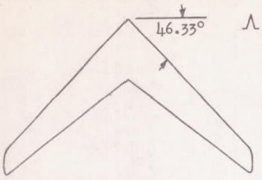


TABLE II.- SUMMARY OF LONGITUDINAL STABILITY CHARACTERISTICS OF A 46.33° SWEPTBACK WING



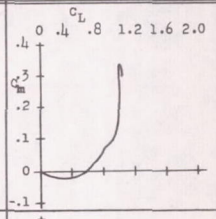
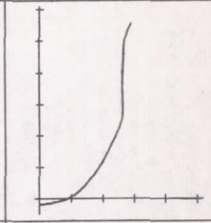
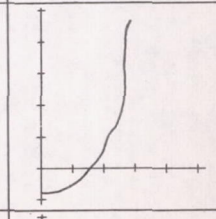
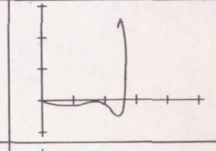
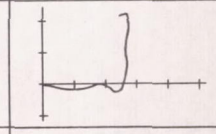
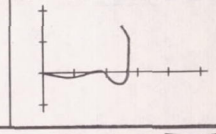
$\Lambda_{c/4} = 45°$ A = 8.02

$\lambda = 0.450$

Airfoil sections (parallel to plane of symmetry)

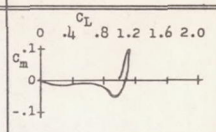
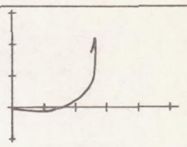
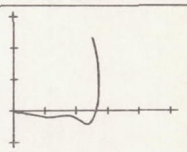
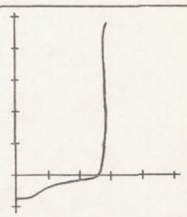
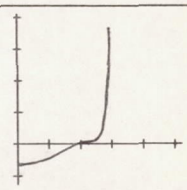
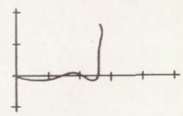
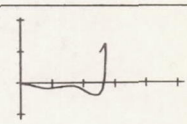
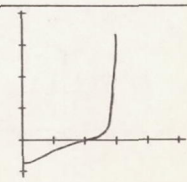
Root: NACA 63_1A012

Tip: NACA 63_1A012

Span of L.E. Device (b/2)	Span of T.E. Device (b/2)	Fence Location (b/2)	Configuration	$C_{L_{max}}$	$\alpha_{C_{L_{max}}}$	L/D at 0.85 $C_{L_{max}}$	C_m Characteristics	Figure
None	None	None		1.01	21.0	8.40		4
			$i_w = 0°$	1.14	31.0	6.05		25
			$i_w = 4°$	1.15	31.0	6.30		25
		.575		1.07	25.0	———		6
		.575		1.10	27.0	———		9
		.575		1.30	27.0	9.60		6, 10

NACA

Table II.- Continued.

Span of L.E. Device (b/2)	Span of T.E. Device (b/2)	Fence Location (b/2)	Configuration	$C_{L_{max}}$	$\alpha_{C_{L_{max}}}$	L/D at 0.85 $C_{L_{max}}$	C_m Characteristics	Figure
None	None	.575		1.13	27.0	———		9
		.80		1.05	27.0	———		6
		.575 .80		1.06	19.0	———		7
		.575 .80	$i_w = 4°$	1.13	22.0	———		28
		.575 .89	$i_w = 4°$	1.19	29.0	———		28
		.575 .80		1.08	27.0	———		8
		.575 .80		1.09	25.0	———		8
		.575 .80	$i_w = 4°$	1.21	31.0	———		28

NACA

Table II.- Continued.

Span of L.E. Device (b/2)	Span of T.E. Device (b/2)	Fence Location (b/2)	Configuration	$C_{L_{max}}$	$\alpha_{C_{L_{max}}}$	L/D at 0.85 $C_{L_{max}}$	C_m Characteristics	Figure
None	None	.575 .80 .89		1.05	19.0	——	C_L 0 .4 .8 1.2 1.6 2.0; C_m .3 .2 .1 0 -.1	7
		.575 .80 .89		1.09	27.0	8.95		8,10
		.575 .80 .89	$i_w = 4^\circ$	1.19	31.0	——		28
	.350 Split Flap	None		1.22	16.6	10.58		12a, 18a
	.500 Split Flap	None		1.29	15.6	10.25		12a, 18a
	.600 Split Flap	None		1.34	15.6	10.25		12a, 18a
	.350 Ext. Split Flap	None		1.30	15.6	11.05		12b, 18b
	.500 Ext. Split Flap	None		1.40	15.6	10.72		12b, 18b
		.575 .80		1.37	14.7	——		12b

NACA

Table II.- Continued.

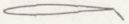
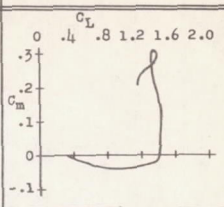
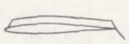
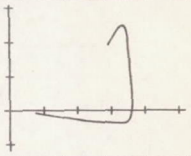
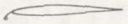
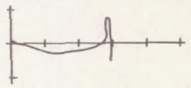
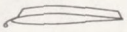
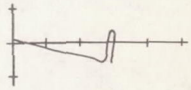
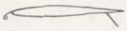
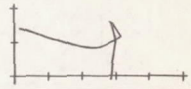
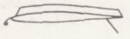
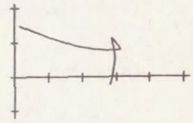
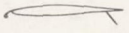
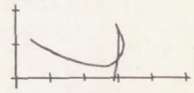
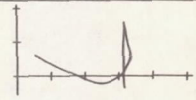
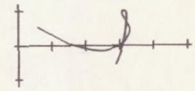
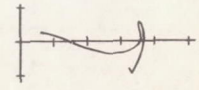
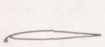
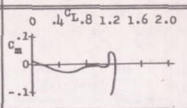
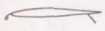
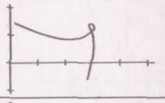
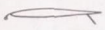
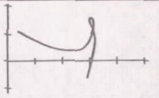
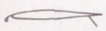
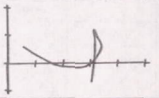
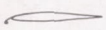
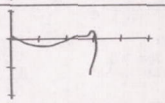
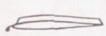
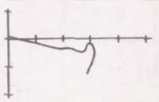
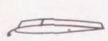
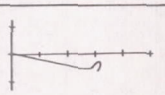
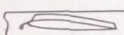
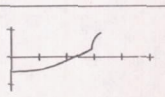
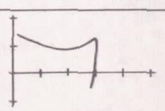
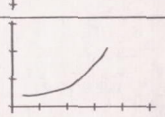
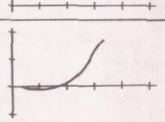
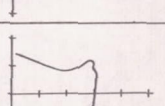
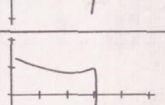
Span of L.E. Device (b/2)	Span of T.E. Device (b/2)	Fence Location (b/2)	Configuration	$C_{L_{max}}$	$\alpha_{C_{L_{max}}}$	L/D at 0.85 $C_{L_{max}}$	C_m Characteristics	Figure
None	.600 Ext. Split Flap	None		1.46	15.7	11.08		12b, 18b
		.575 .80		1.44	14.8	10.46		12b, 18b
.350 L.E. Flap	None	None		1.18	28.6	9.52		13, 19
		.575 .80		1.19	26.6	——		13
	.350 Split Flap	None		1.26	15.6	——		14a
		.575 .80		1.26	15.6	——		14a
	.500 Split Flap	None		1.29	14.6	——		14b
	.600 Split Flap	None		1.34	14.6	——		14c
		.575 .80		1.30	15.0	——		14c
	.600 Ext. Split Flap	.575 .80		1.45	27.7	——		15b

Table II.- Continued.

Span of L.E. Device (b/2)	Span of T.E. Device (b/2)	Fence Location (b/2)	Configuration	$C_{l_{max}}$	$\alpha_{C_{l_{max}}}$	L/D at 0.85 $C_{l_{max}}$	C_m Characteristics	Figure
.400 L.E. Flap	None	None		1.21	28.6	———		13
	.350 Split Flap	None		1.23	15.6	———		14a
	.500 Split Flap	None		1.26	15.0	———		14b
	.600 Split Flap	None		1.34	15.4	———		14c
.450 L.E. Flap	None	None		1.22	27.0	8.95		13, 19
		.575 .80		1.25	27.0	9.00		13, 19
		.575 .80 .89		1.28	27.0	———		22
		.475 .80	 $i_w = 4°$	1.31	31.0	———		29
	.350 Split Flap	None		1.22	16.6	11.58		14a, 20a
			$i_w = 0°$	1.39	30.7	———		31
			$i_w = 4°$	1.34	30.7	———		30a
		.575		1.23	24.6	———		23
		.80		1.24	24.0	———		23

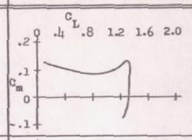
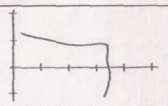
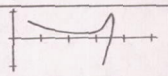
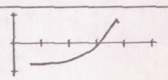
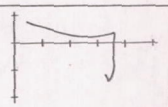
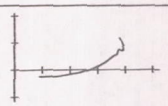
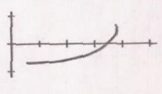
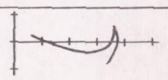
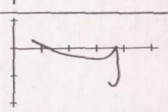
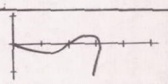
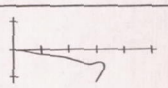
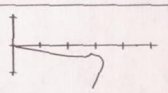
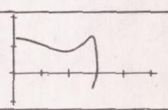
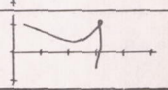
NACA

Table II.- Continued.

Span of L.E. Device (b/2)	Span of T.E. Device (b/2)	Fence Location (b/2)	Configuration	$C_{L_{max}}$	$\alpha_{C_{L_{max}}}$	L/D at 0.85 $C_{L_{max}}$	C_m Characteristics	Figure
.450 L.E. Flap	.350 Split Flap	.575 .80		1.27	24.6	10.87		14a, 20a
		.575 .80	$i_w = 0°$	1.40	28.7	——		31
		.575 .80	$i_w = 4°$	1.35	30.7	——		30a
		.575 .89	$i_w = 4°$	1.36	30.7	——		30a
	.500 Split Flap	None		1.26	15.6	10.40		14b, 20a
		None	$i_w = 4°$	1.35	30.7	——		30b
		.575 .80		1.28	16.0	10.52		14b, 20a
		.575 .80	$i_w = 4°$	1.38	28.7	——		30b
		.575 .89	$i_w = 4°$	1.38	28.7	——		30b
	.600 Split Flap	None		1.33	15.5	10.27		14c, 20a
		.575 .80		1.33	15.5	9.92		14c, 20a

NACA

Table II.- Continued.

Span of L.E. Device (b/2)	Span of T.E. Device (b/2)	Fence Location (b/2)	Configuration	$C_{L_{max}}$	$^{a}C_{L_{max}}$	L/D at 0.85 $C_{L_{max}}$	C_m Characteristics	Figure
.450 L.E. Flap	.350 Ext. Split Flap	None		1.37	17.6	11.64		15a, 20b
		.575 .80		1.36	16.6	———		15a
	.500 Ext. Split Flap	None		1.42	15.6	11.39		15a, 20b
			$i_w = 4°$	1.52	28.8	———		30c
		.575 .80		1.43	16.6	———		15a
		.575 .80	$i_w = 0°$	1.58	27.0	———		31
		.575 .80	$i_w = 4°$	1.53	26.8	———		30c
	.600 Ext. Split Flap	None		1.49	22.7	11.08		15b, 20b
		.575 .80		1.54	24.7	———		15b
.500 L.E. Flap	None	None		1.24	26.8	———		13
		.575 .80		1.30	26.8	———		13
		.575 .80 .89		1.29	26.8	———		22
	.350 Split Flap	None		1.21	16.6	———		14a
	.500 Split Flap	None		1.29	16.0	———		14b

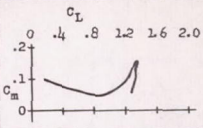
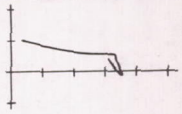
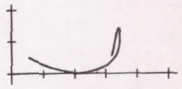
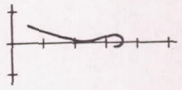
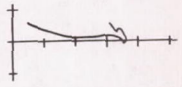
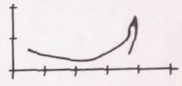
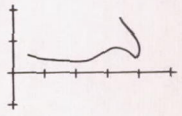
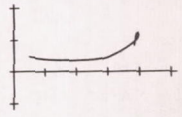
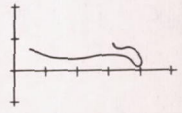
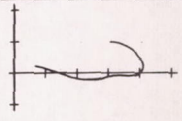
NACA

Table II.- Continued

Span of L.E. Device (b/2)	Span of T.E. Device (b/2)	Fence Location (b/2)	Configuration	$C_{L_{max}}$	$\alpha_{C_{L_{max}}}$	L/D at 0.85 $C_{L_{max}}$	C_m Characteristics	Figure
.500 L.E. Flap	.500 Split Flap	.80		1.27	20.7	———		16
		.575 .80		1.32	16.6	———		14b
		.575 .80 .89		1.32	15.8	———		22
	.600 Split Flap	None		1.32	15.0	———		14c
		.575 .80		1.38	16.2	———		14c
	.500 Ext. Split Flap	None		1.45	24.0	———		15a
		.575 .80		1.50	24.7	———		15a
	.600 Ext. Split Flap	None		1.52	24.7	———		15b
		.575 .80		1.55	24.0	———		15b
.575 L.E. Flap	None	None		1.24	27.0	7.32		13, 19
		.575 .80		1.29	26.2	———		13
	.350 Split Flap	None		1.25	24.0	———		14a
		.575 .80		1.31	24.6	———		14a

NACA

Table II.- Concluded.

Span of L.E. Device (b/2)	Span of T.E. Device (b/2)	Fence Location (b/2)	Configuration	$C_{L_{max}}$	$\alpha_{C_{L_{max}}}$	L/D at 0.85 $C_{L_{max}}$	C_m Characteristics	Figure
.575 L.E. Flap	.500 Split Flap	None		1.34	24.6	——		14b
		.575 .80		1.40	24.6	——		14b
	.600 Split Flap	None		1.37	23.6	——		14c
		.475 .80		1.42	24.7	——		16
		.575 .80		1.43	24.7	——		14c
	.500 Ext. Split Flap	None		1.56	24.0	——		15a
		.575		1.59	22.8	——		16
		.80		1.57	25.0	——		16
		.575 .80		1.62	22.7	——		15a
	.600 Ext. Split Flap	.575 .80		1.66	22.7	——		15b

NACA

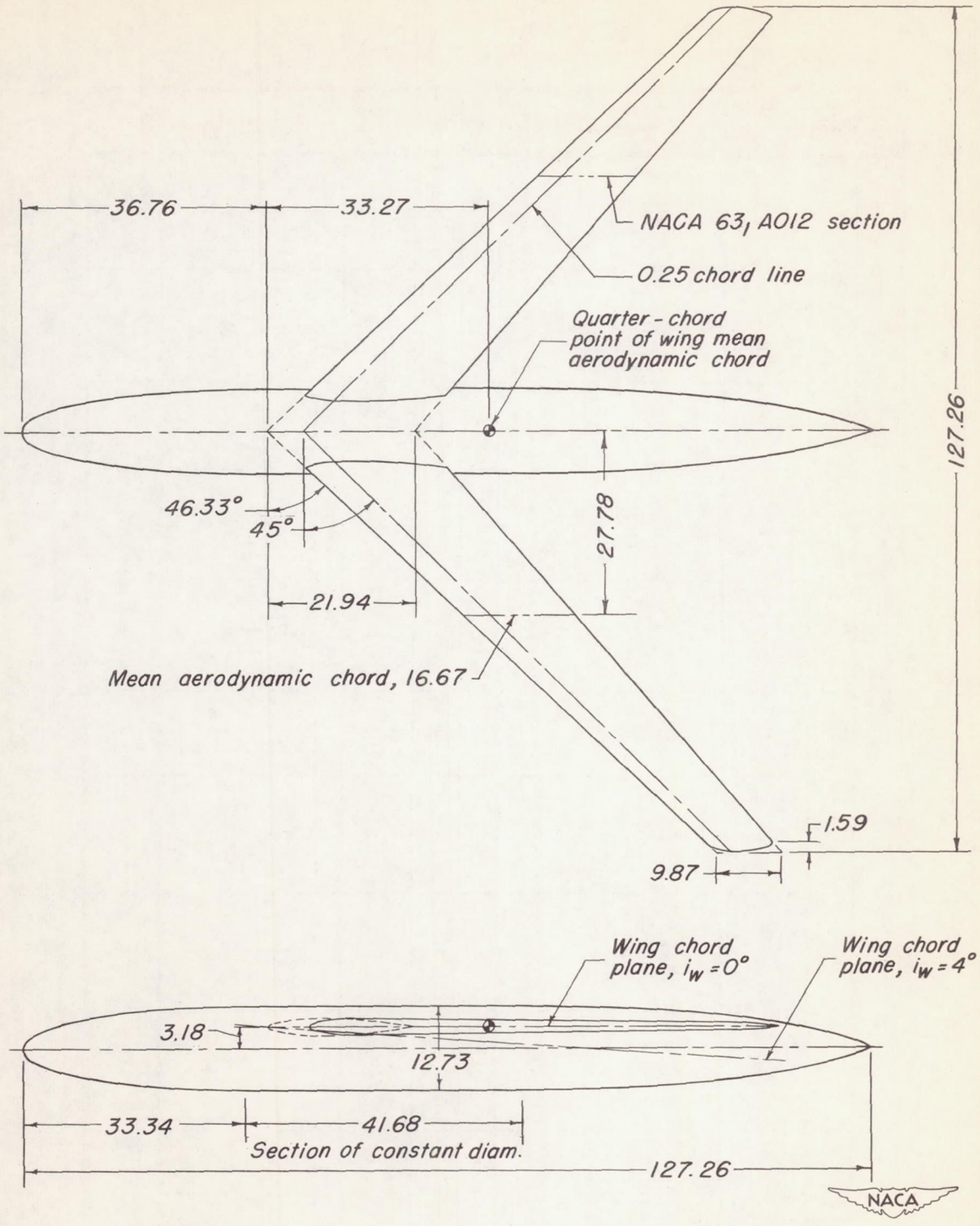
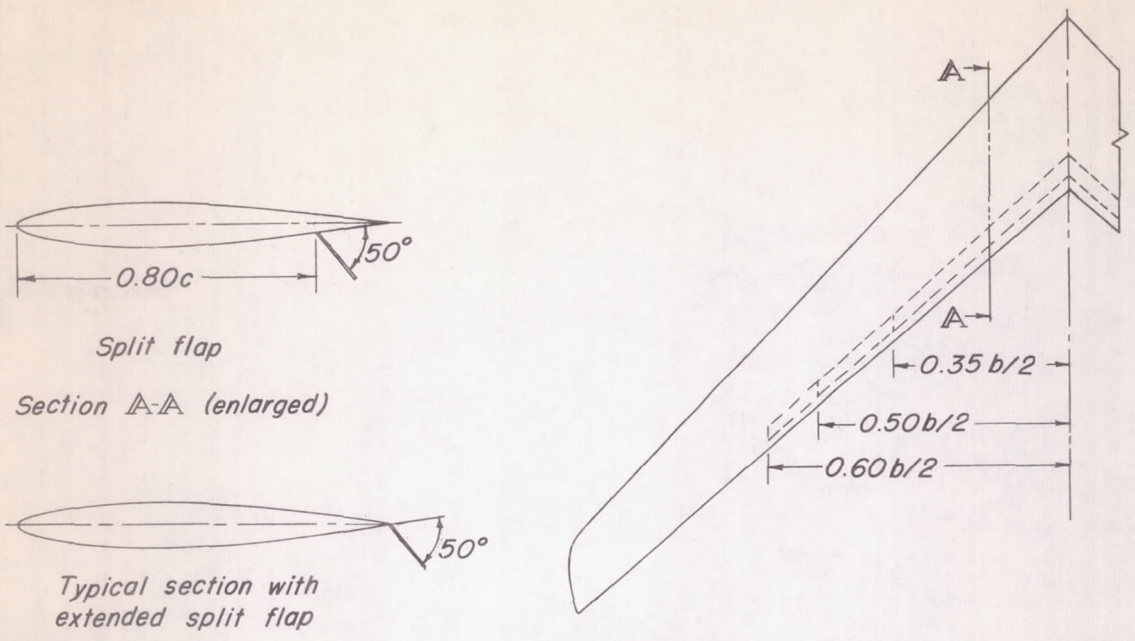
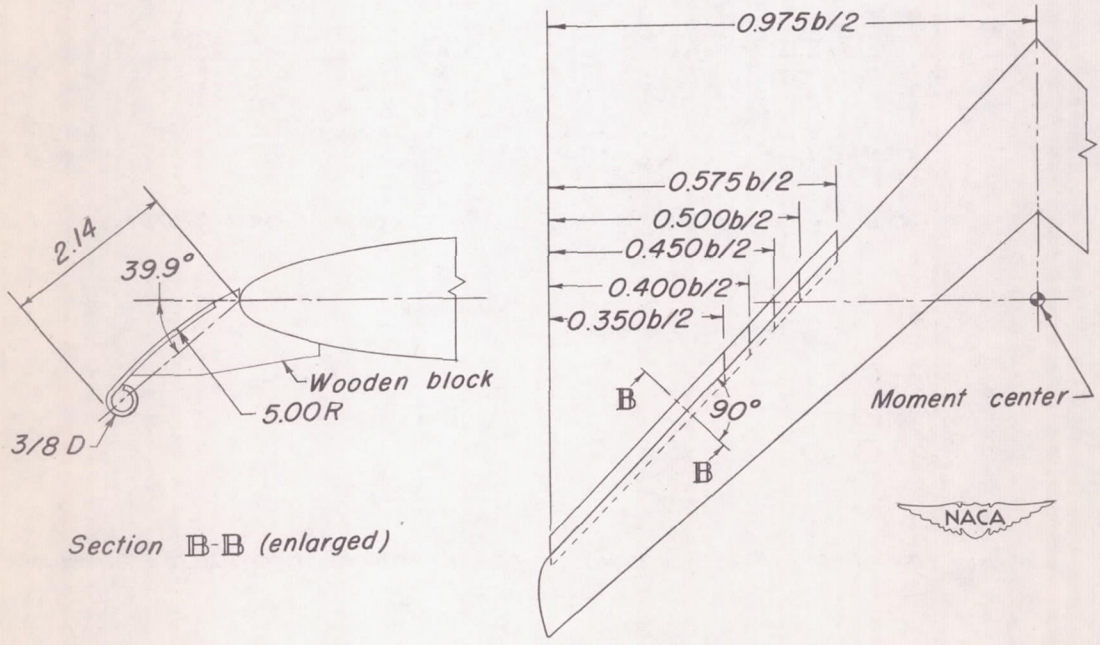


Figure 1.- Principal dimensions of wing with fuselage. (Dimensions are in inches.)

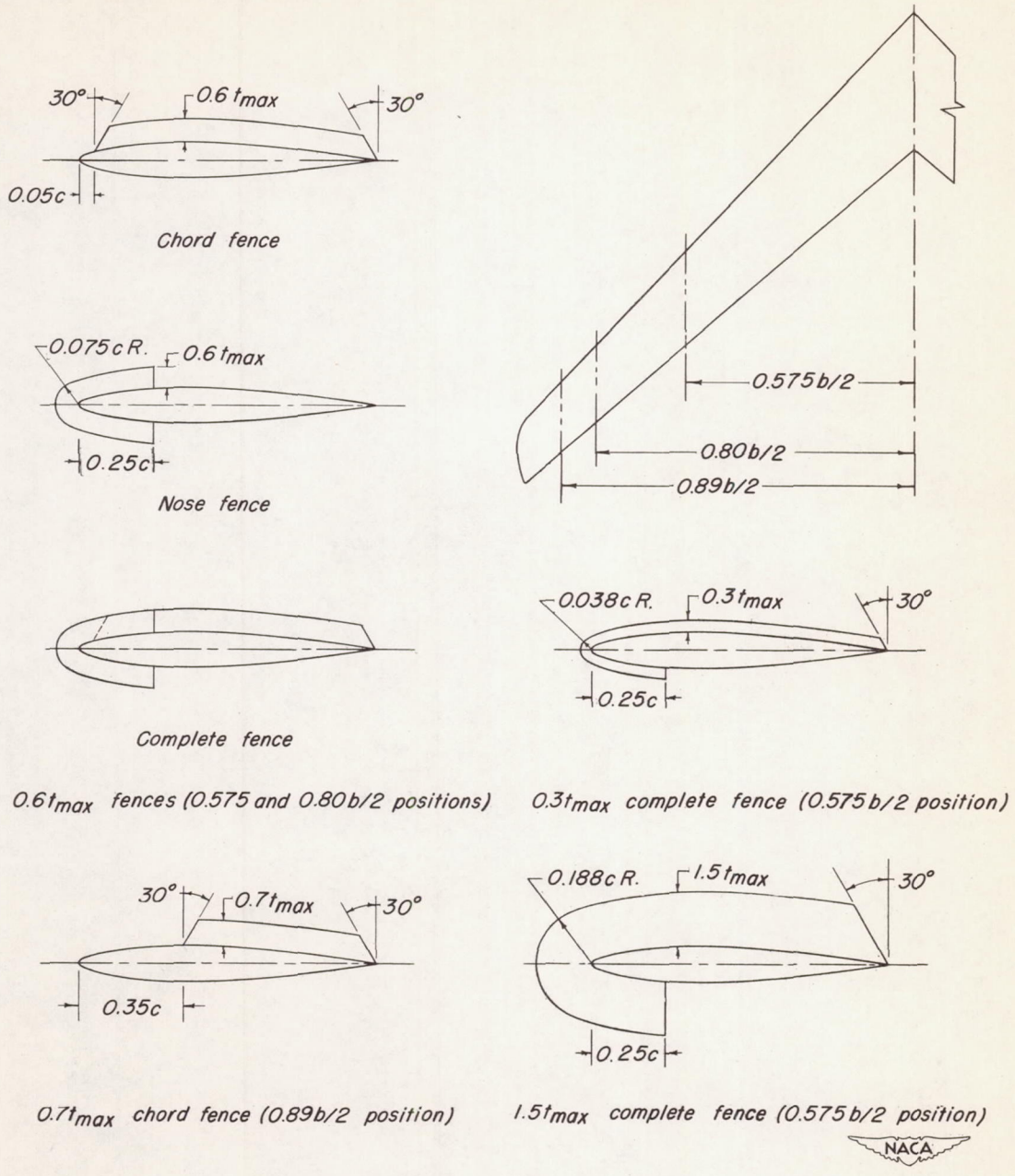


(a) Trailing-edge flaps.



(b) Leading-edge flaps.

Figure 2.- Details of high-lift and stall-control devices. (Dimensions are in inches.)



(c) Upper-surface fences.

Figure 2.- Concluded.

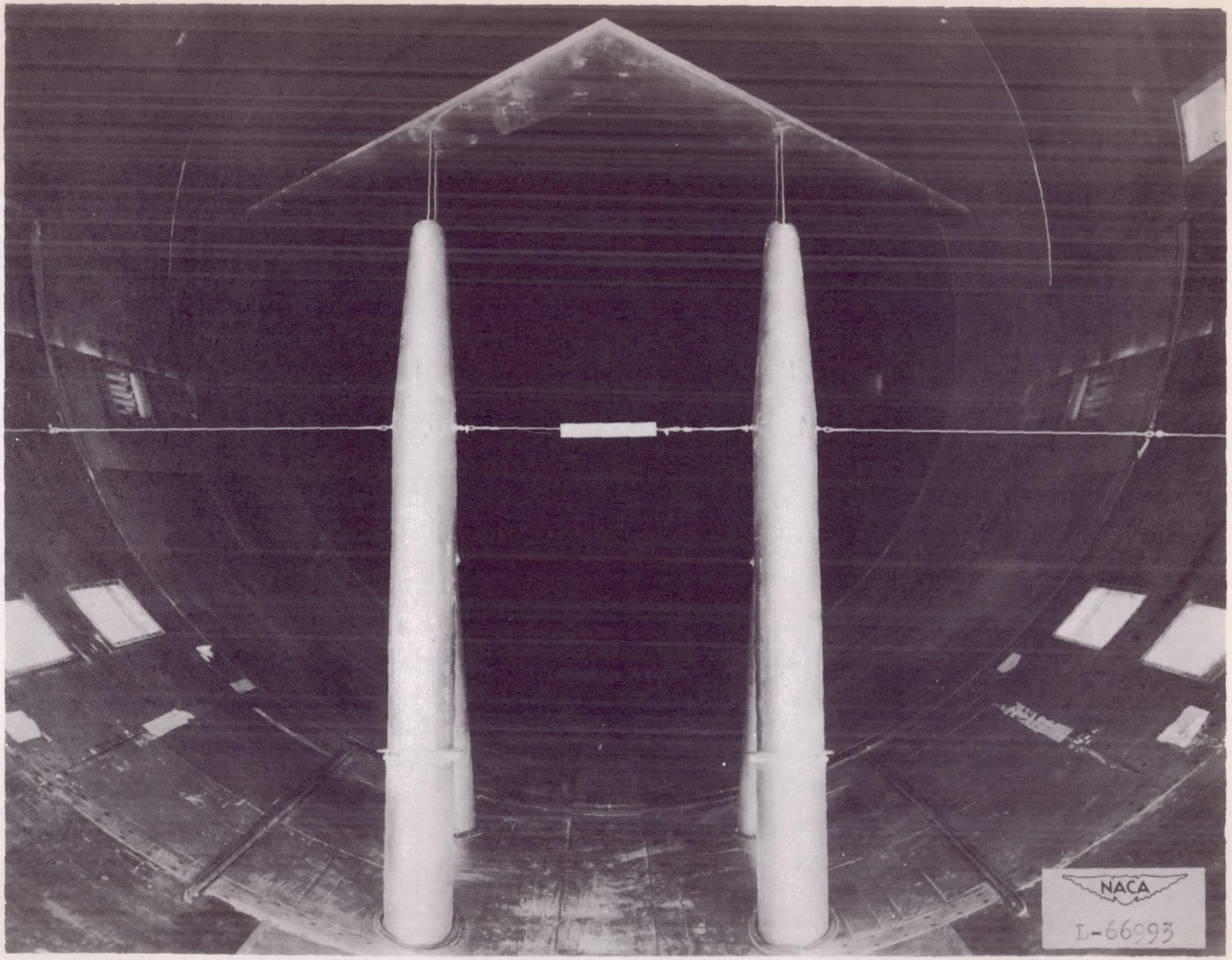
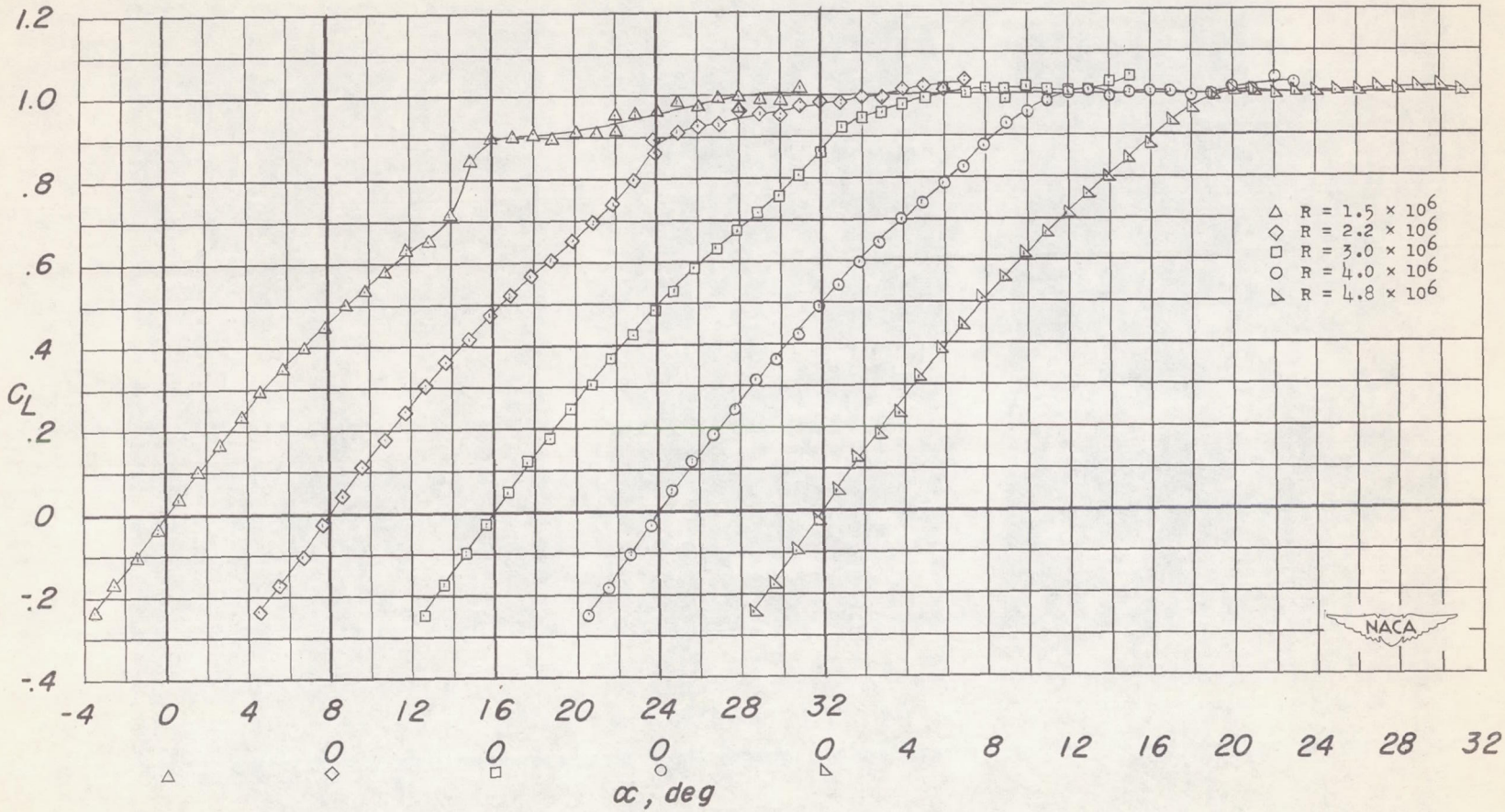
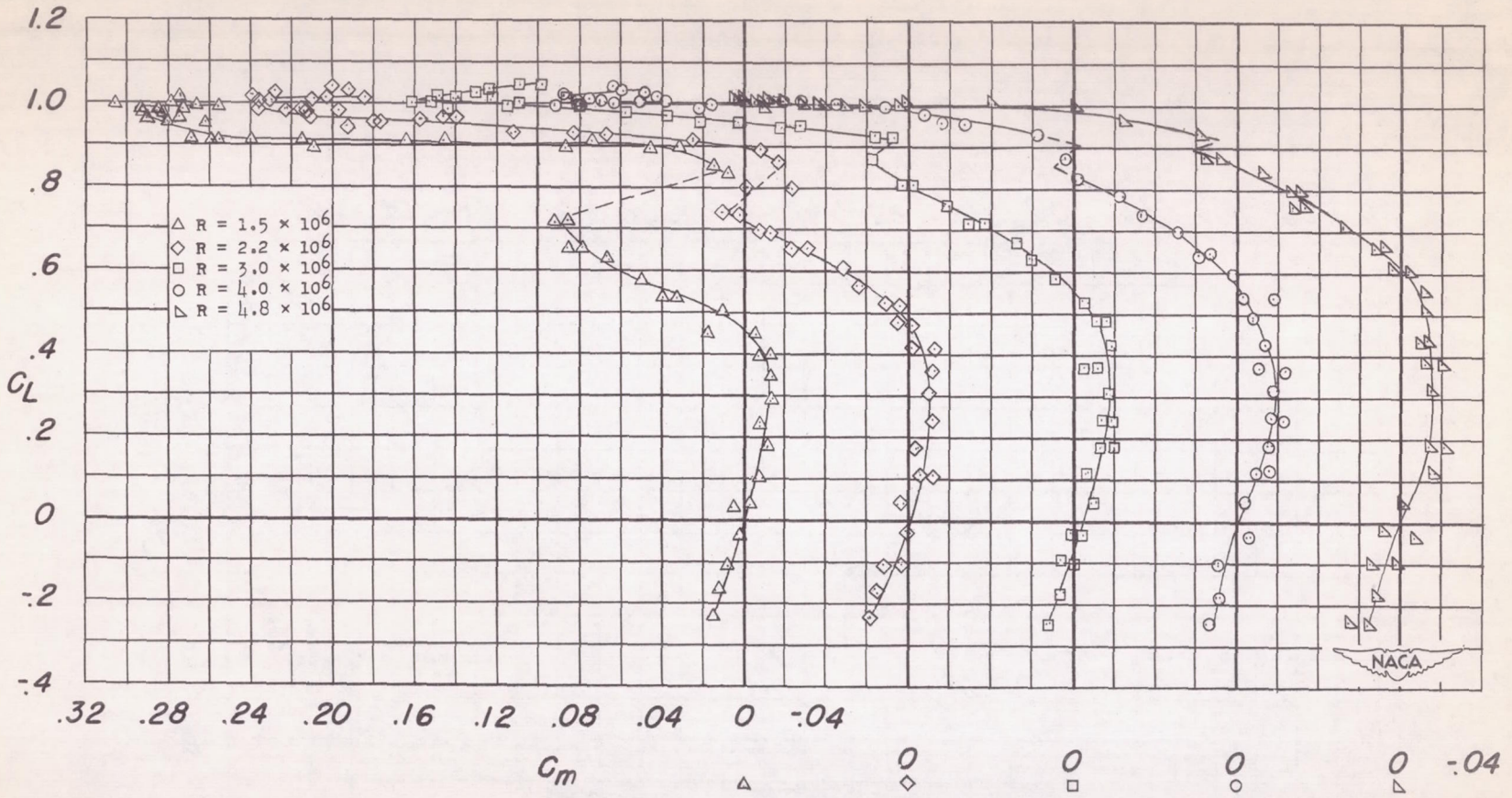


Figure 3.- The wing mounted for testing in the Langley 19-foot pressure tunnel.



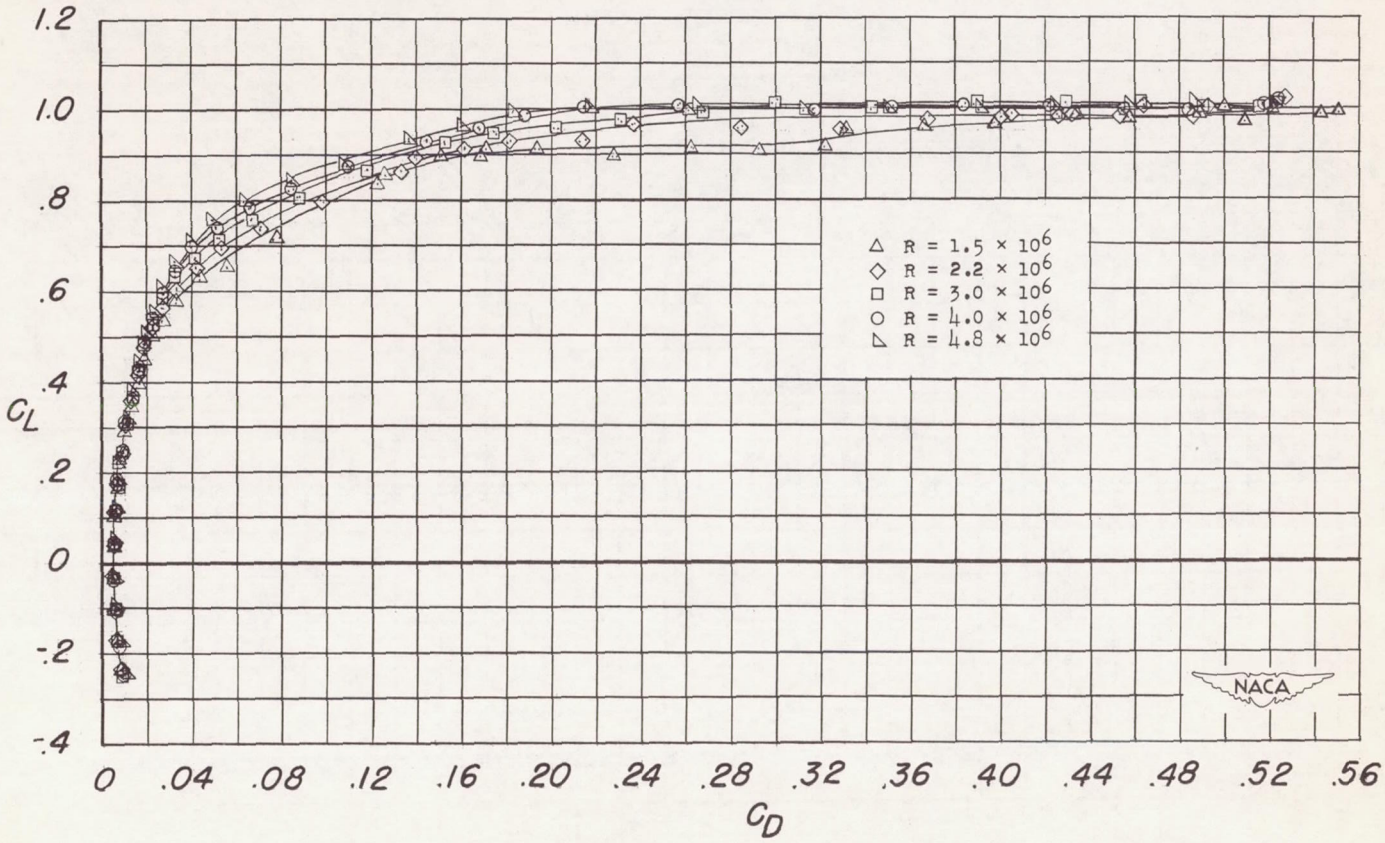
(a) C_L against α.

Figure 4.- Effect of Reynolds number on lift, drag, and pitching-moment characteristics on the plain wing.



(b) C_L against C_m.

Figure 4.- Continued.



(c) C_L against C_D.

Figure 4.- Concluded.

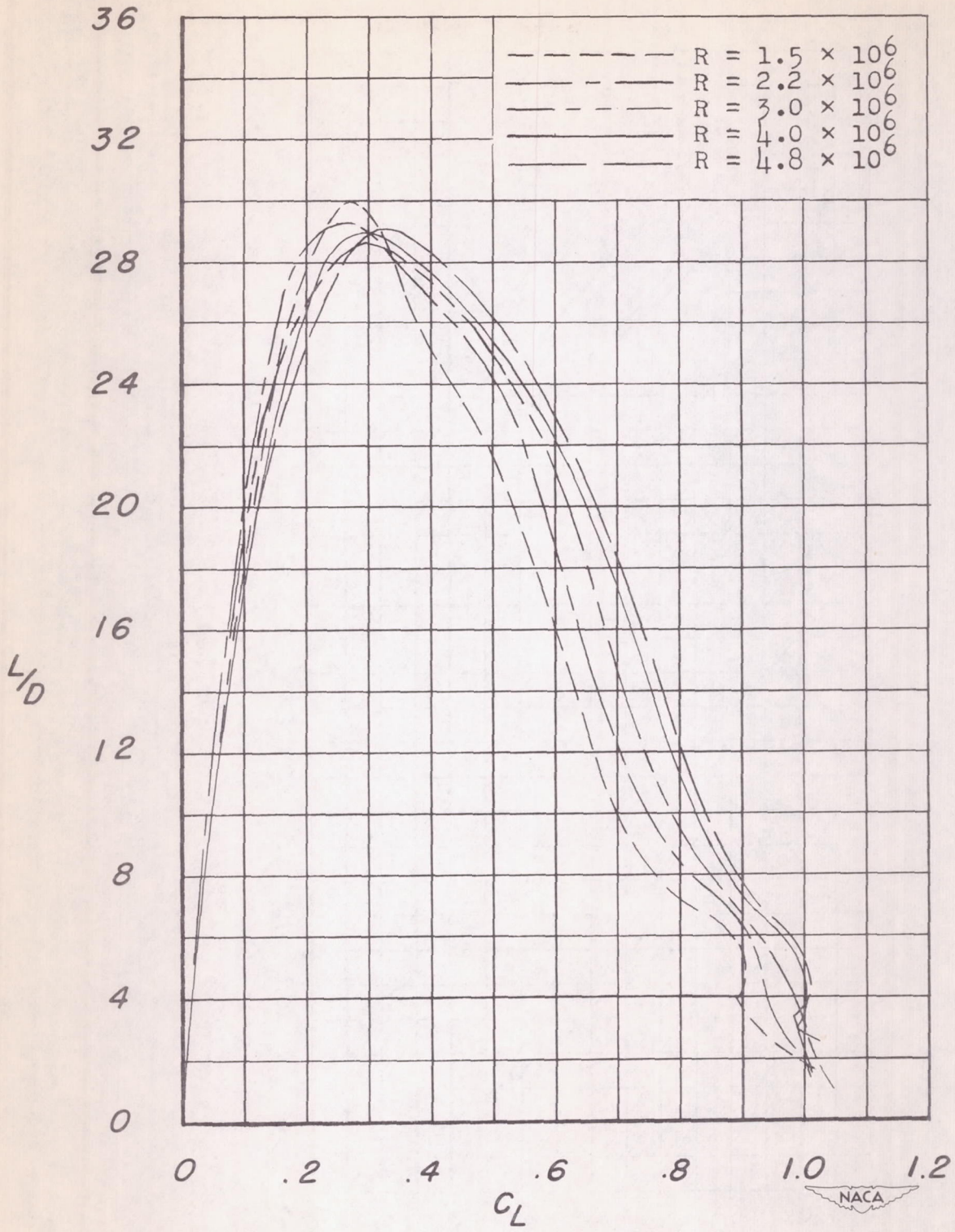
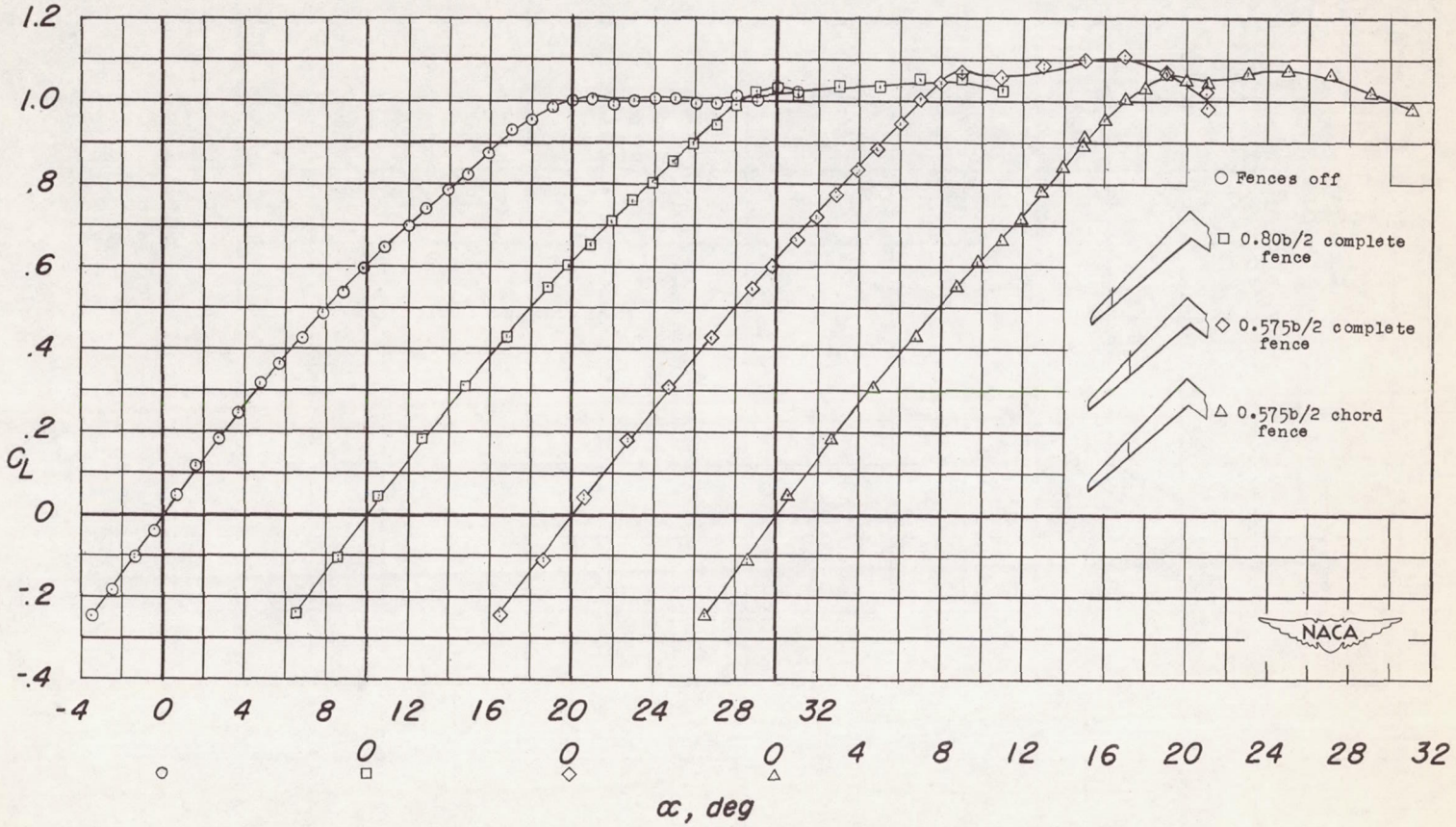
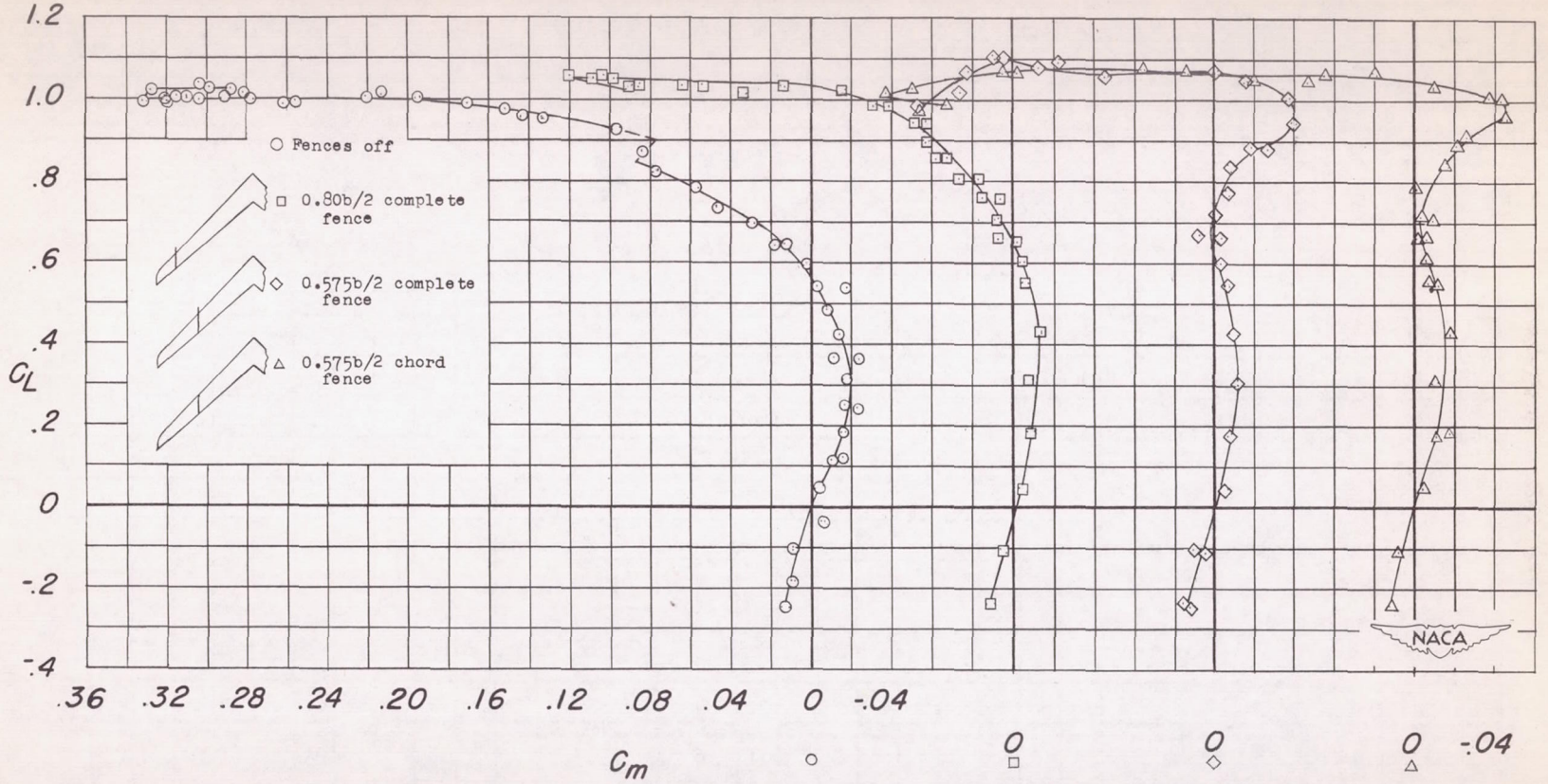


Figure 5.- Effect of Reynolds number on lift-drag ratios of basic wing.



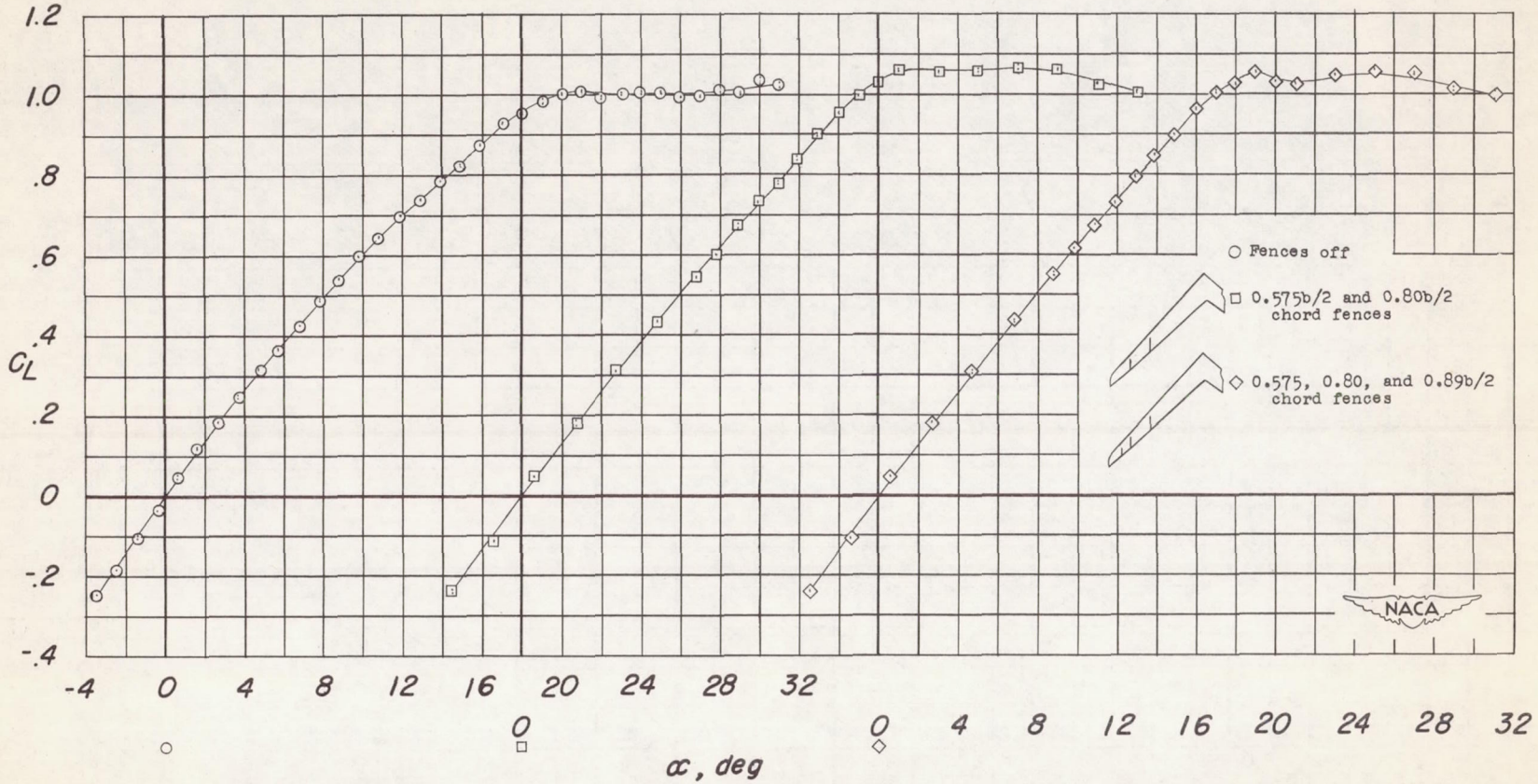
(a) C_L against α.

Figure 6.- Effect of single fences on lift and pitching-moment characteristics.



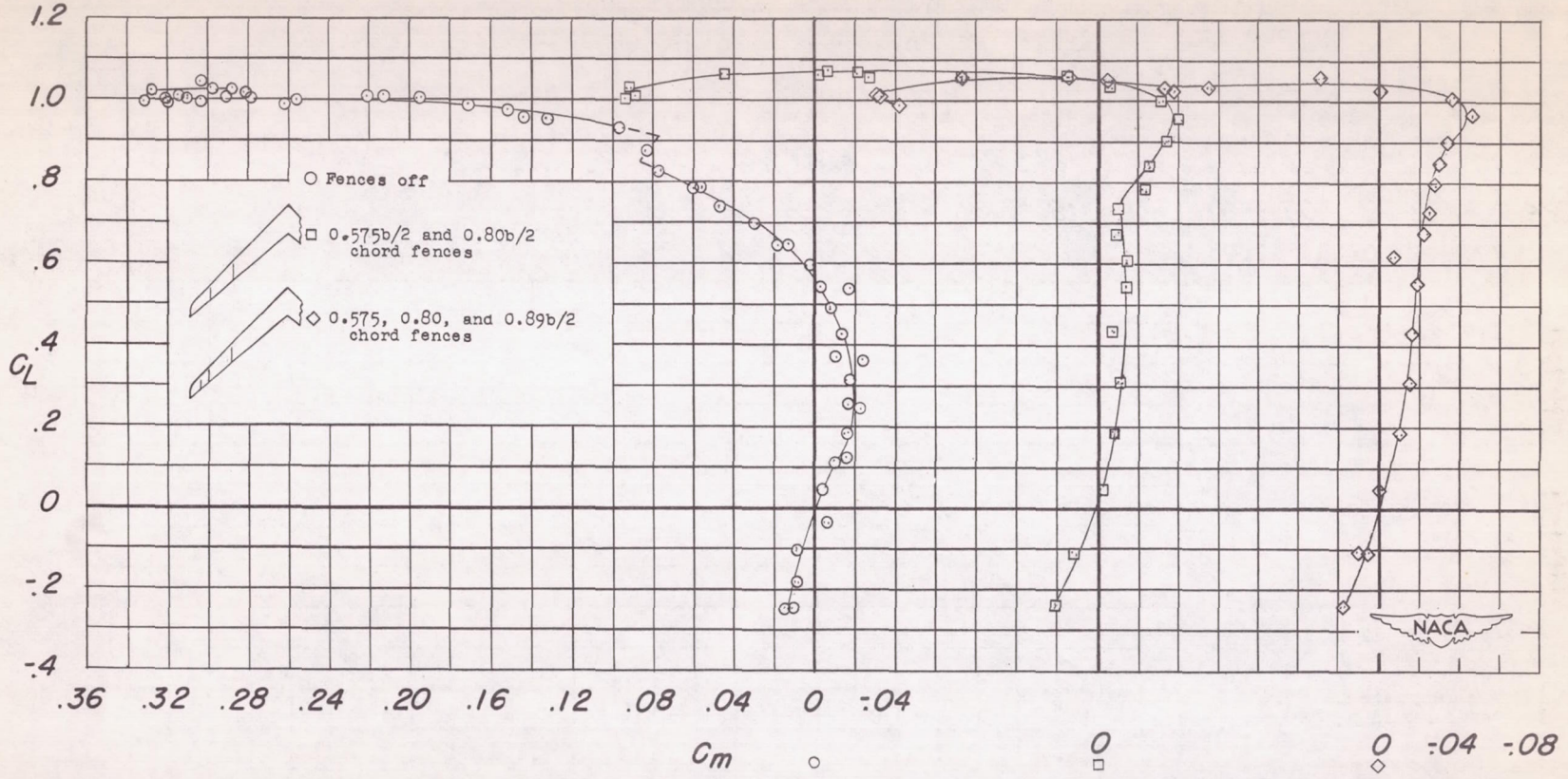
(b) C_L against C_m.

Figure 6.- Concluded.



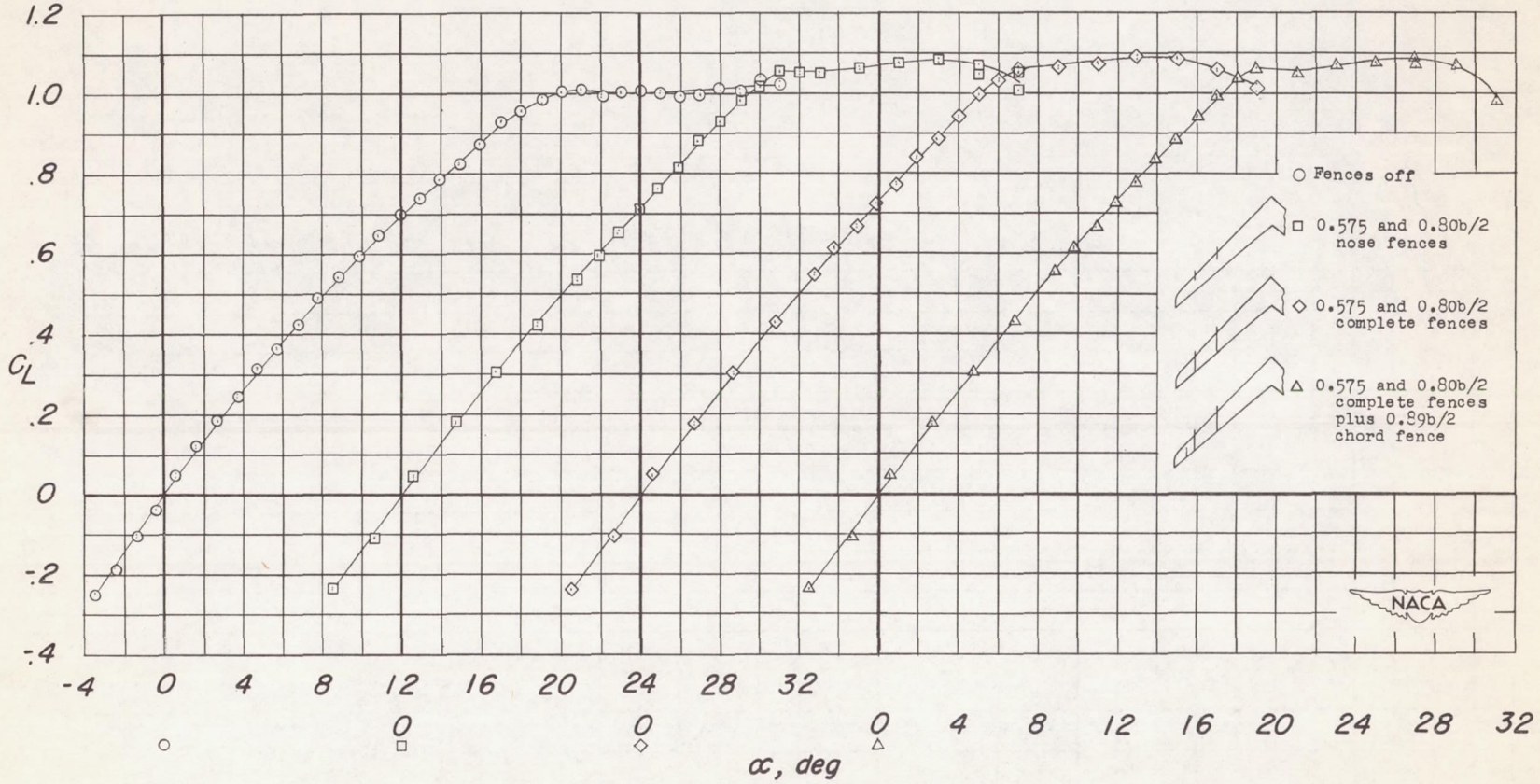
(a) C_L against α.

Figure 7.- Effect of multiple chord fences on lift and pitching-moment characteristics.



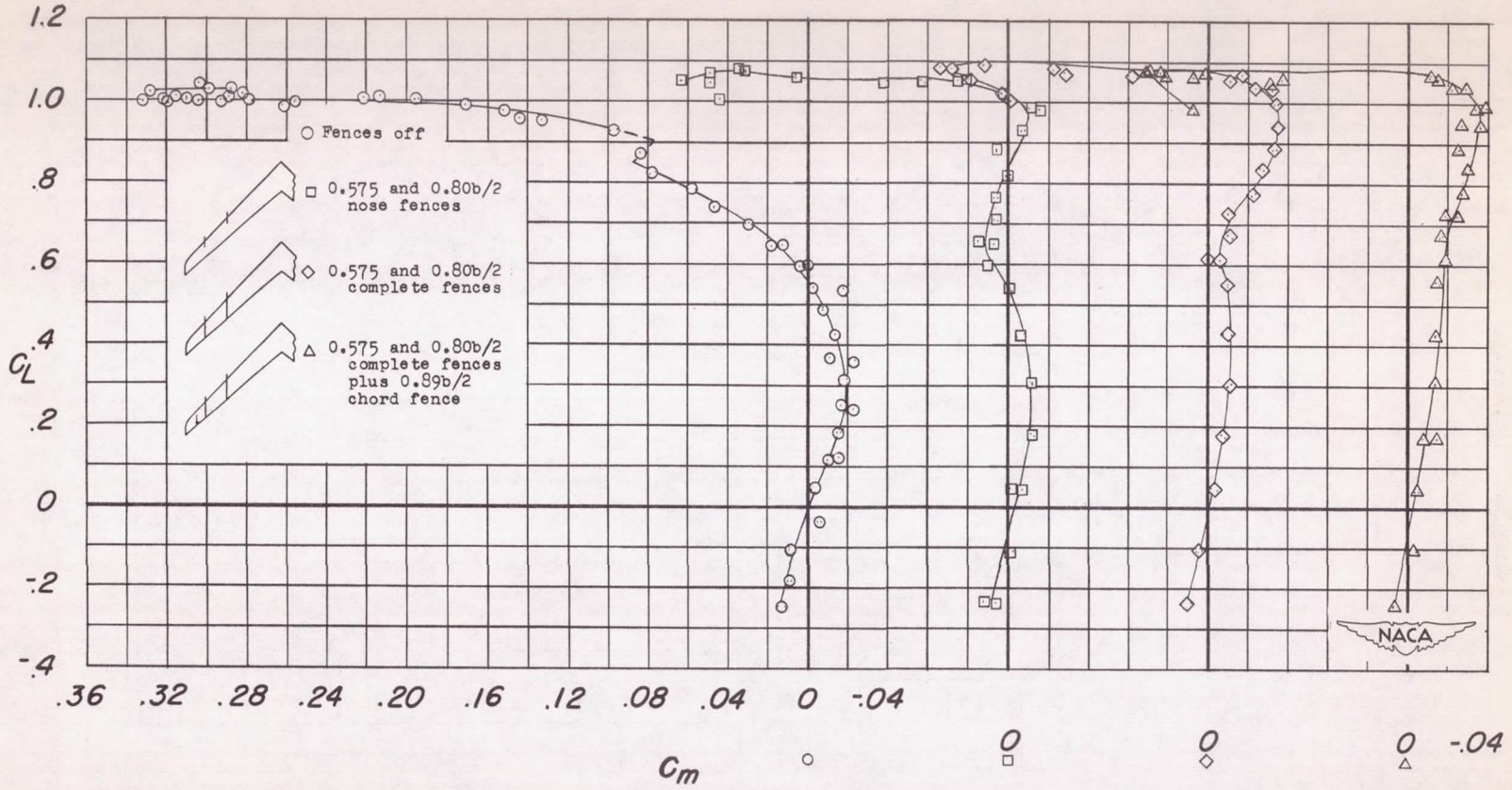
(b) C_L against C_m.

Figure 7.- Concluded.



(a) C_L against α.

Figure 8.- Effect of multiple nose and complete fences on lift and pitching-moment characteristics.



(b) C_L against C_m.

Figure 8.- Concluded.

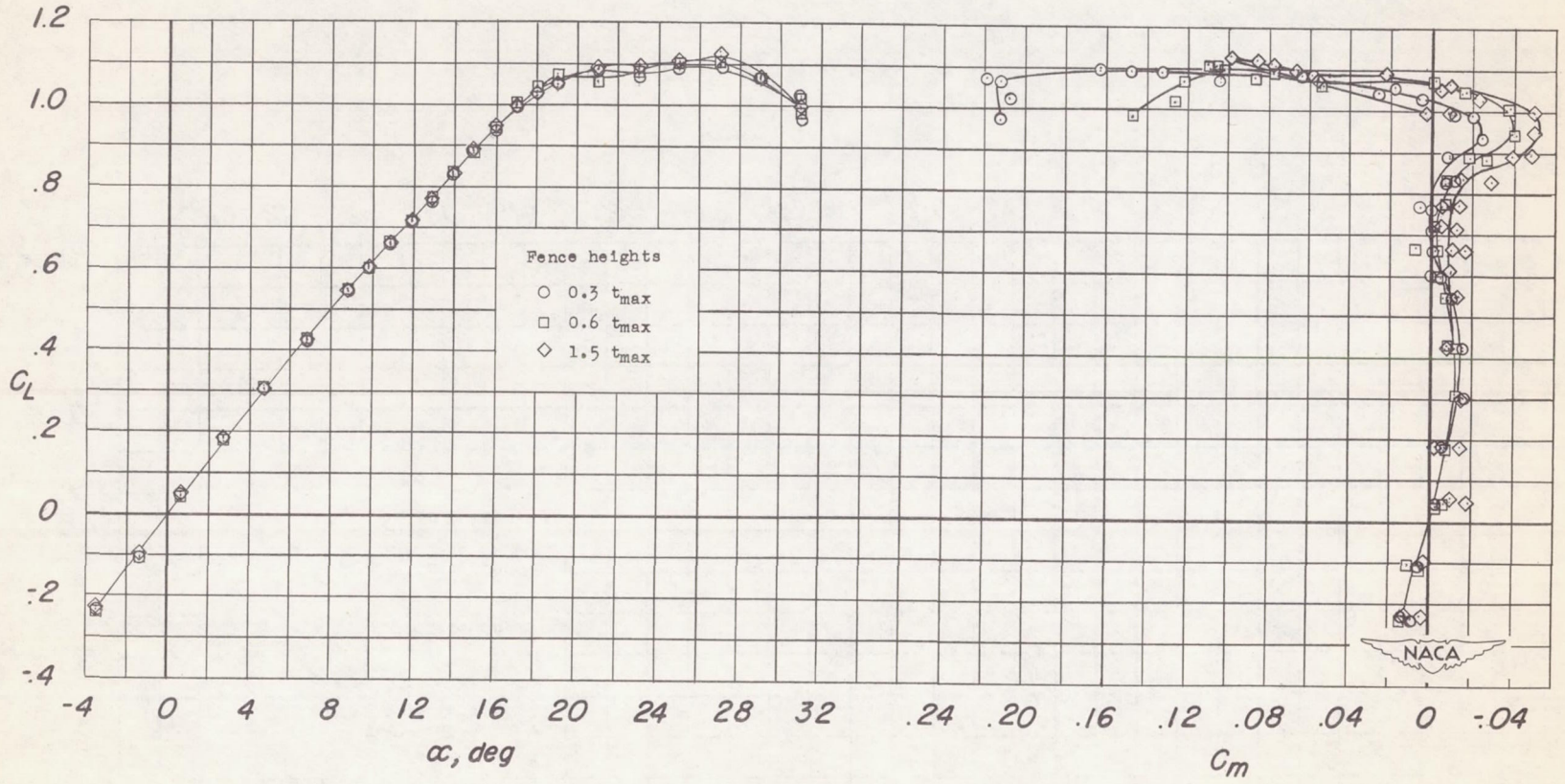


Figure 9.- Effect of varying height of 0.575b/2 complete fence on lift and pitching-moment characteristics.

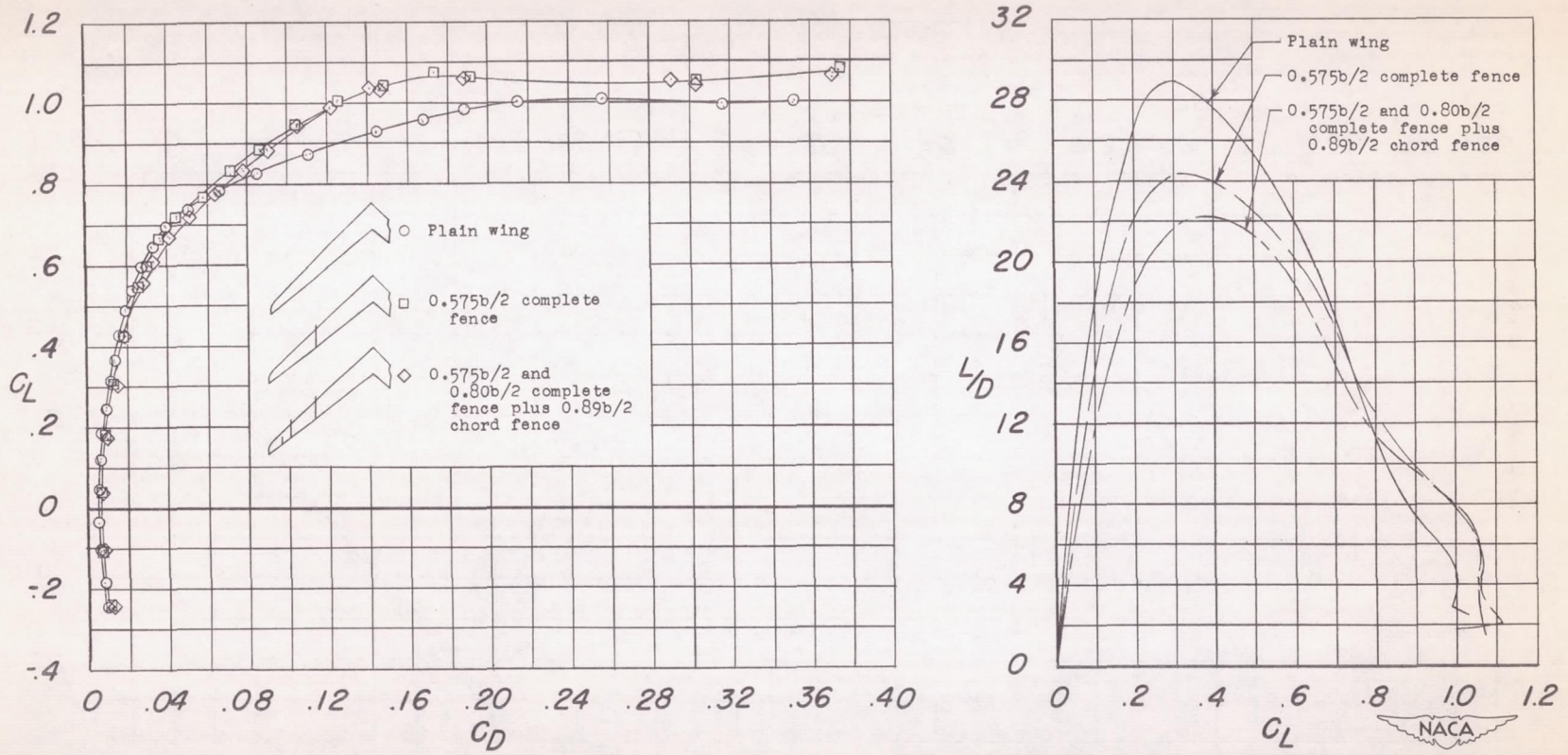
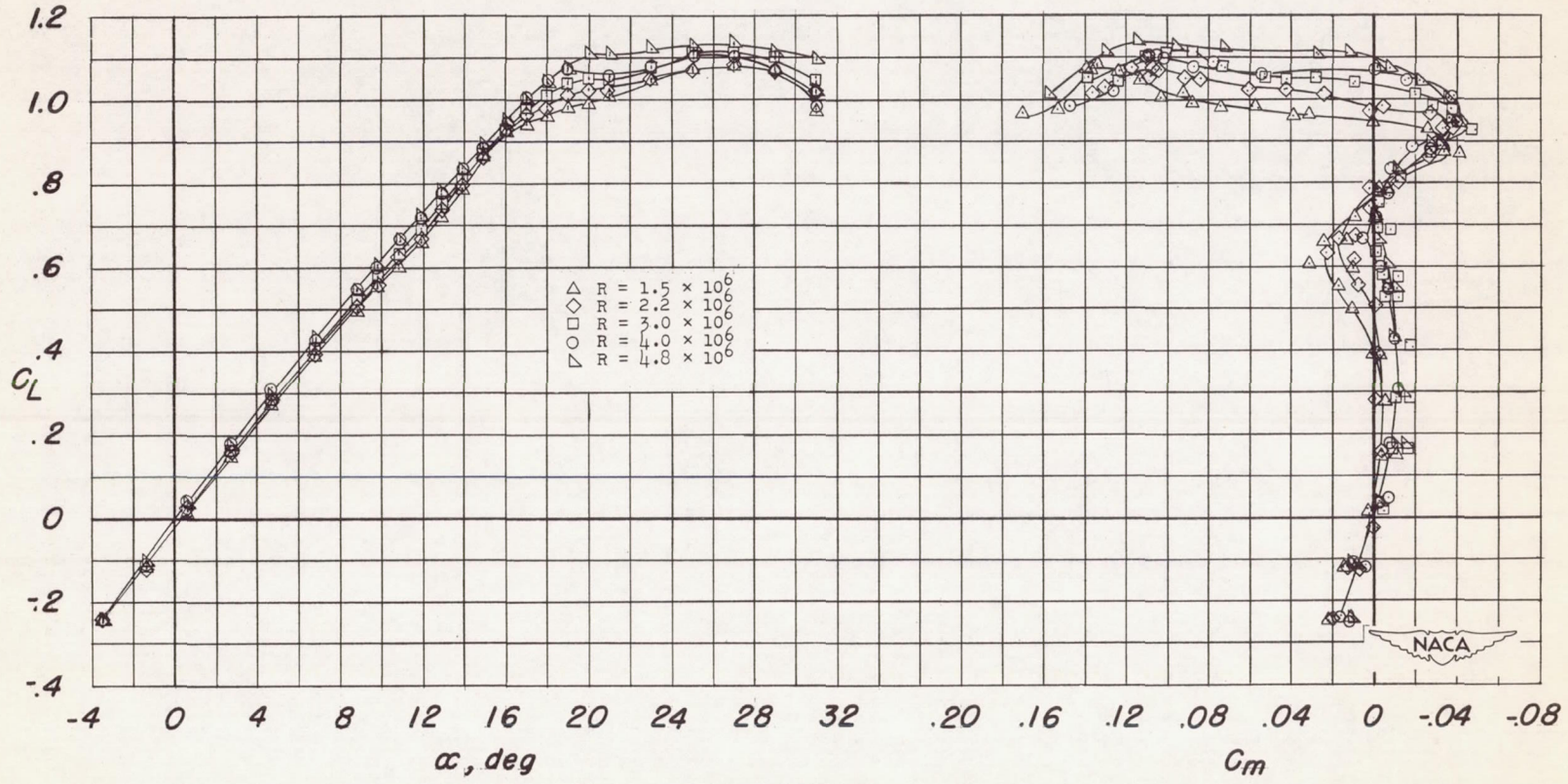
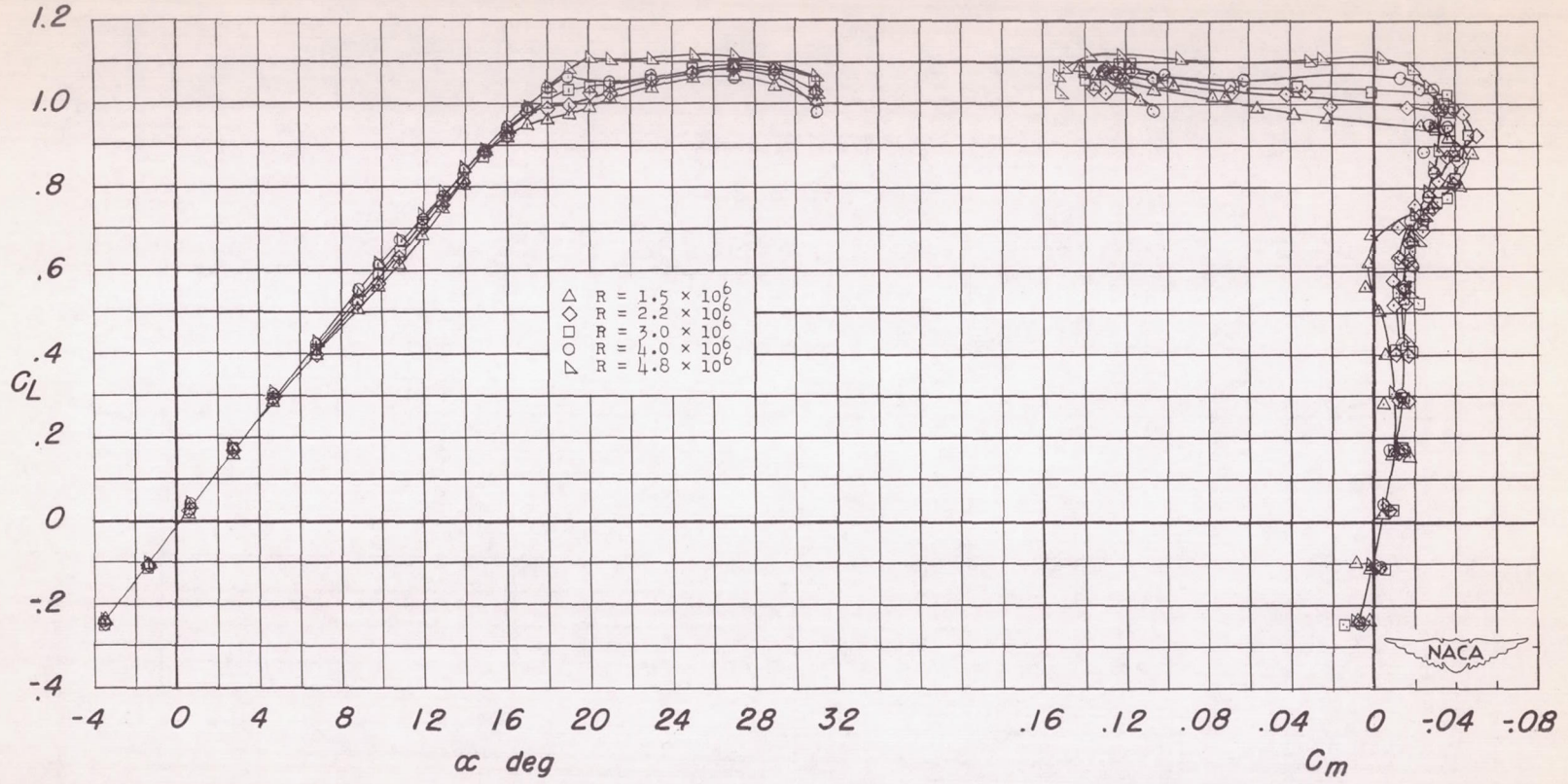


Figure 10.- Effect of fences on drag characteristics of basic wing.



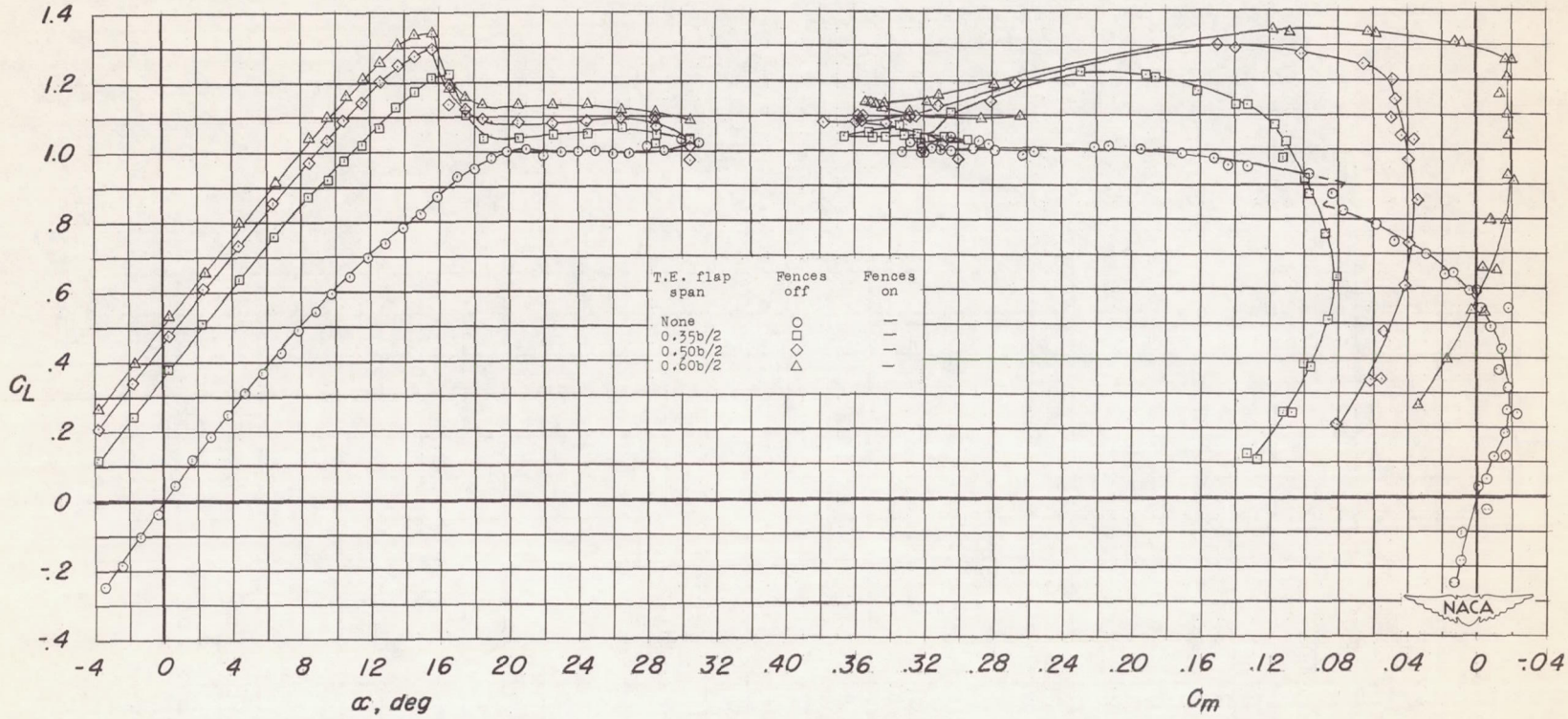
(a) 0.575b/2 complete fence.

Figure 11.- Effect of Reynolds number on lift and pitching-moment characteristics of wing with fences.



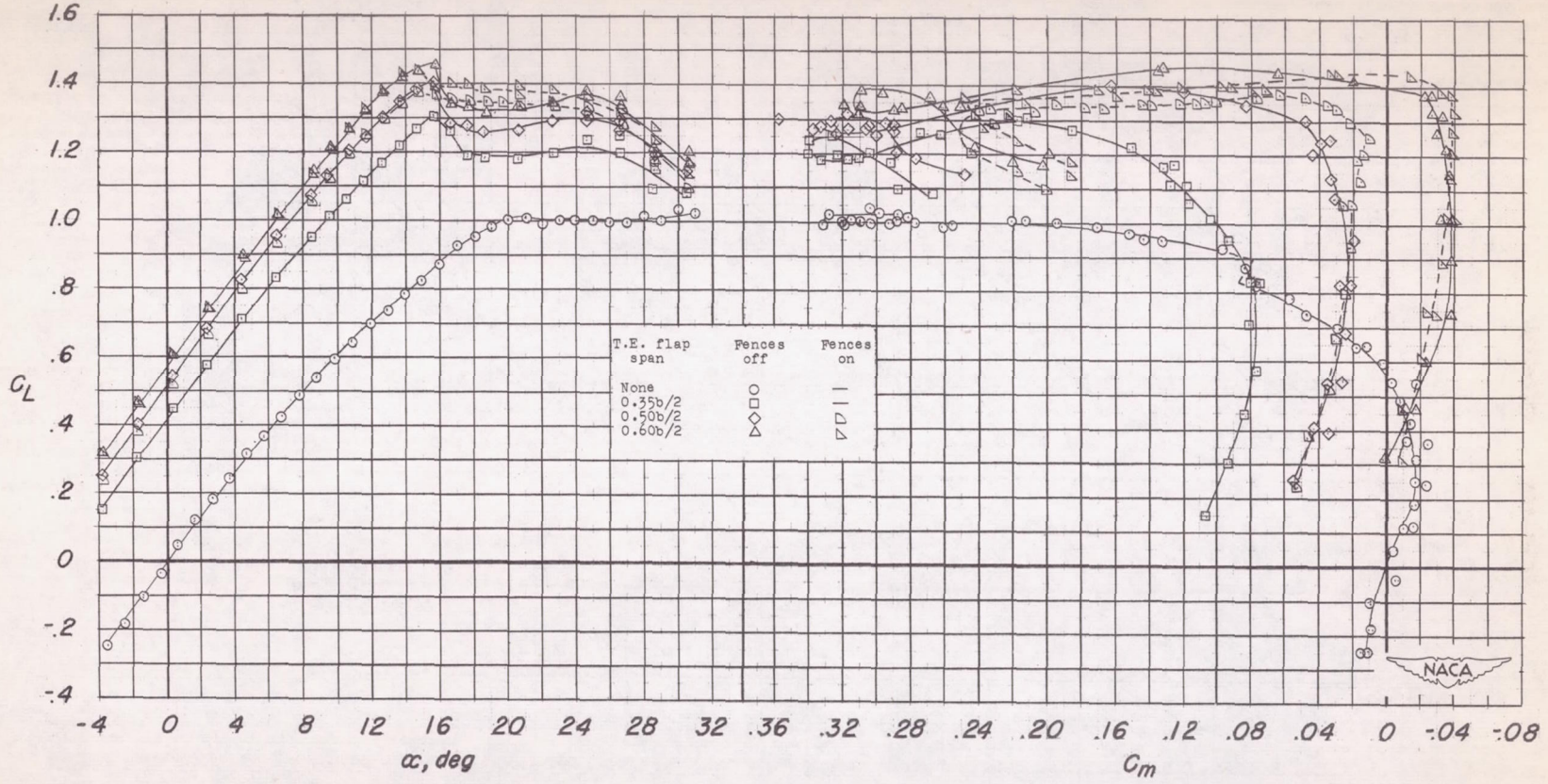
(b) 0.575b/2 and 0.80b/2 complete fences plus 0.89b/2 chord fence.

Figure 11.- Concluded.



(a) Split flaps.

Figure 12.- Effect of trailing-edge flap span on lift and pitching-moment characteristics with and without 0.575b/2 and 0.80b/2 chord fences.



(b) Extended split flaps.

Figure 12.- Concluded.

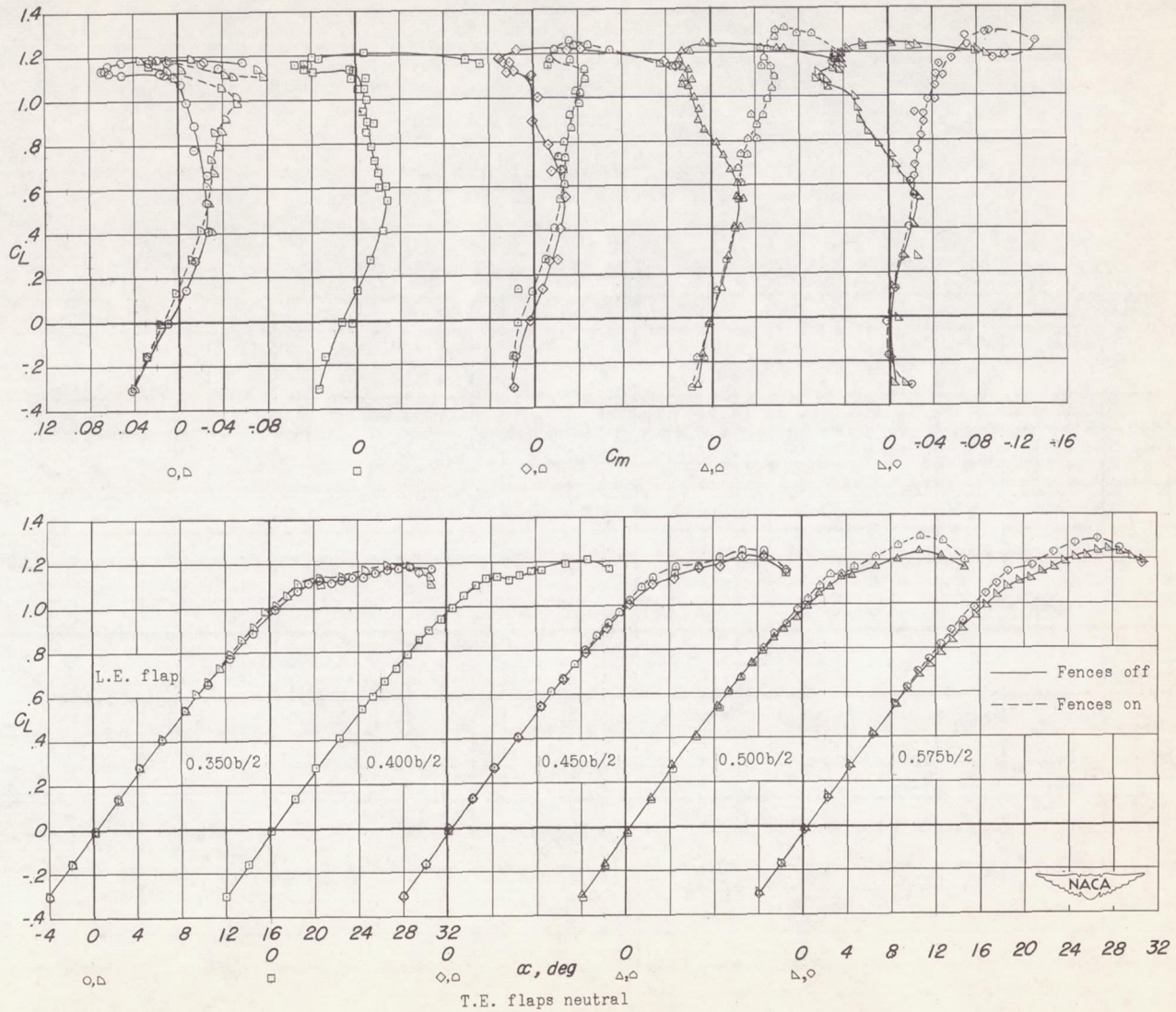
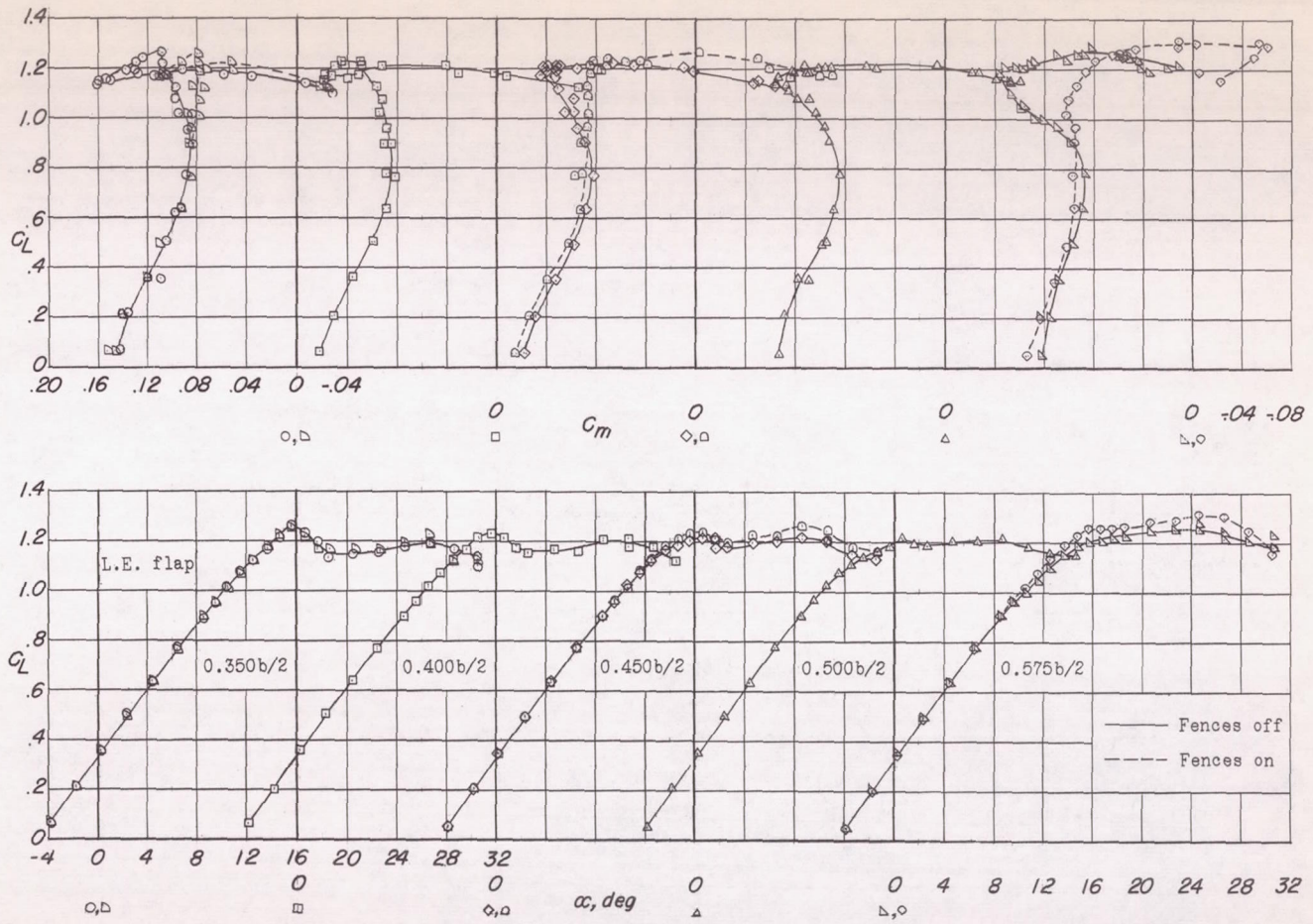
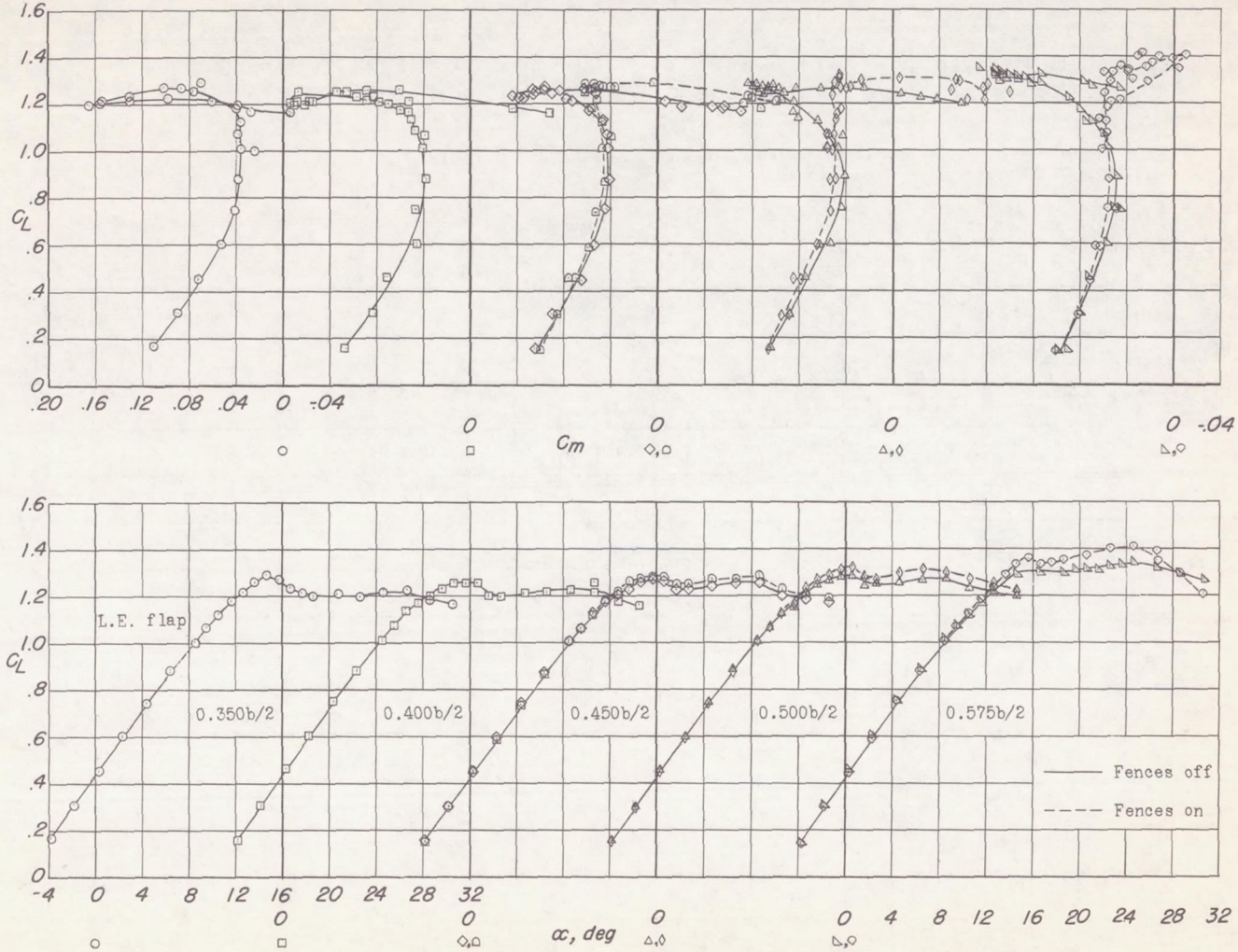


Figure 13.- Effect of leading-edge flap span on lift and pitching-moment characteristics with and without 0.575b/2 and 0.80b/2 chord fences.



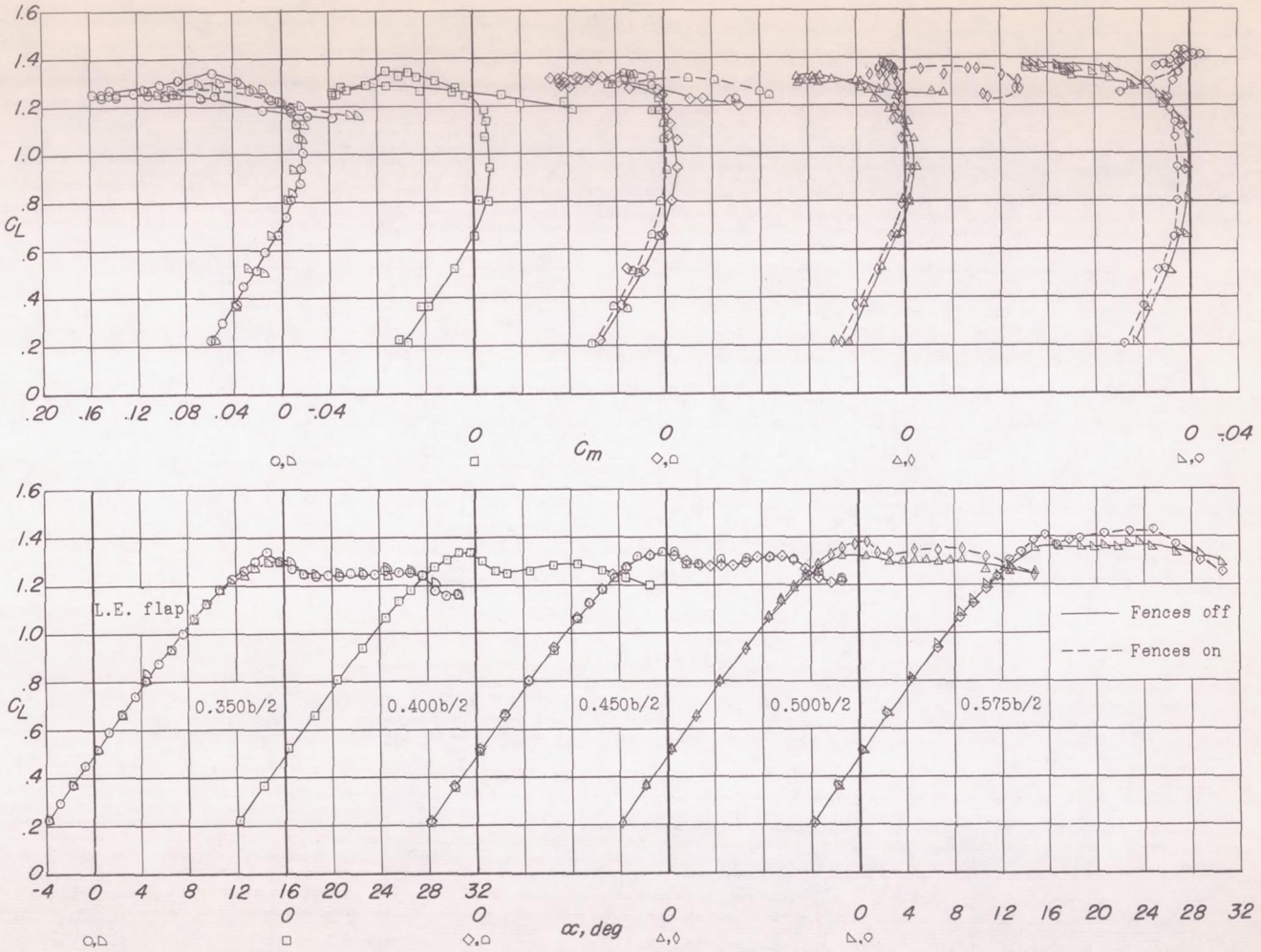
(a) 0.350b/2 split flaps.

Figure 14.- Effect of leading-edge flap span with split flaps deflected on lift and pitching-moment characteristics with and without 0.575b/2 and 0.80b/2 chord fences.



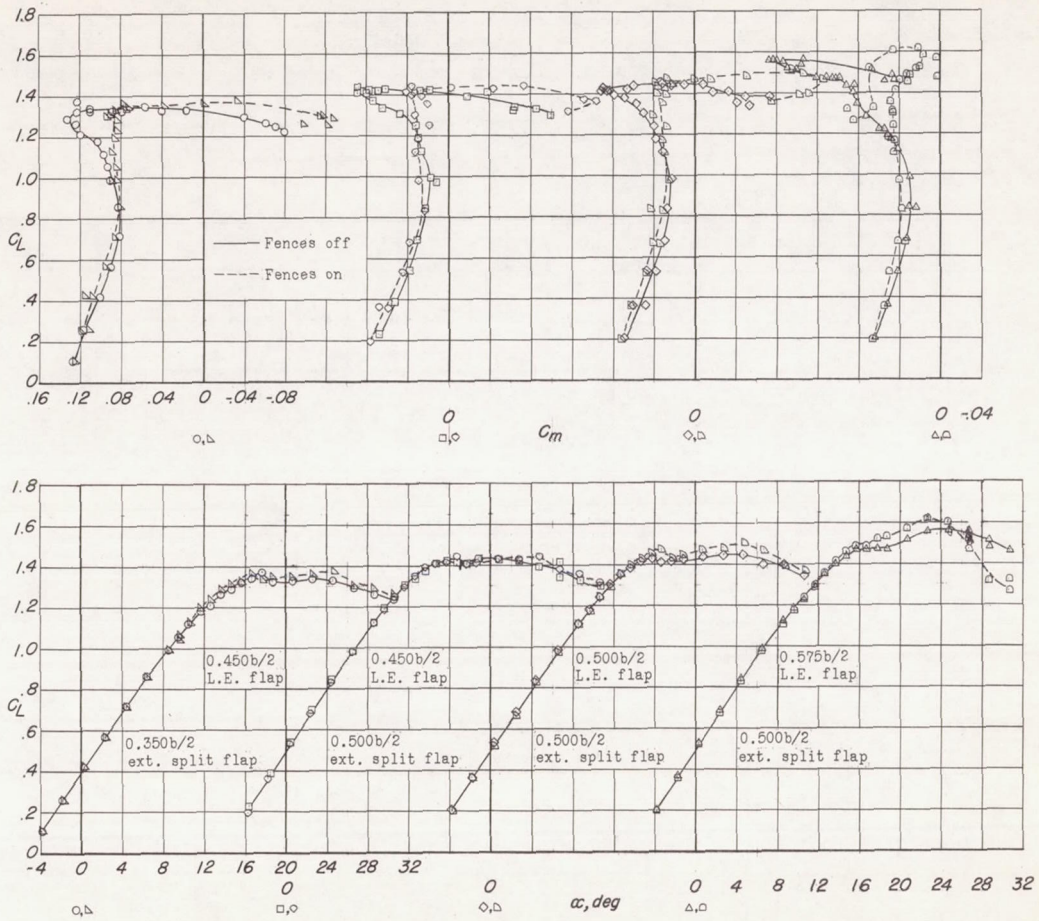
(b) 0.500b/2 split flaps.

Figure 14.- Continued.



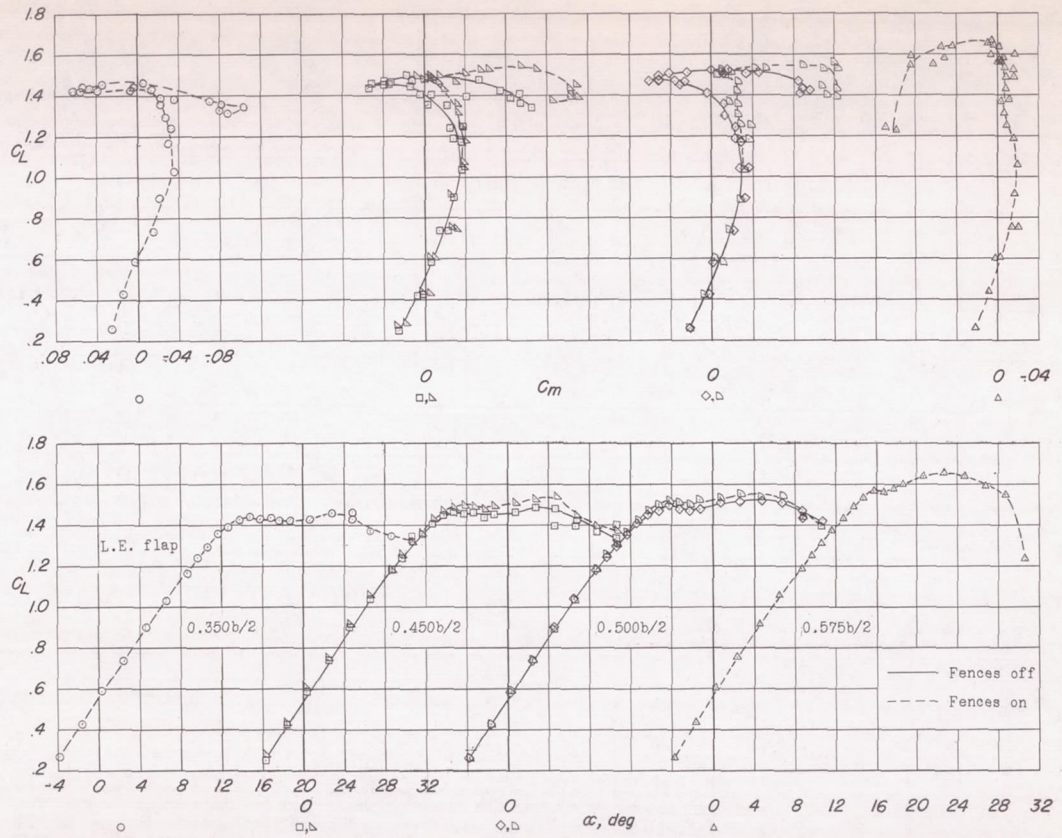
(c) 0.600b/2 split flaps.

Figure 14.- Concluded.



(a) 0.350b/2 and 0.500b/2 extended split flaps.

Figure 15.- Effect of leading-edge flap span with extended split flaps deflected on lift and pitching-moment characteristics with and without 0.575b/2 and 0.80b/2 chord fences.



(b) 0.600b/2 extended split flaps.

Figure 15.- Concluded.

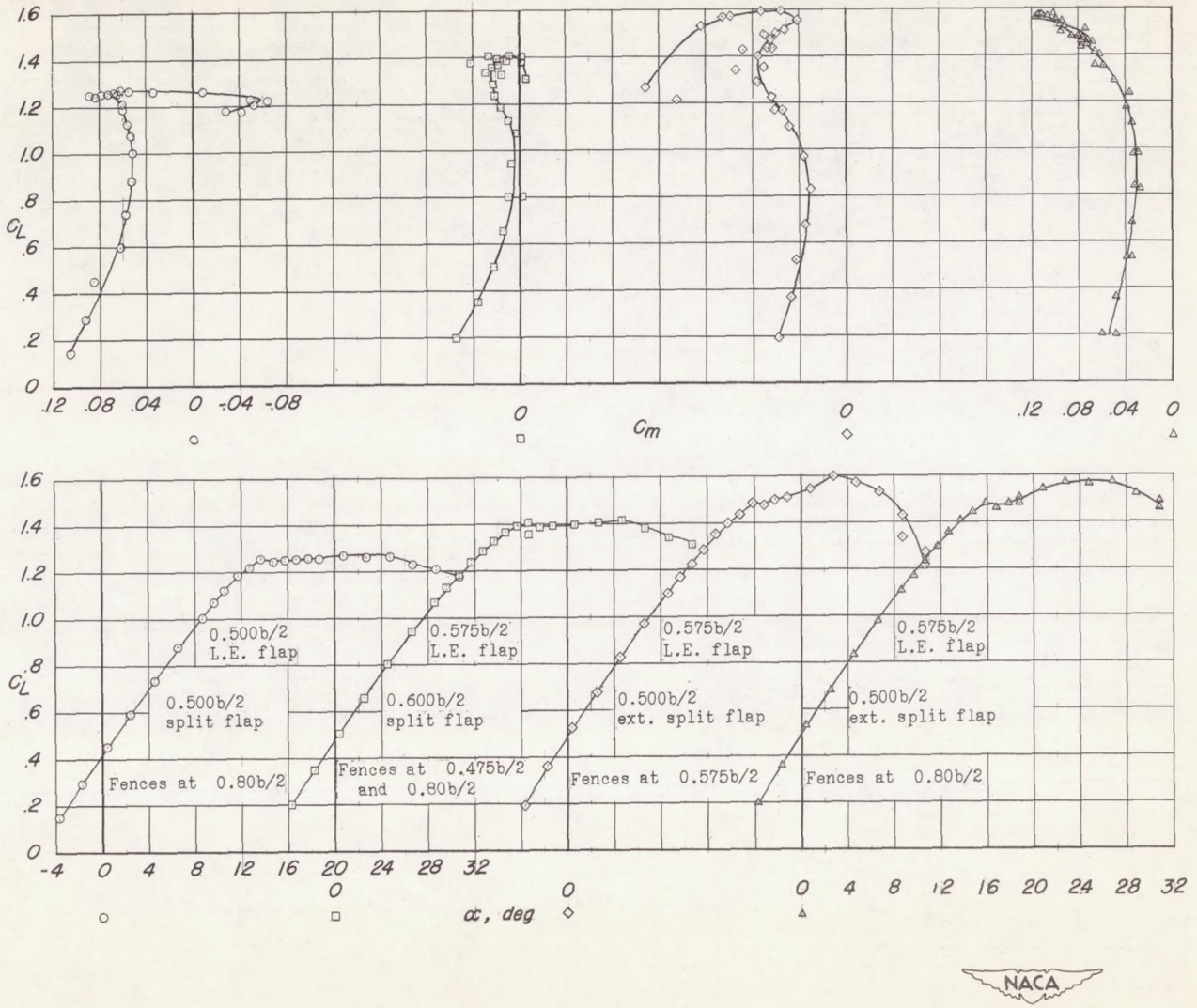
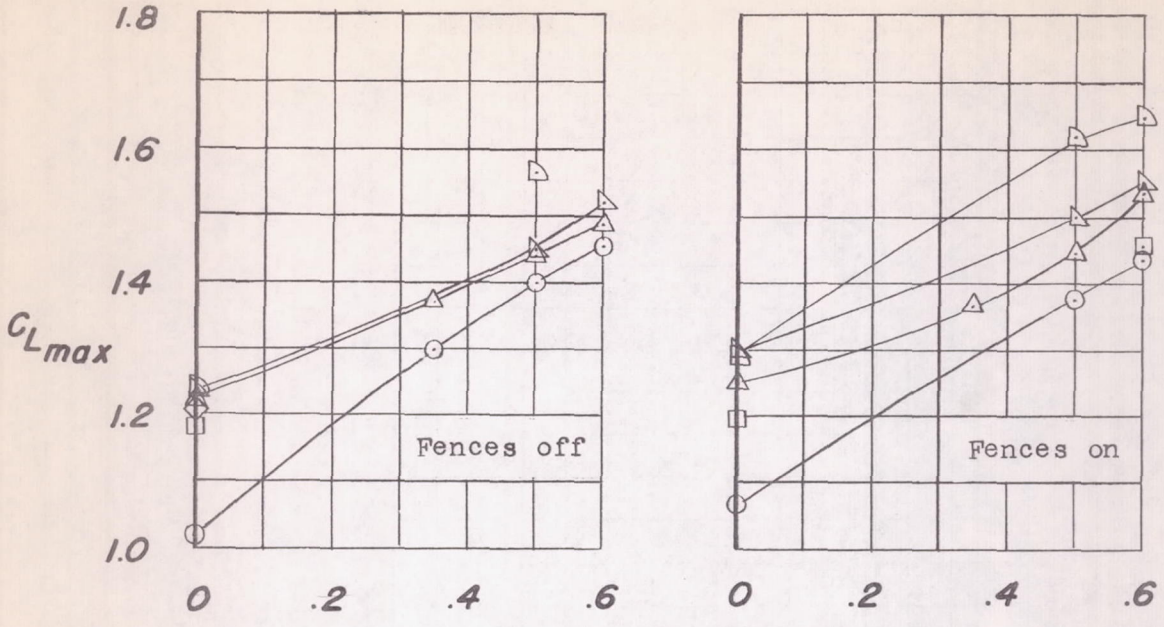
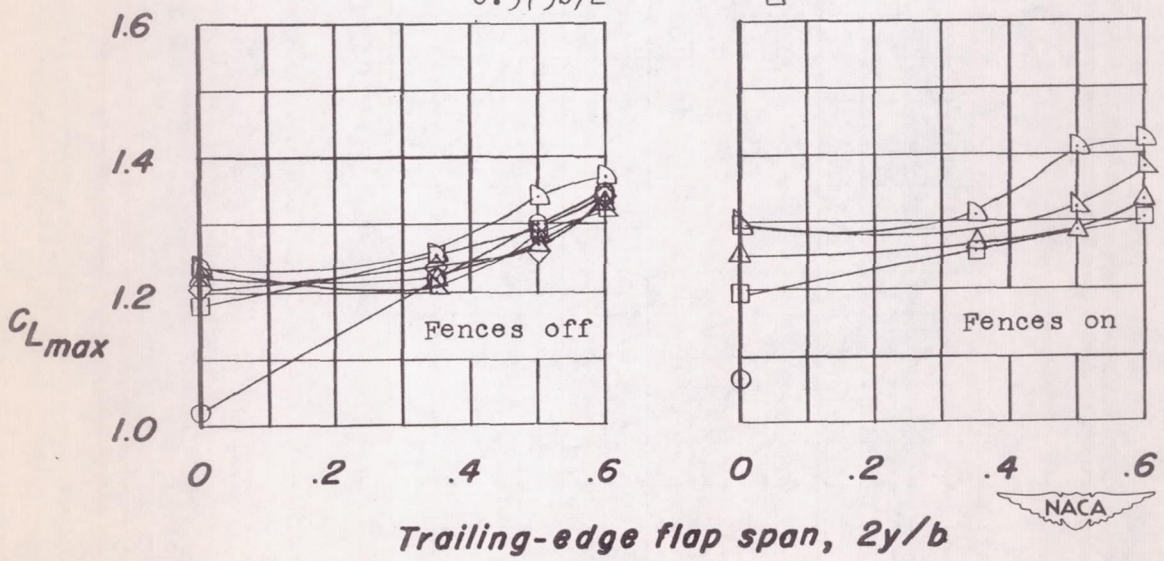


Figure 16.- The lift and pitching-moment characteristics of several additional fence-flap combinations.



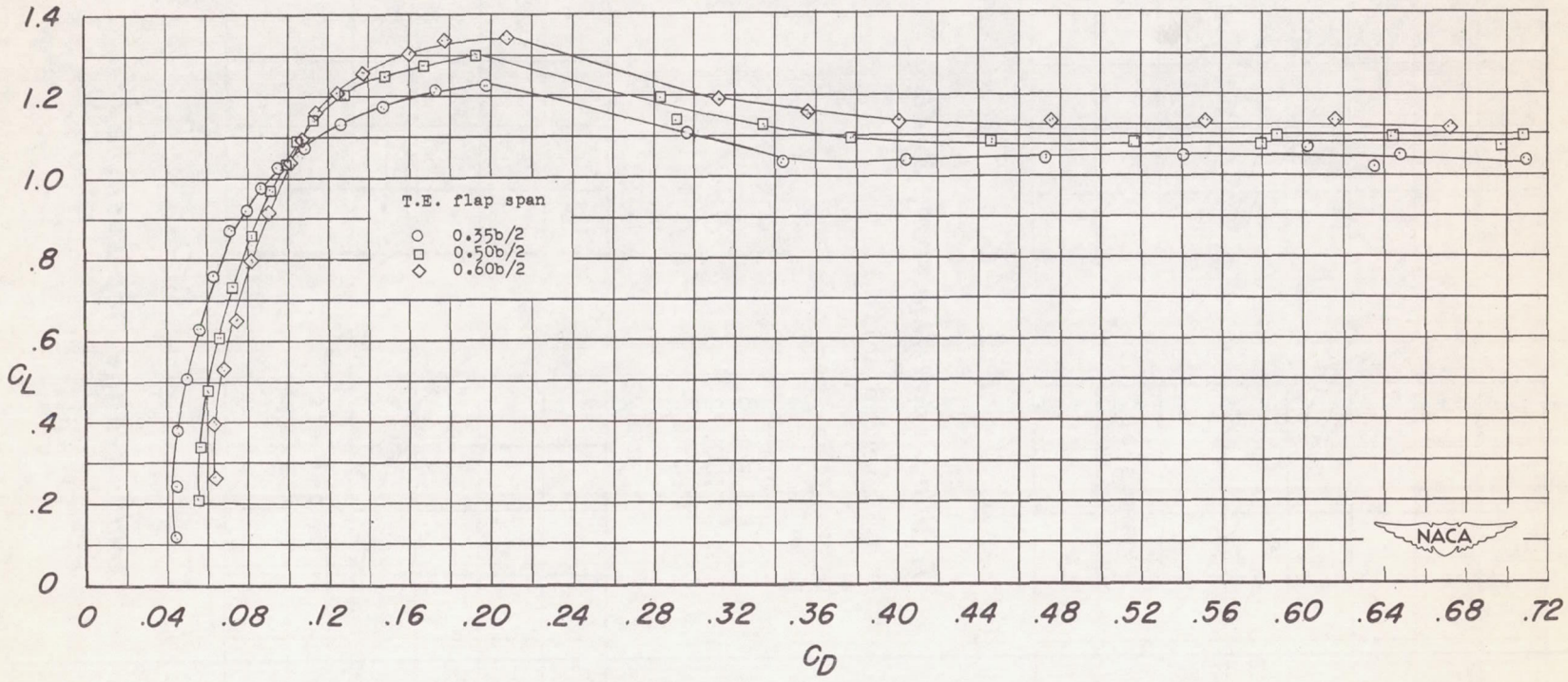
(a) Extended split flaps.

L.E. flap span	Symbol
Off	○
0.35b/2	□
0.40b/2	◇
0.45b/2	△
0.50b/2	◁
0.575b/2	◻



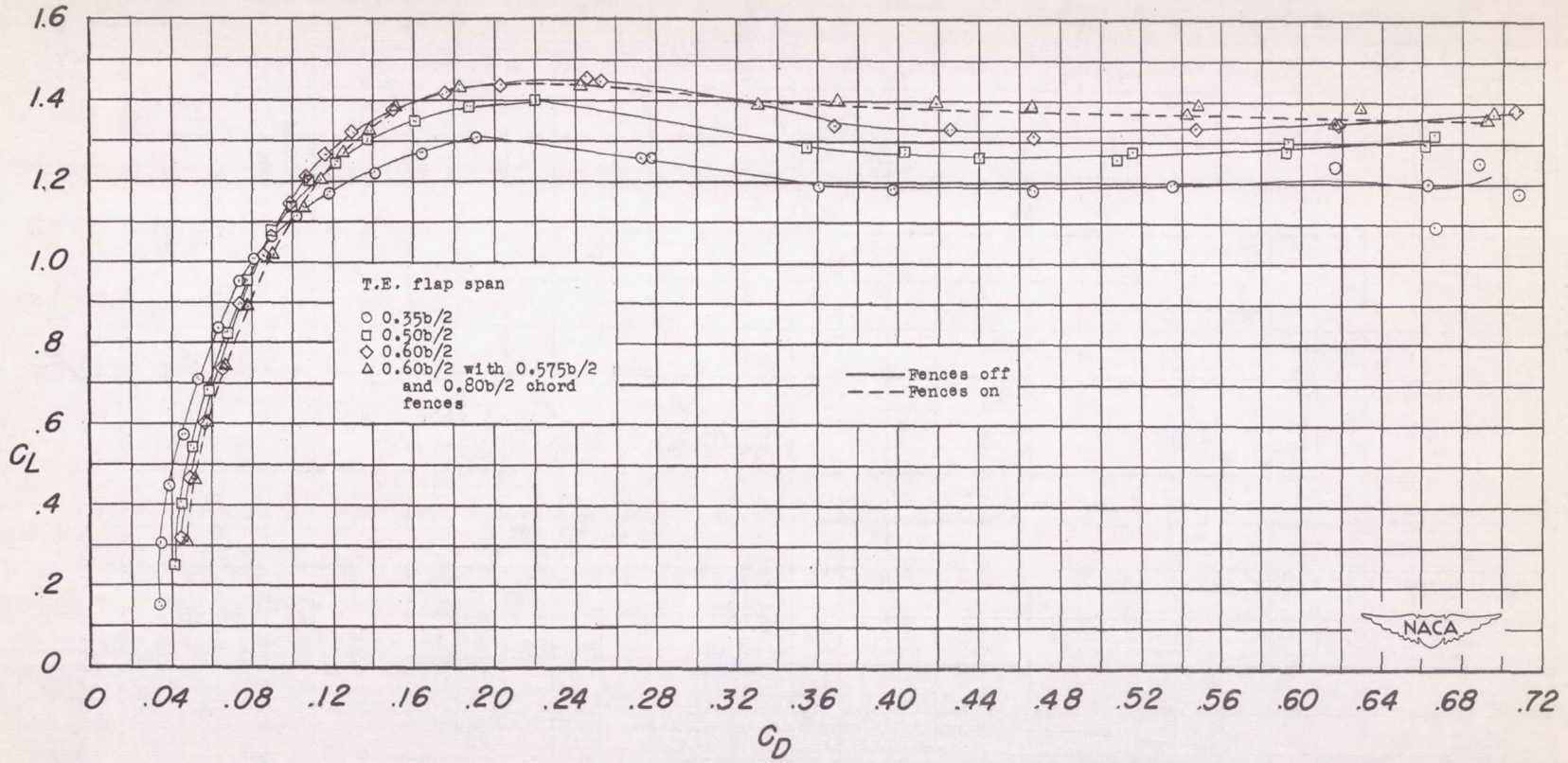
(b) Split flaps.

Figure 17.- Maximum-lift characteristics of various combinations of leading- and trailing-edge flaps with and without 0.575b/2 and 0.80b/2 chord fences.



(a) Split flaps.

Figure 18.- Effect of trailing-edge flap span and location on drag characteristics.



(b) Extended split flaps

Figure 18.- Concluded.

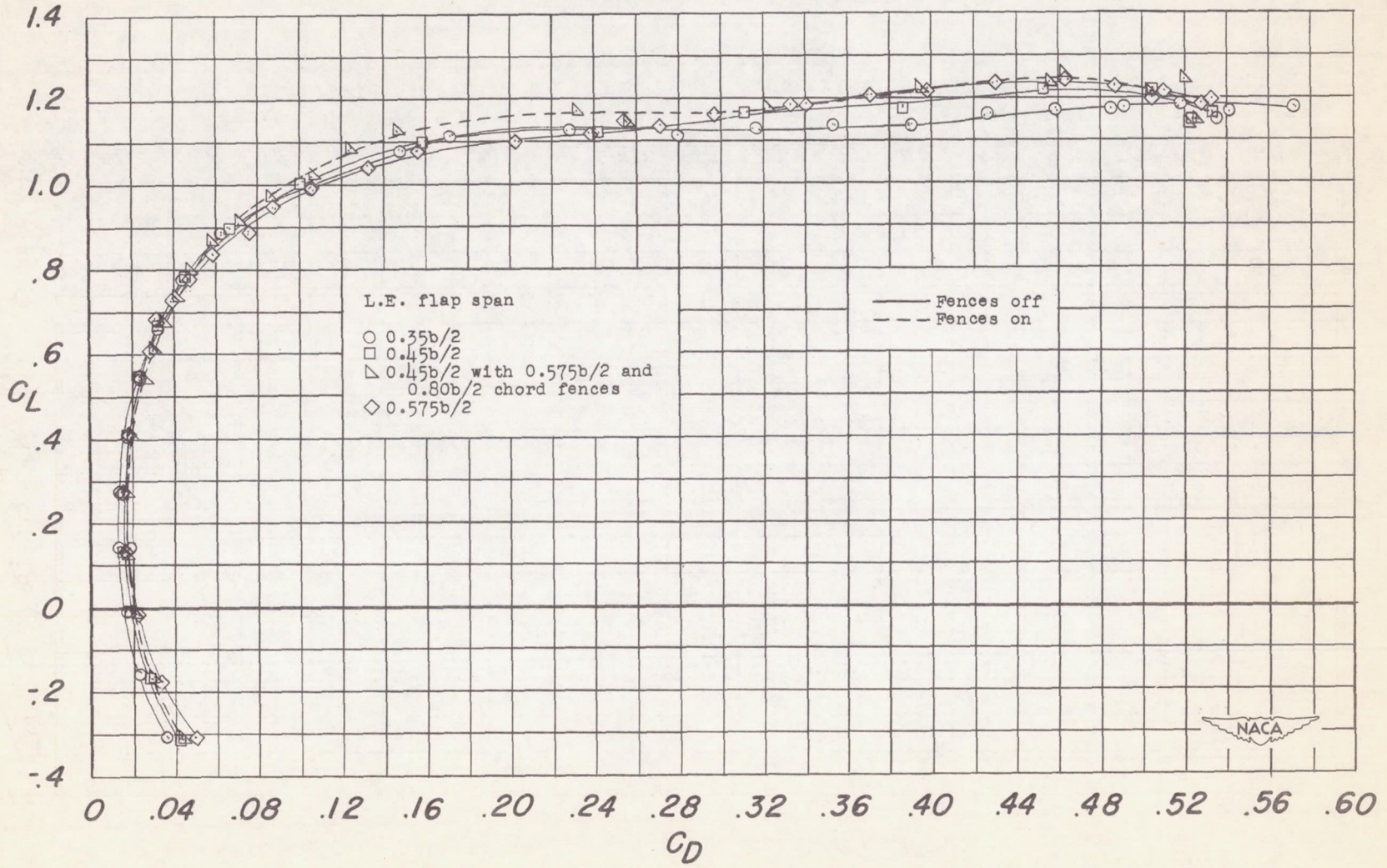
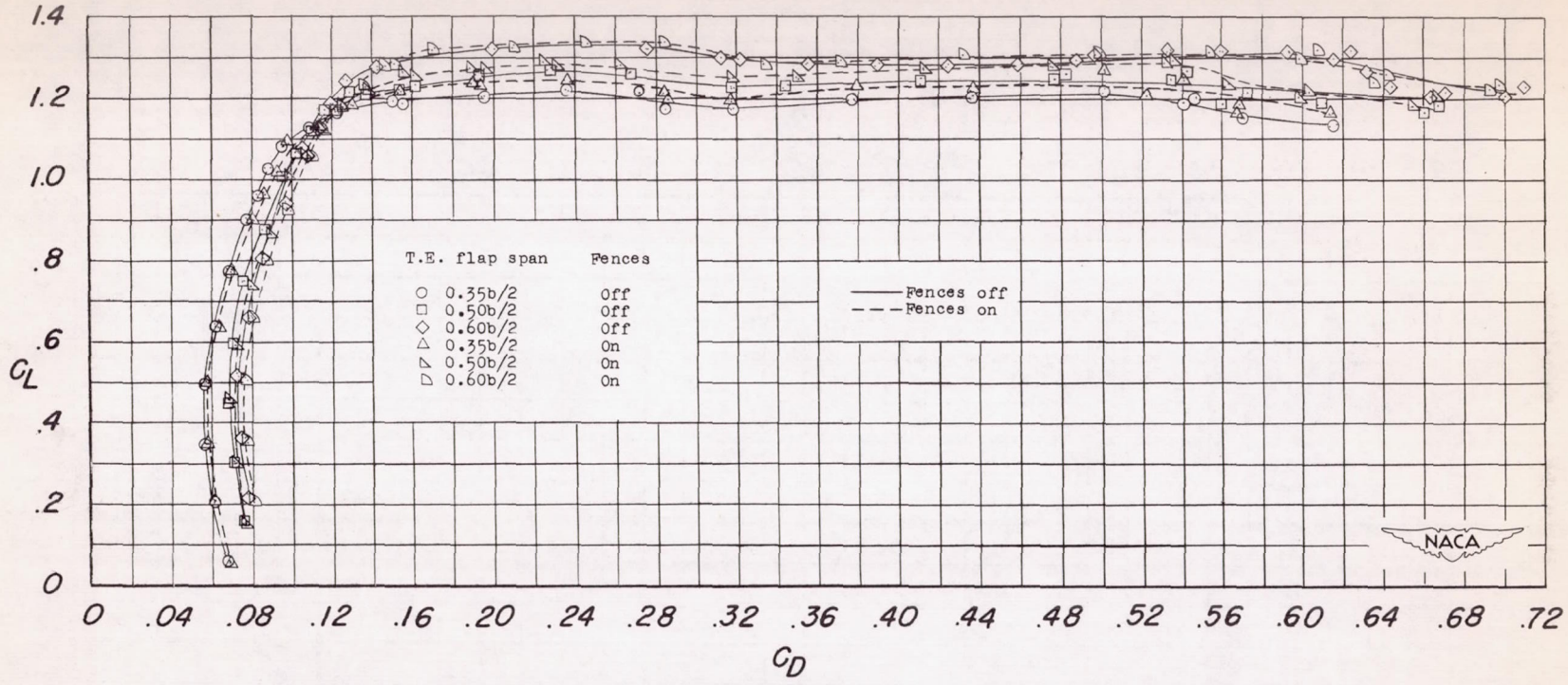
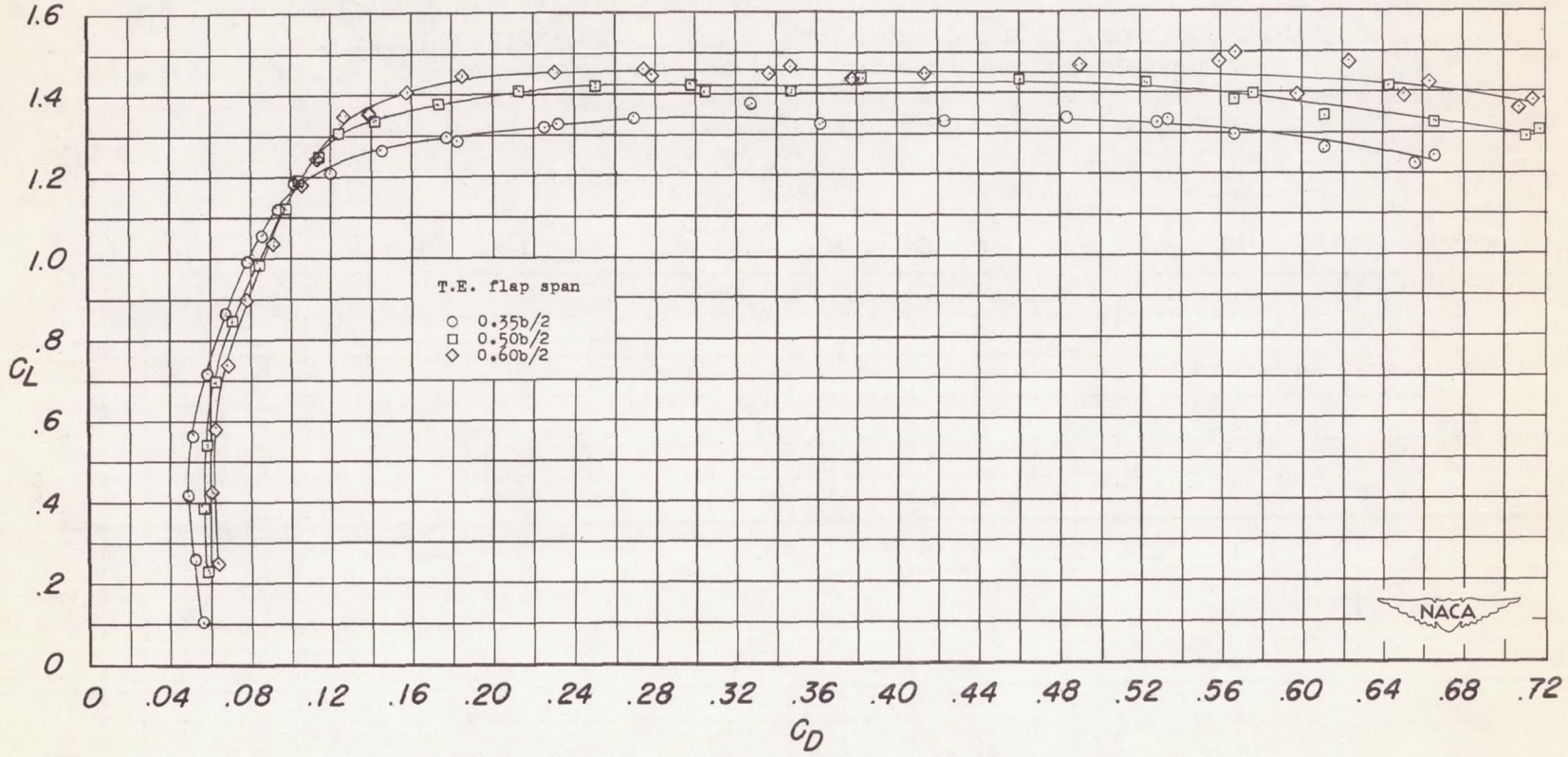


Figure 19.- Effect of leading-edge flap span on drag characteristics.



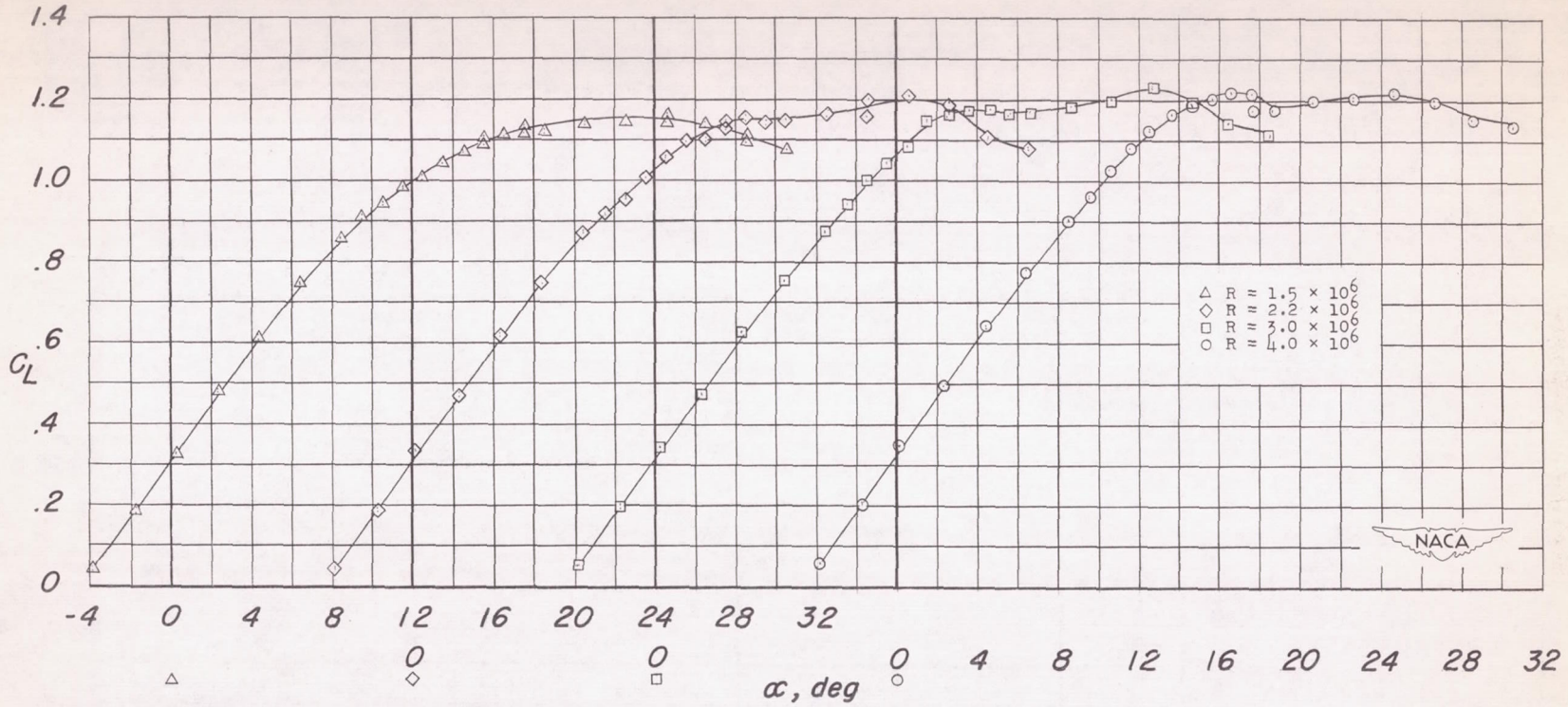
(a) Split flaps.

Figure 20.- Effect of trailing-edge flap span and location with 0.45b/2 leading-edge flaps on drag characteristics with and without 0.575b/2 and 0.80b/2 chord fences.



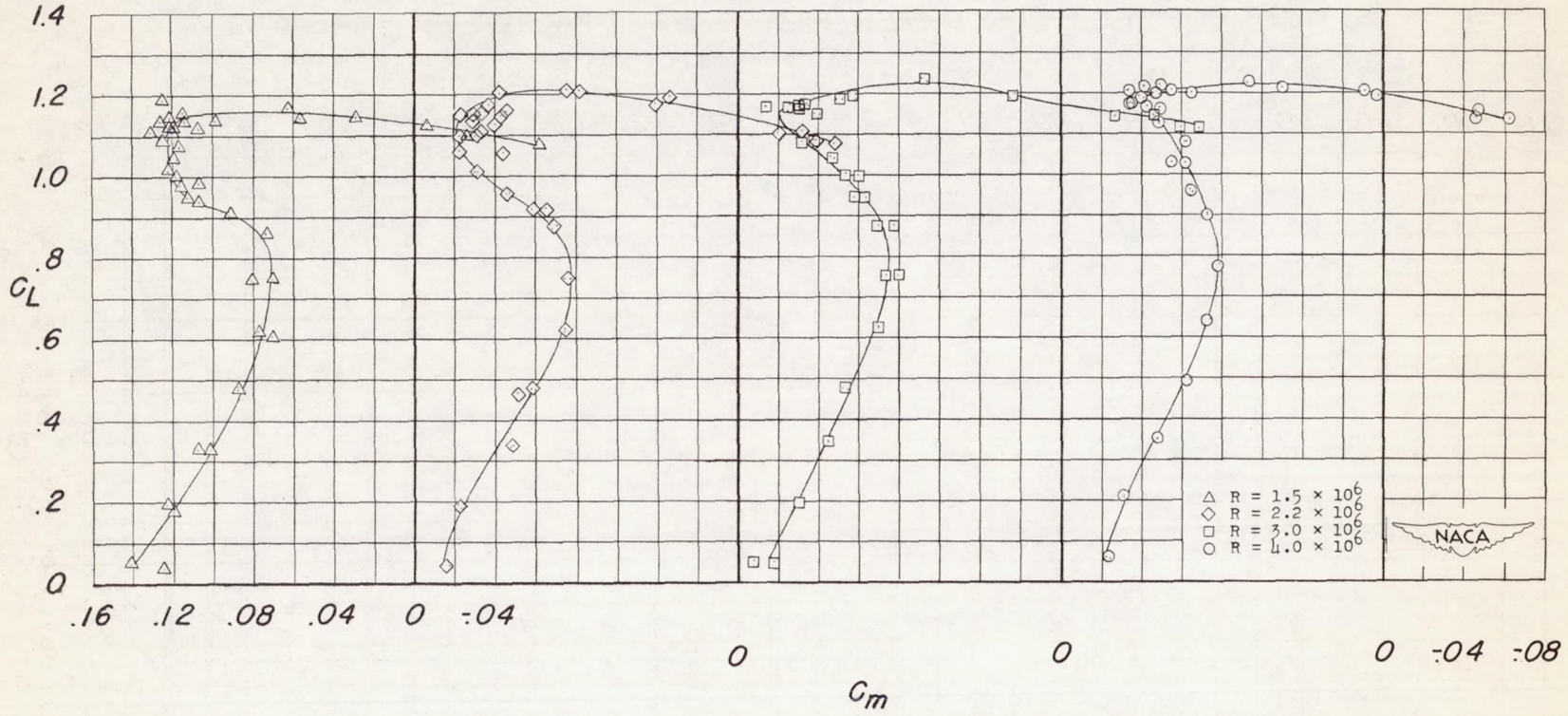
(b) Extended split flaps.

Figure 20.- Concluded.



(a) C_L against α.

Figure 21.- Effect of Reynolds number on lift and pitching-moment characteristics with 0.45b/2 leading-edge flaps and 0.35b/2 split flaps.



(b) C_L against C_m.

Figure 21.- Concluded.

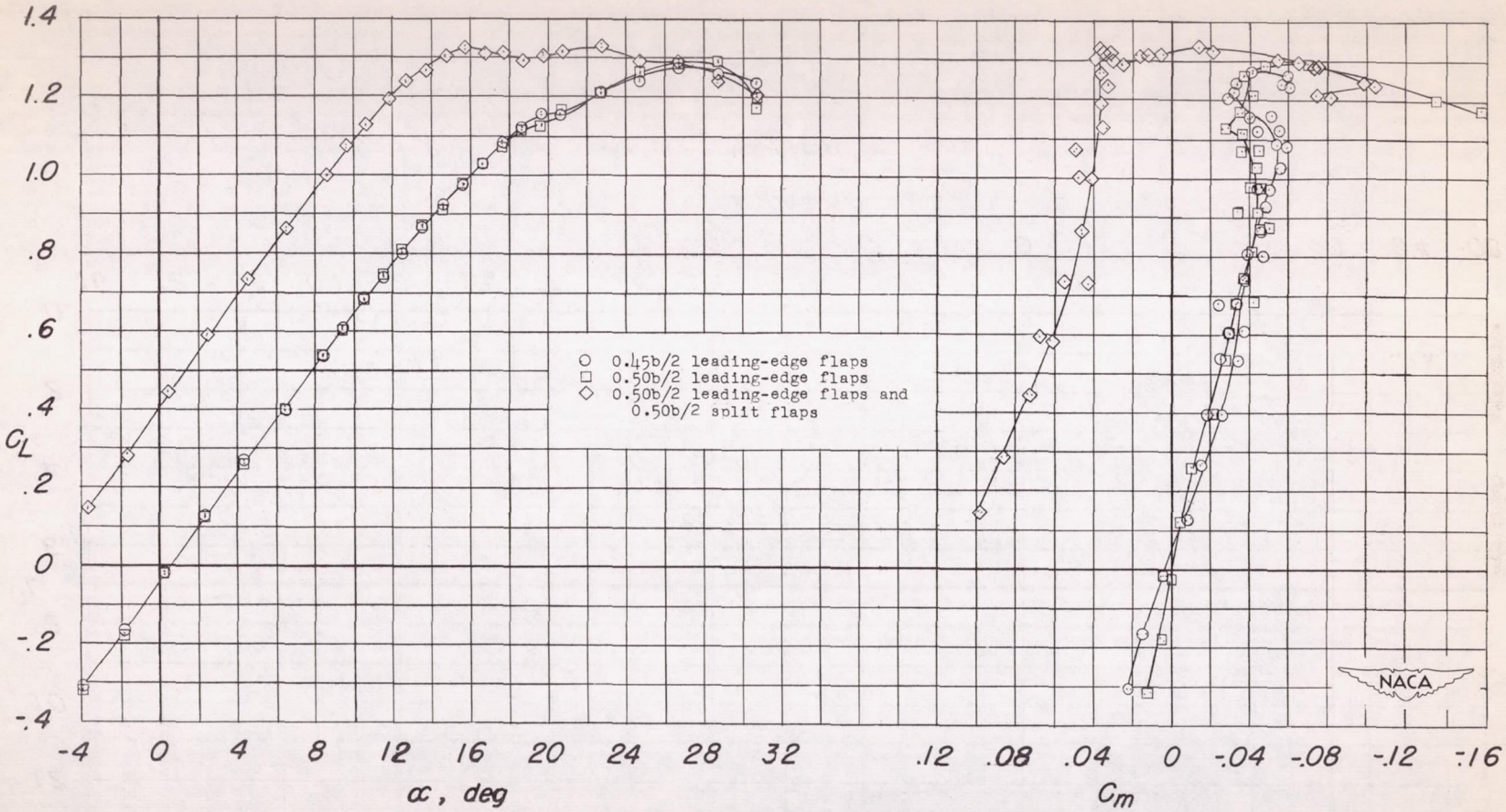
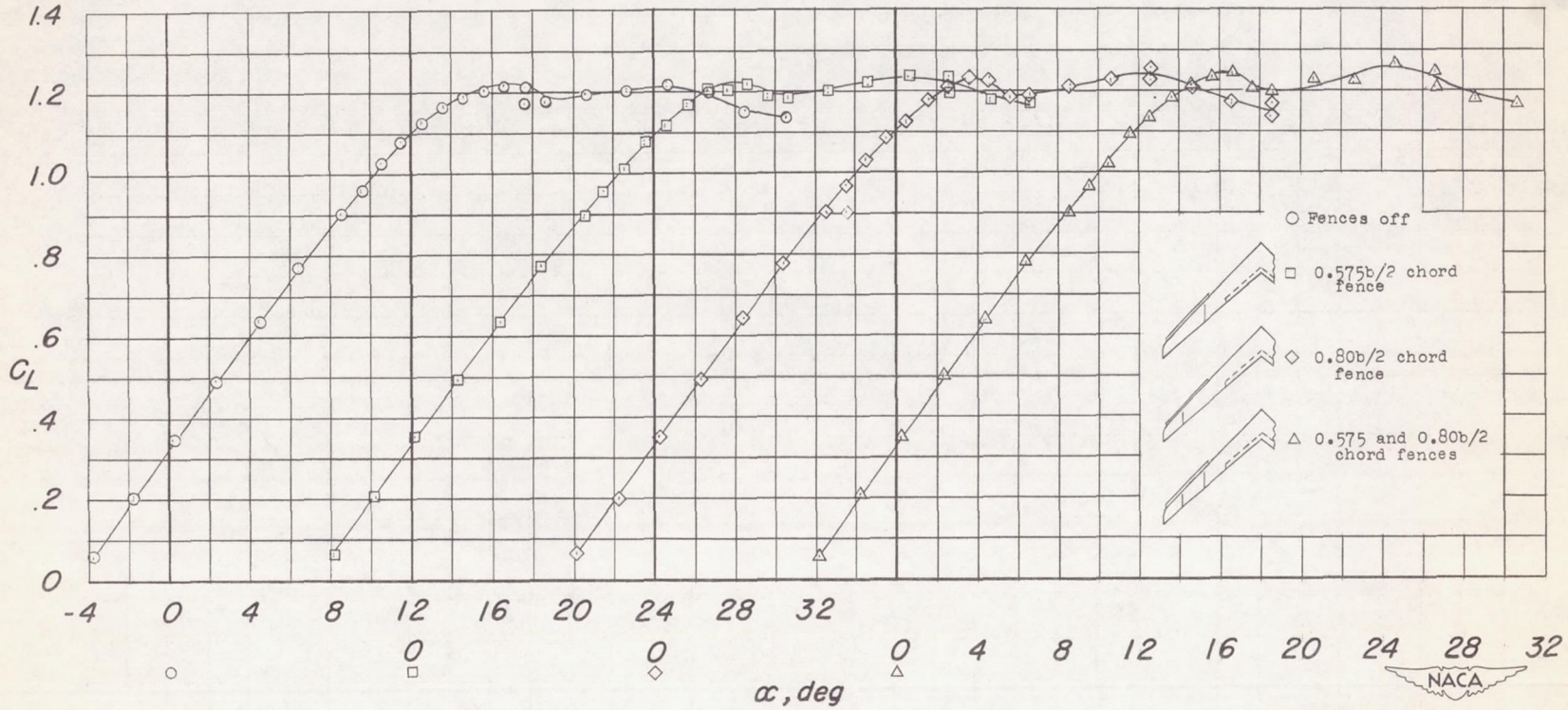
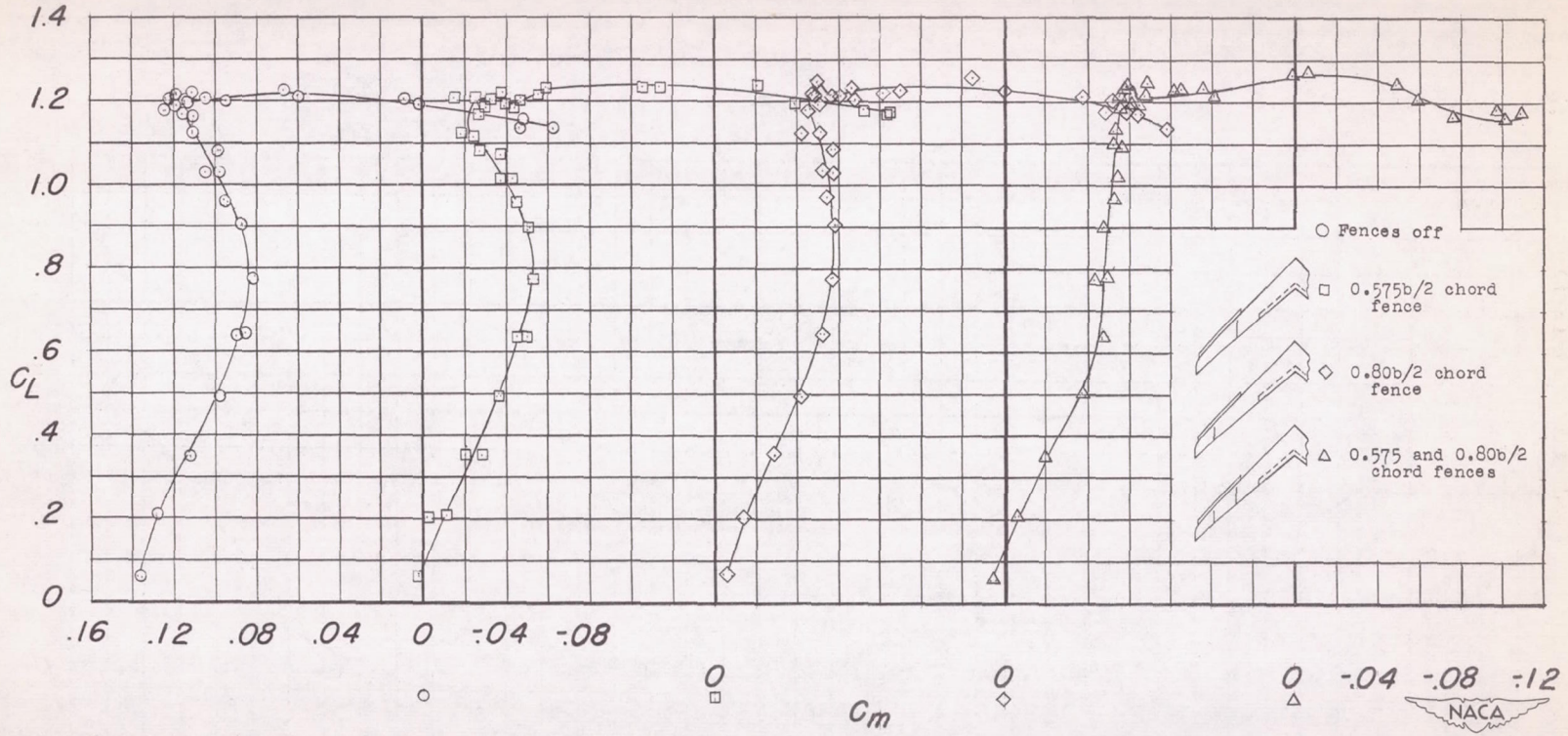


Figure 22.- The lift and pitching-moment characteristics with leading-edge and trailing-edge flaps and 0.575b/2, 0.80b/2, and 0.89b/2 chord fences.



(a) C_L against α.

Figure 23.- Effect of fence number and location on wing with 0.45b/2 leading-edge flaps and 0.35b/2 split flaps.



(b) C_L against C_m.

Figure 23.- Concluded.

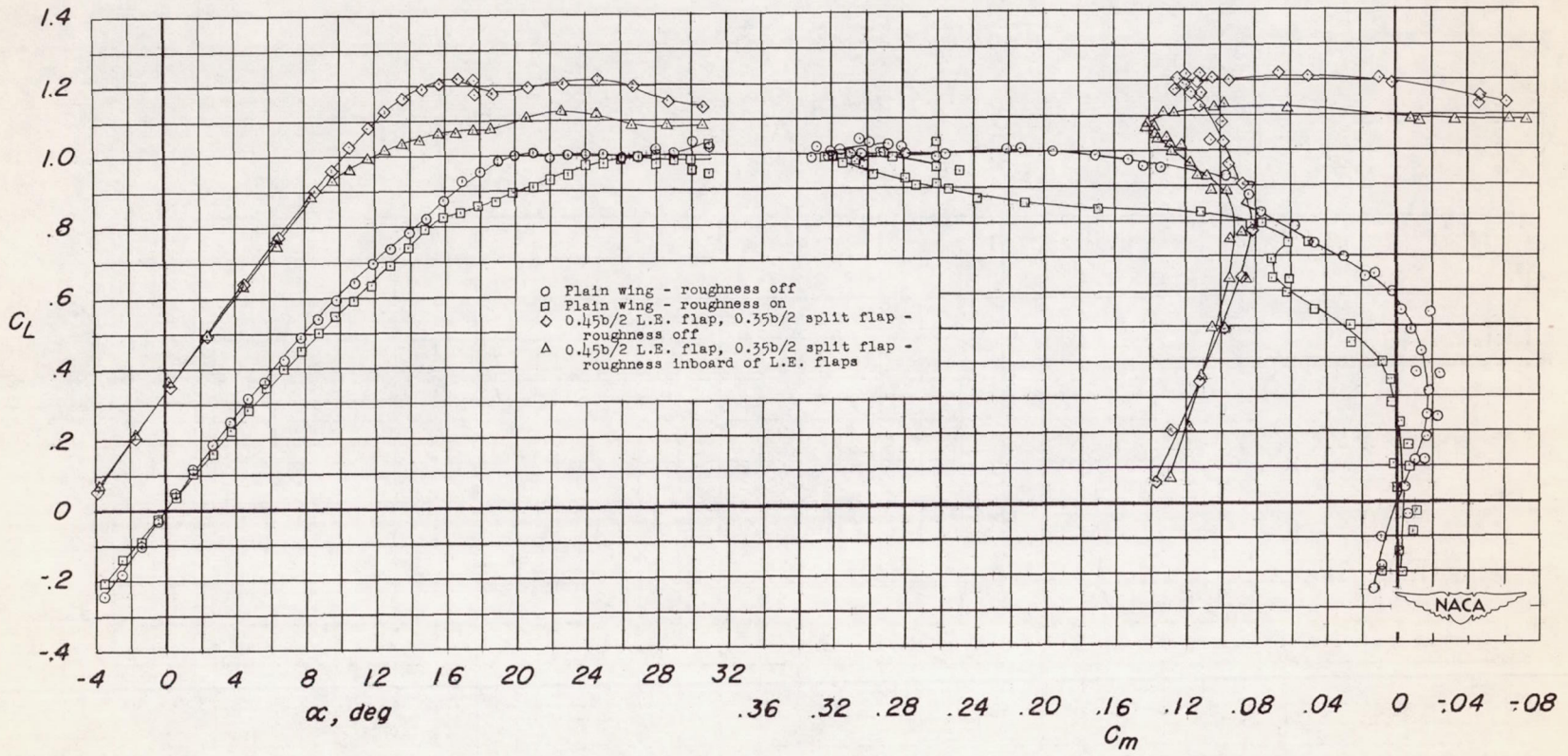
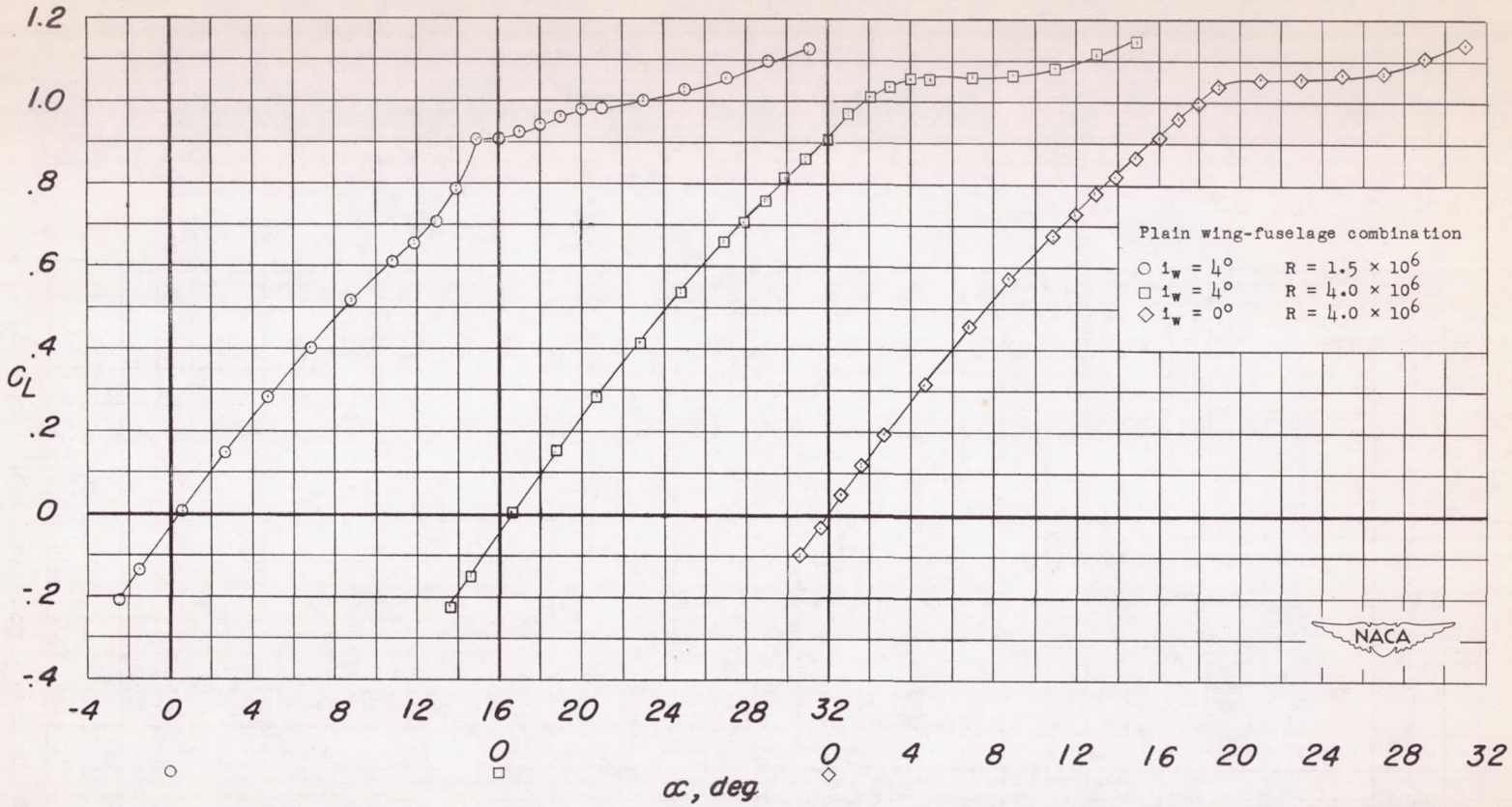
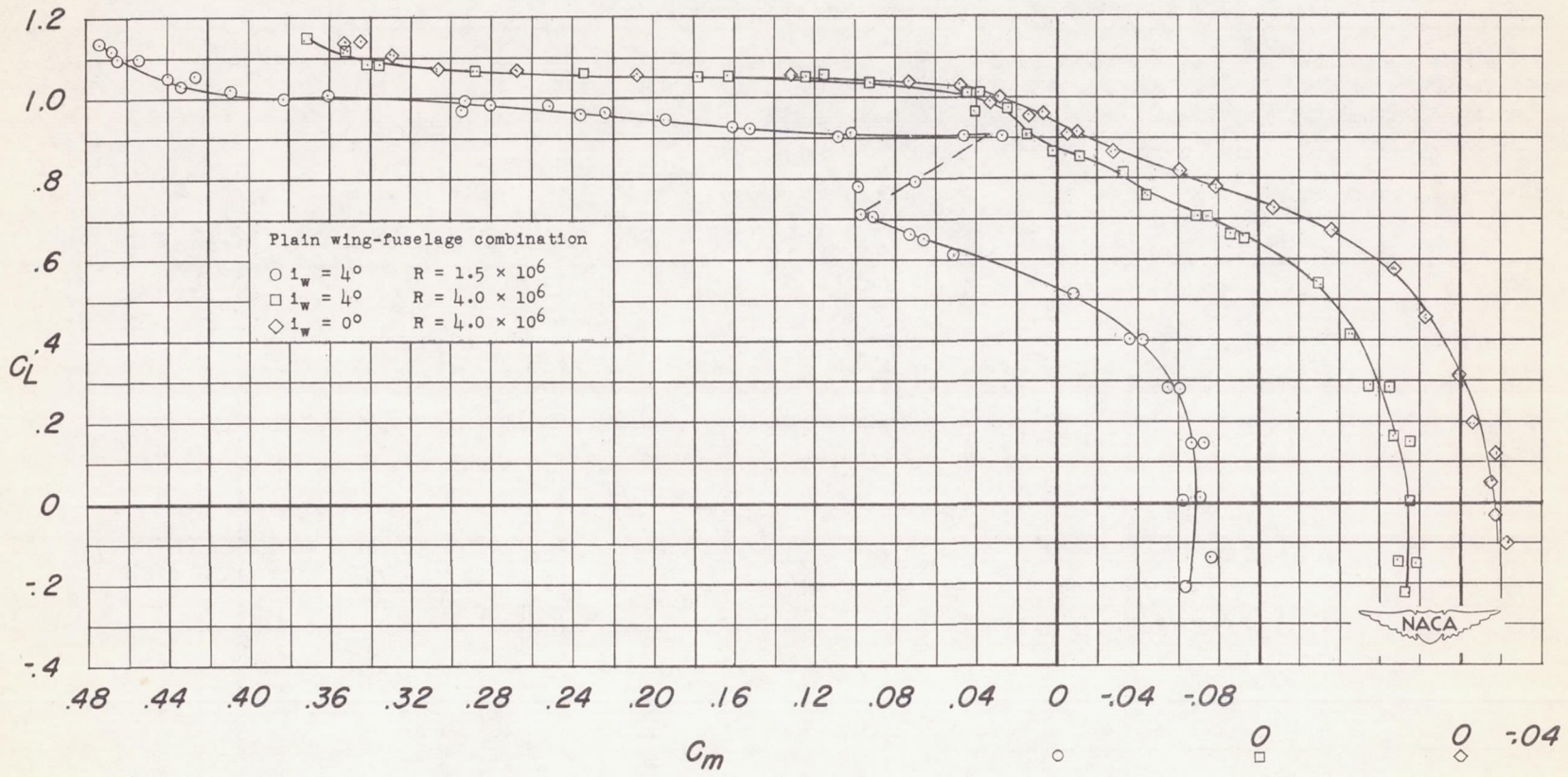


Figure 24.- Effect of leading-edge roughness on lift and pitching-moment characteristics.



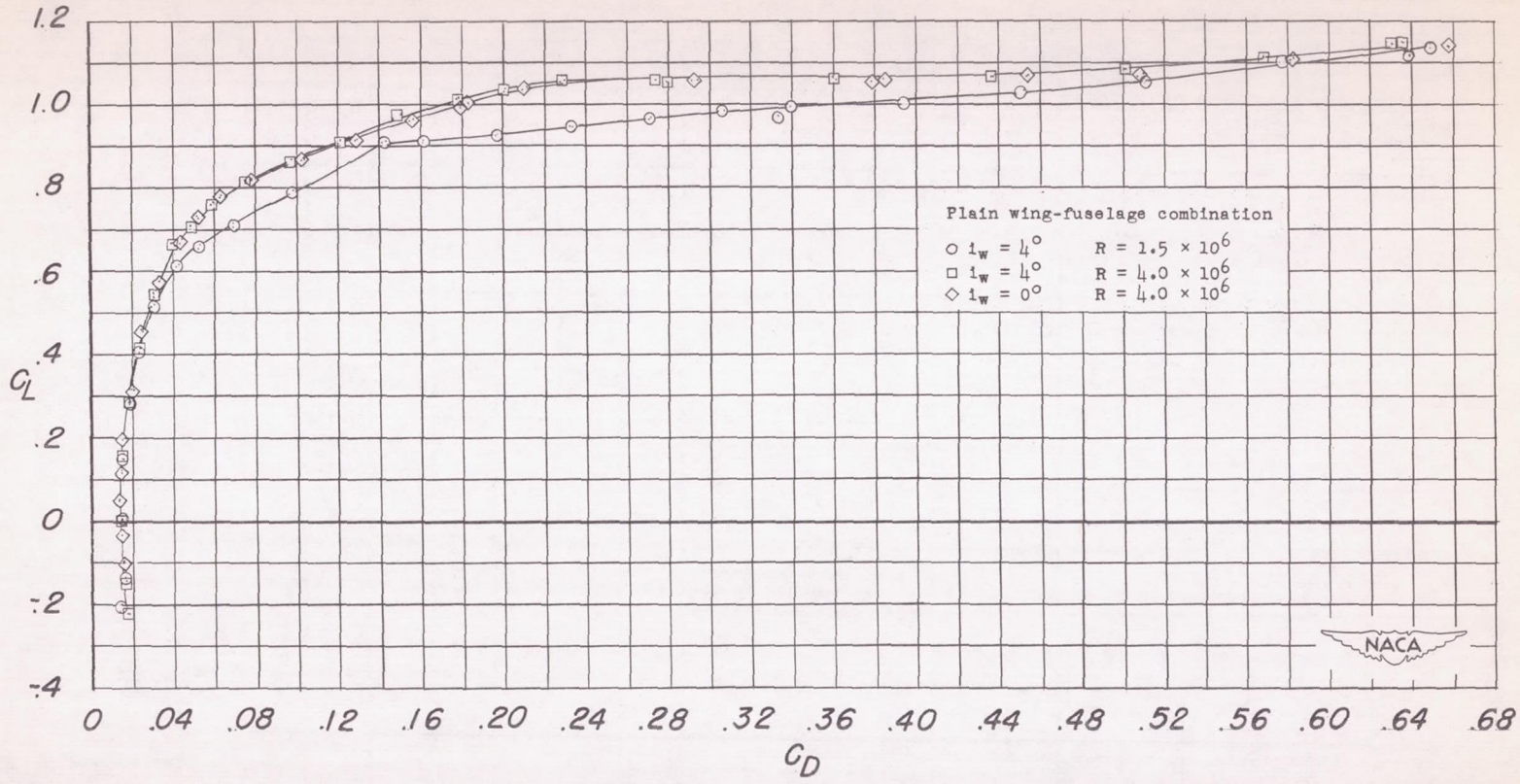
(a) C_L against α.

Figure 25.- Lift, pitching-moment, and drag characteristics with fuselage installed.



(b) C_L against C_m.

Figure 25.- Continued.



(c) C_L against C_D.

Figure 25.- Concluded.

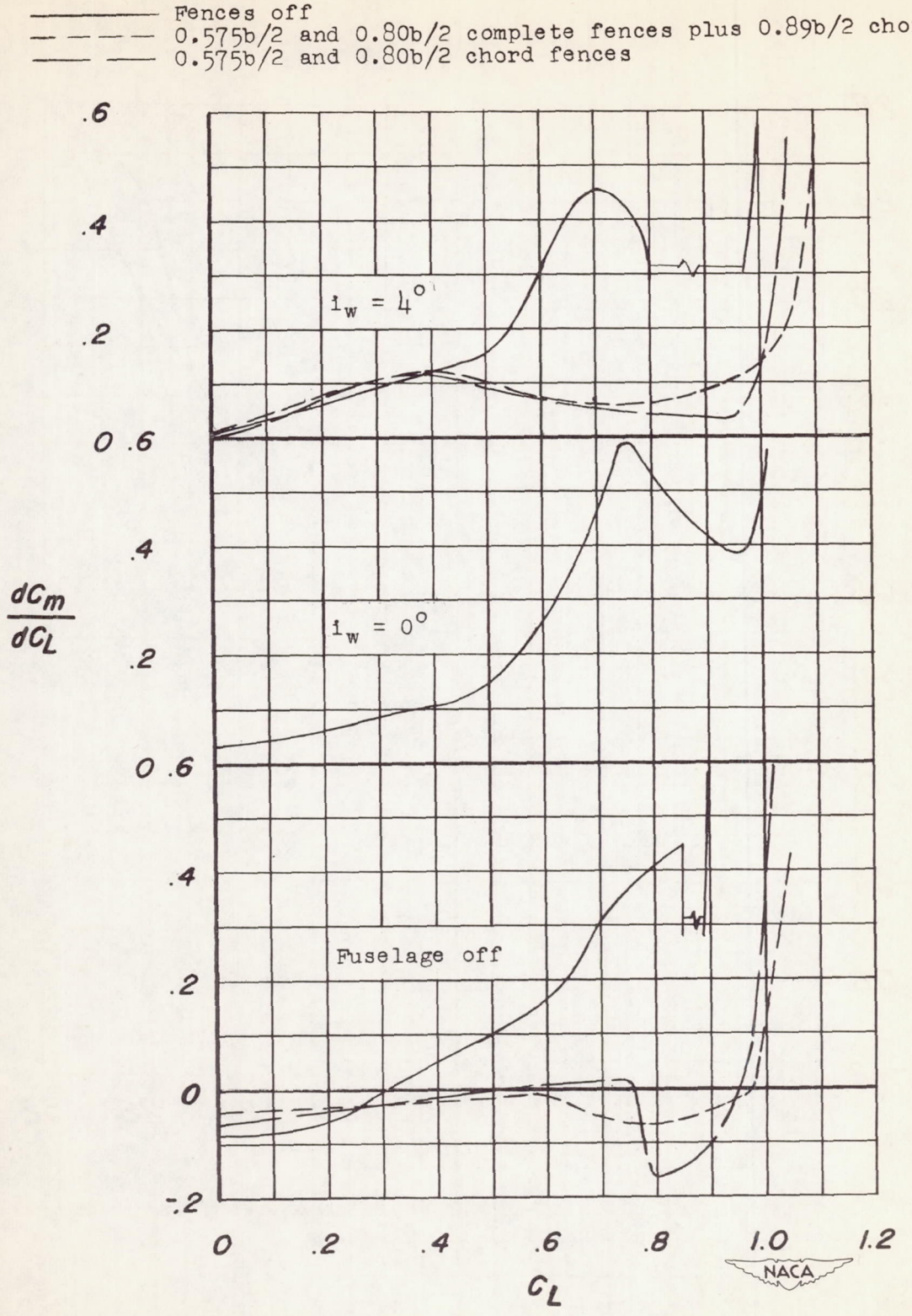


Figure 26.- Effect of fuselage and fences on dC_m/dC_L.

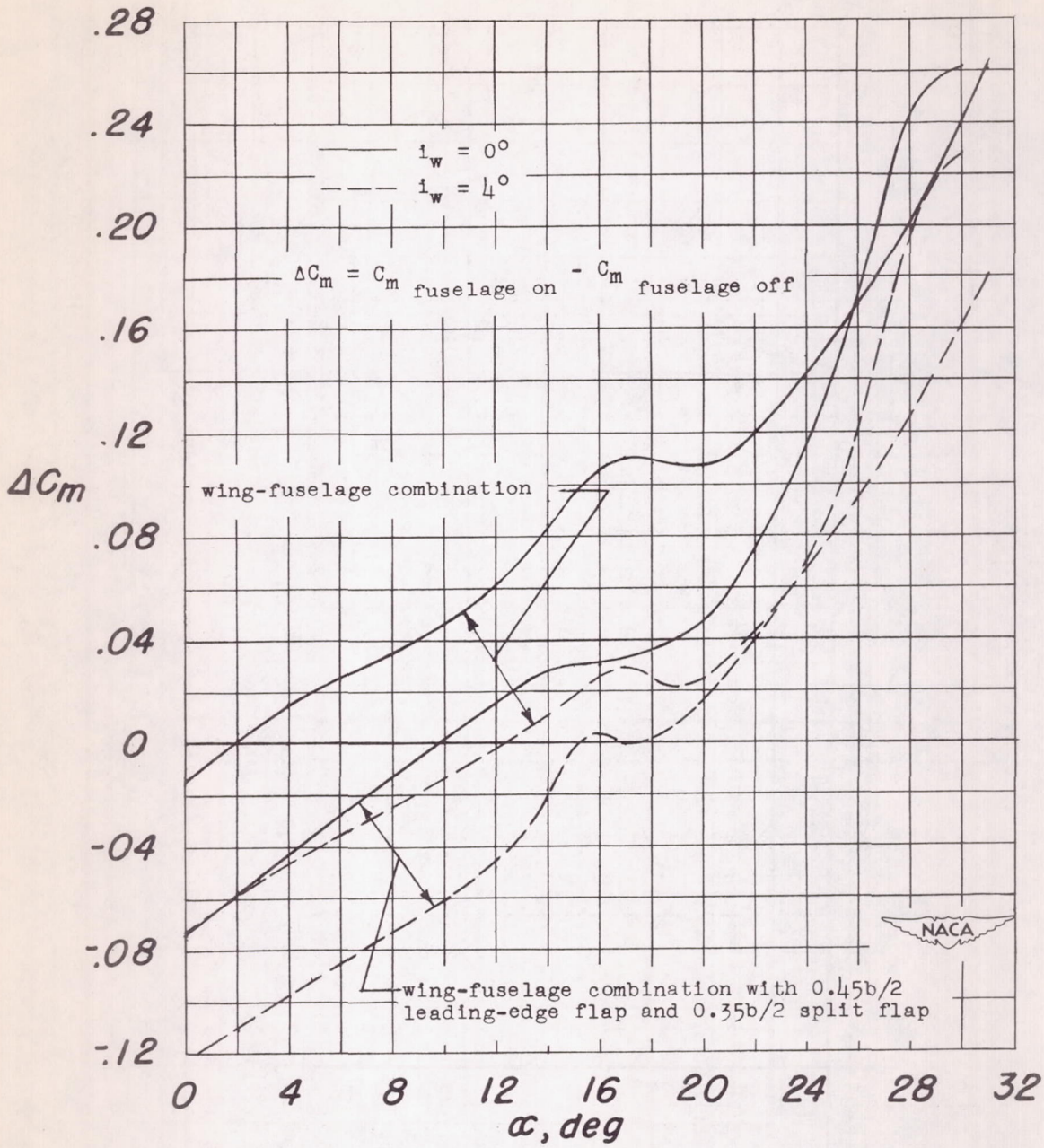
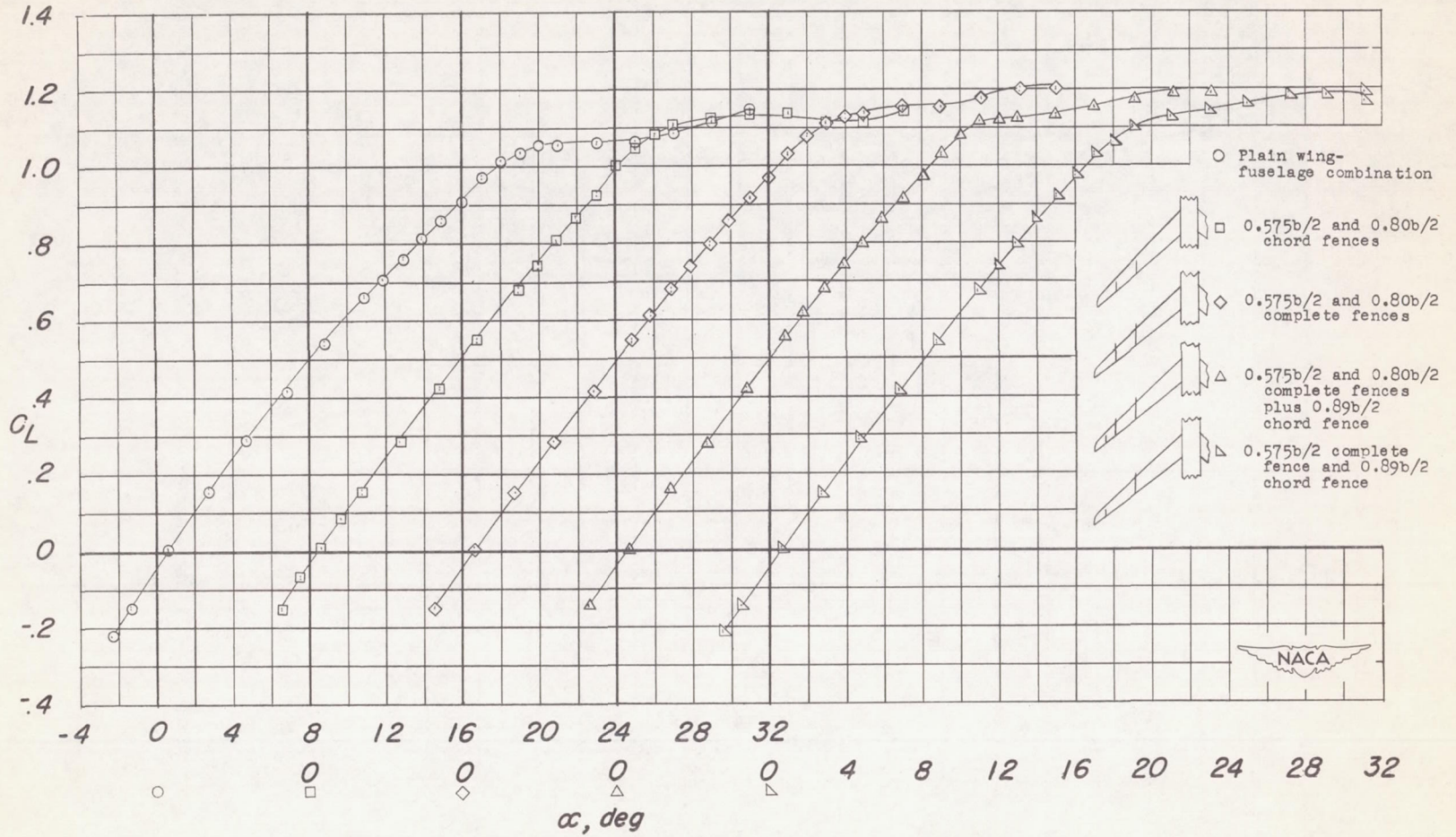
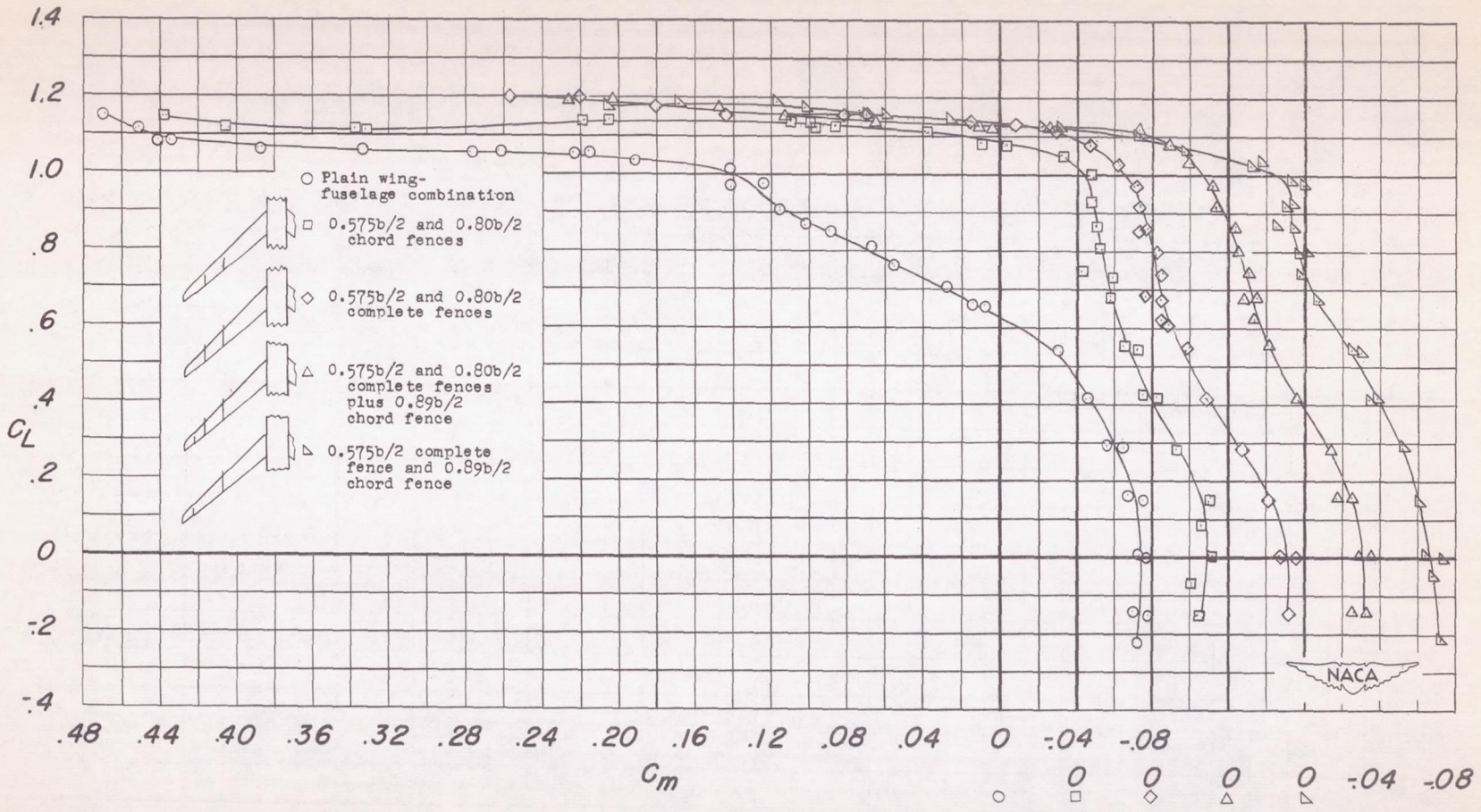


Figure 27.- Increment of pitching-moment coefficient resulting from the addition of the fuselage.



(a) C_L against α.

Figure 28.- Effect of fences on lift and pitching-moment characteristics of wing-fuselage combination. $i_w = 4^o$.



(b) C_L against C_m.

Figure 28.- Concluded.

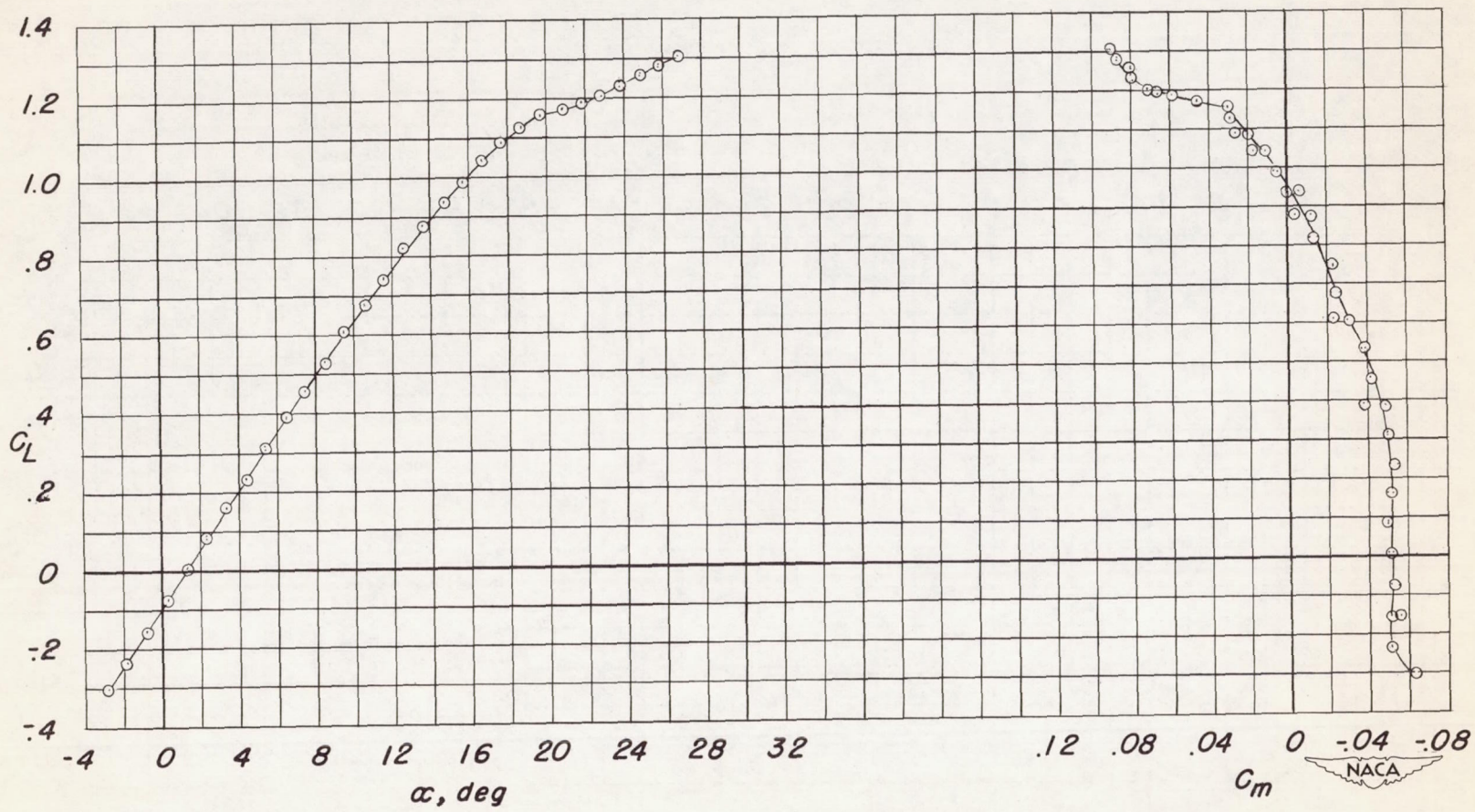
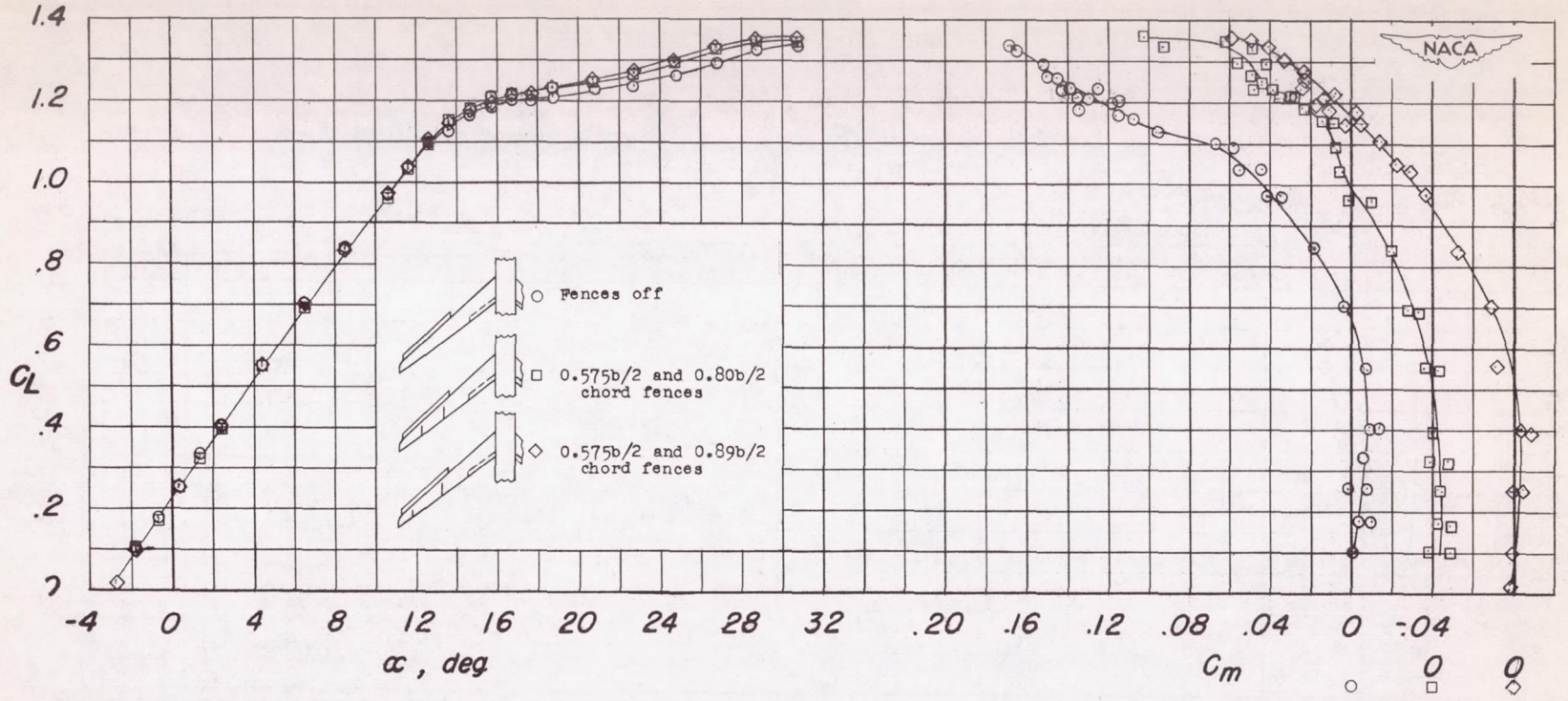
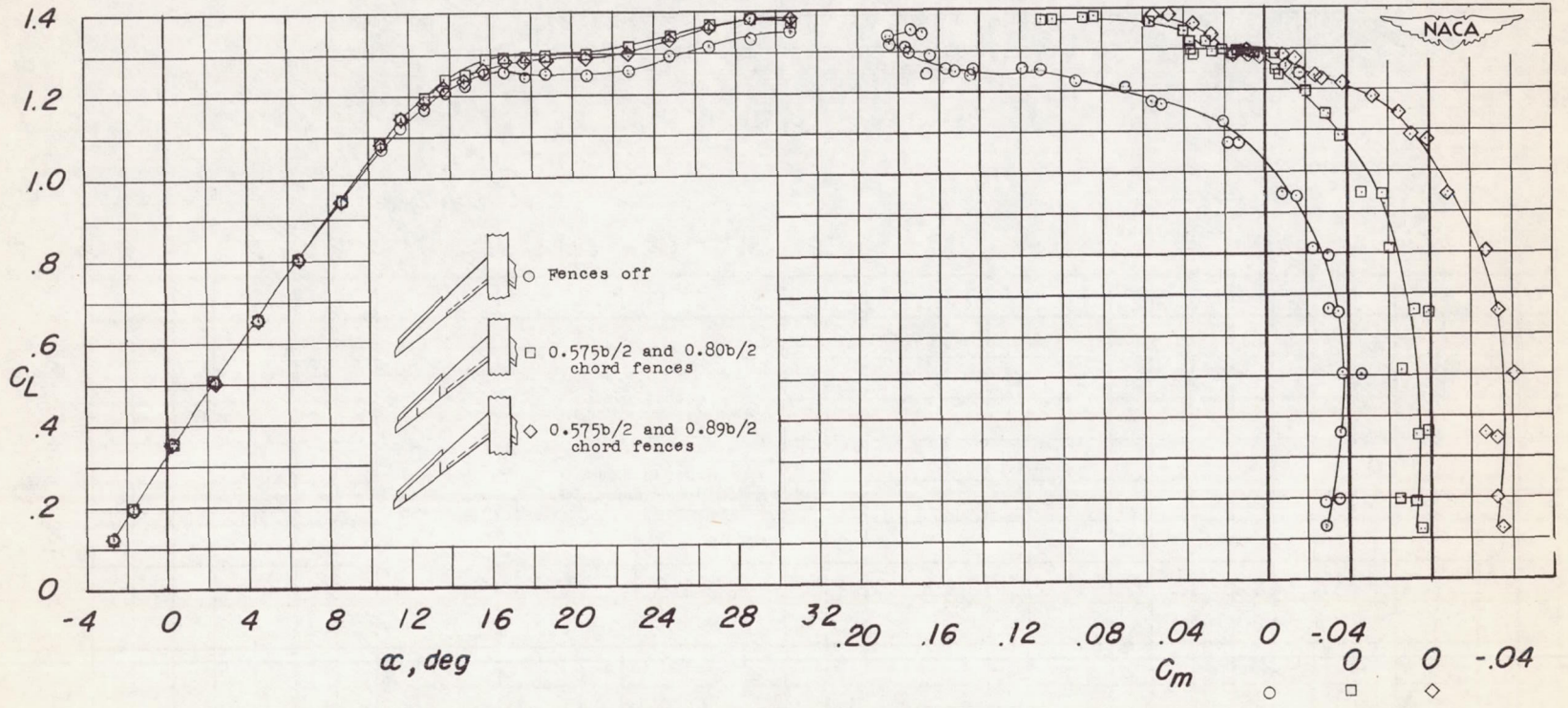


Figure 29.- Lift and pitching-moment characteristics of wing-fuselage combination with 0.45b/2 leading-edge flaps and 0.475b/2 and 0.80b/2 chord fences. $i_w = 4^o$.



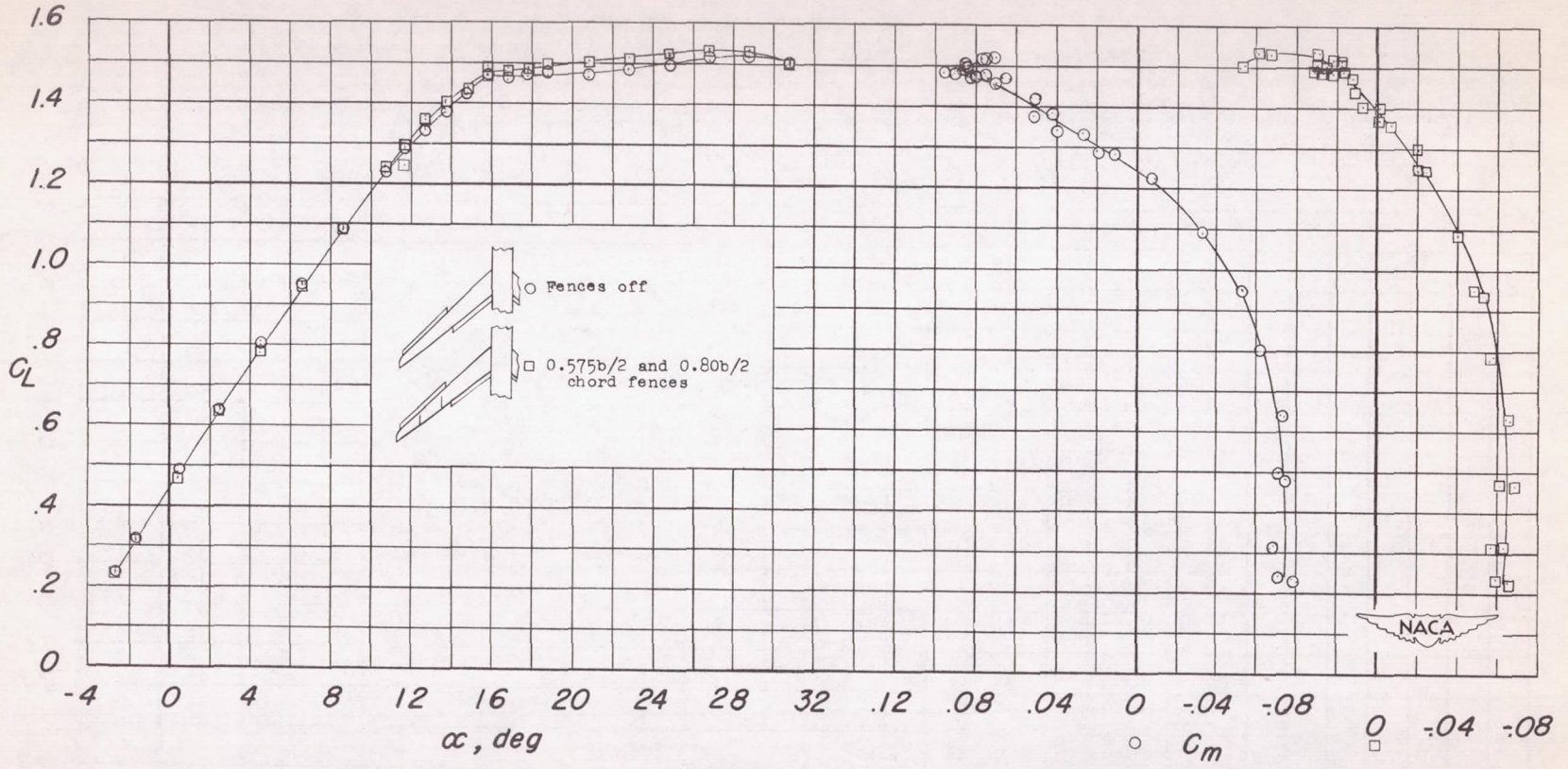
(a) 0.35b/2 split flaps.

Figure 30.- Lift and pitching-moment characteristics of wing-fuselage combination with trailing-edge flaps and 0.45b/2 leading-edge flaps with and without fences. $i_w = 4^\circ$.



(b) 0.50b/2 split flaps.

Figure 30.- Continued.



(c) 0.50b/2 extended split flaps.

Figure 30.- Concluded.

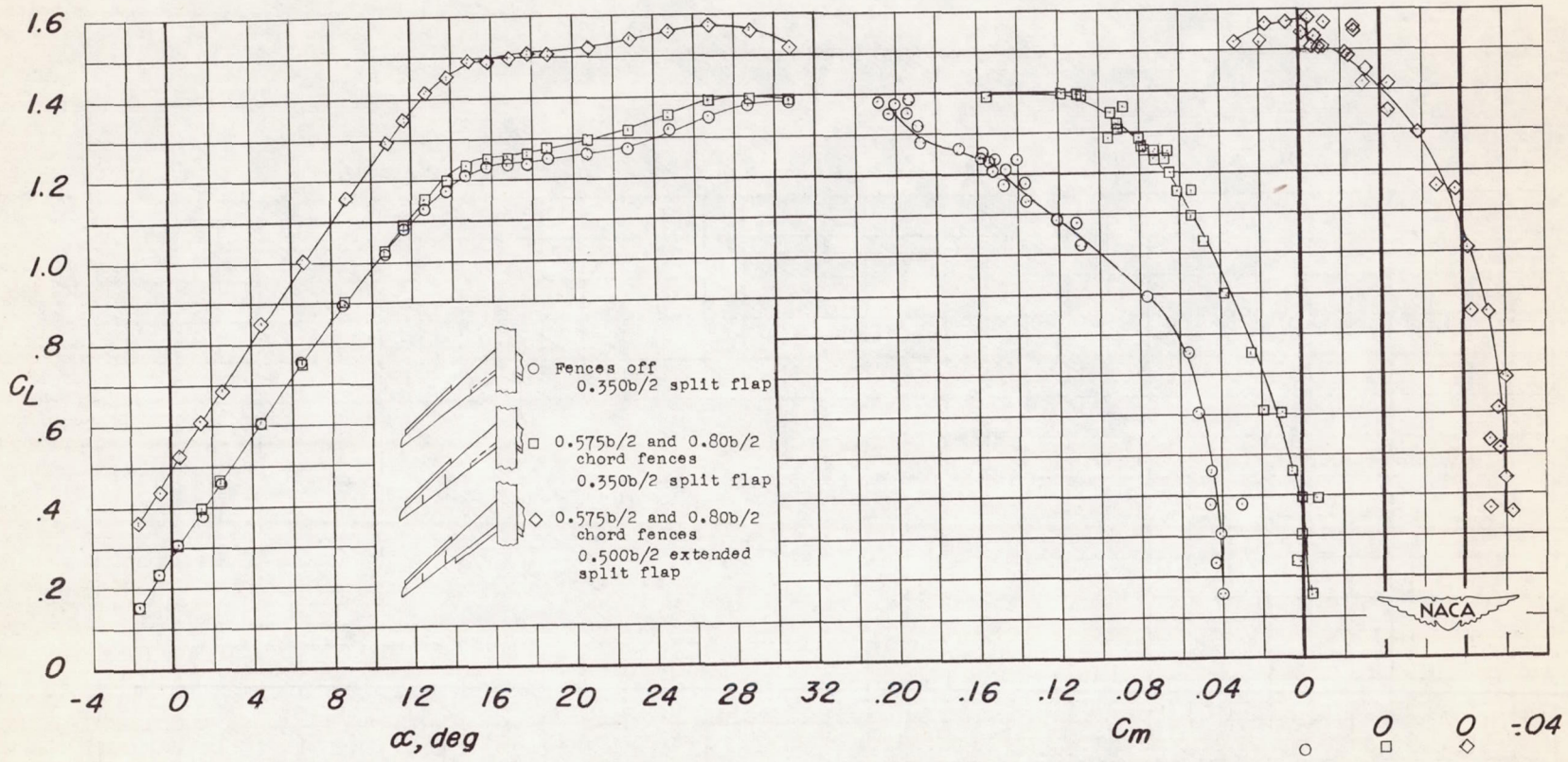


Figure 31.- Lift and pitching-moment characteristics of wing-fuselage combination with trailing-edge flaps and 0.45b/2 leading-edge flaps with and without fences. $i_w = 0^\circ$.